NASA Contractor Report 181940

Crew Emergency Return Vehicle Autoland Feasibility Study

J. A. Bossi
M. A. Langehough
K. L. Lee

Boeing Aerospace & Electronics
20403 68th Ave South
18-26 bldg Kent, WA 98032

Contract NAS1-18762

December 1989

NASA
National Aeronautics and
Space Administration

Langley Research Center
Hampton, Virginia 23665-5225

TABLE OF CONTENTS

TABLE OF CONTENTS (Continued)

LIST OF FIGURES

LIST OF TABLES

1.0 Introduction

1.1 Background

The Crew Emergency Return Vehicle (CERV) autoland feasibility study has been performed as one of the tasks under NASA contract No. NAS1-18762, "Aircraft and Spacecraft Guidance and Control Technology".

The CERV is an emergency support vehicle for the Space Station. The vehicle is be docked at the Space Station, and furnishes a quick exit from the Space Station in case of emergency on board. The vehicle will support return to Earth for one to eight astronauts. The NASA Langley vehicle prescribed in this task would reenter the Earth atmosphere and land on a prescribed runway. The purpose of this task is to determine the feasibility of automatically landing the CERV horizontally in the presence of winds. The feasibility of autoland is determined by 1) the ability of an autoland control system (to be designed) to satisfactorily track the nominal trajectories and 2) the definition of acceptable preliminary requirements on maximum control surface deflections and rates for this system.

The nominal trajectory, aerodynamic data and vehicle mass properties for the CERV model were provided by NASA Langley. The mission starts aligned to the runway centerline at 15000 ft altitude and Mach 0.6, and ends at touchdown on the runway. No engine is available for the autoland operation. The touchdown requirements are a landing speed from 160 to 180 knots with a sink rate less than 2 fps.

A control system shall be developed with the capability of tracking the trajectory in the presence of turbulence and wind shear; both head and side wind conditions. The design shall be verified using non-linear 6DOF simulation. Preliminary requirements shall be developed for control surface positions and rates.

1.2 Technical Approach

The CERV autoland feasibility study focused on determining the controllability of the NASA Langley CERV for performing an automatic landing at a prescribed runway. The study consisted of three prescribed tasks:

1) Design a multi-input, multi-output (MIMO) autoland system control law.

2) Develop a non-linear simulation.

1

3) Determine autoland control system feasibility and preliminary requirements.

Our technical approach consisted of developing the MIMO autoland system including pitch, yaw, and roll autopilots, lateral steering, altitude and speed controller. The autopilots were designed using the integral-LQG control technique with state estimation. The integral-LQG technique consists of using state weighting for transmission zero placement which allows direct design in the frequency domain. The resulting design, by using high gain on the integral control, offers excellent DC characteristics, robust to parameter biases. The control weighting is based on decoupling the control surface effectors. Only partial state feedback, representing modes to be phase stabilized, is included in the LQG design process, thereby minimizing the estimator design. Our design process uses a discrete LQR design technique with computational delay . compensation. Details of the design systhesis are contained in section 5.0.

The resulting MIMO autoland system has been verified using a non-linear 6DOF simulation. A block diagram for the simulation is shown in figure 1-1. Our existing 6DOF simulation has been upgraded with the CERV vehicle characteristic, subsonic aerodynamic model and baseline digital autoland control system. Details of the simulation are described in Appendix B. The stability, control, and performance of the CERV configuration have been verified for the complete autoland mission including the constant glide path flight, the flares and the decrab maneuver. Requirements for this mission are identified in section 3.0. The mission performance has been verified for various wind conditions including wind shear, wind gusts, and wind turbulence. Details of the 6DOF analysis are described in section 6.0

Control surface actuator position requirements have been developed using an initial static trim program followed by 6DOF simulation verification runs. The control surface rate requirements were developed using the 6DOF simulation.

1.3 Summary of Results

A MIMO autoland control system has been developed and feasibility of the CERV configuration for landing on a prescribed runway has been demonstrated through simulation. Reasonable control surface actuator requirements have been demonstrated.

The recommended baseline control surface configuration is shown in figure 1-2. The wing elevons are deflected together for pitch control, the body flaps are split for speed control, both the body flaps and wing elevons are differentiated for roll control, and the vertical center rudder is used for yaw control. The marginal roll control associated with using either the elevons or body flaps independently is improved by using both sets together. This roll control configuration is

2
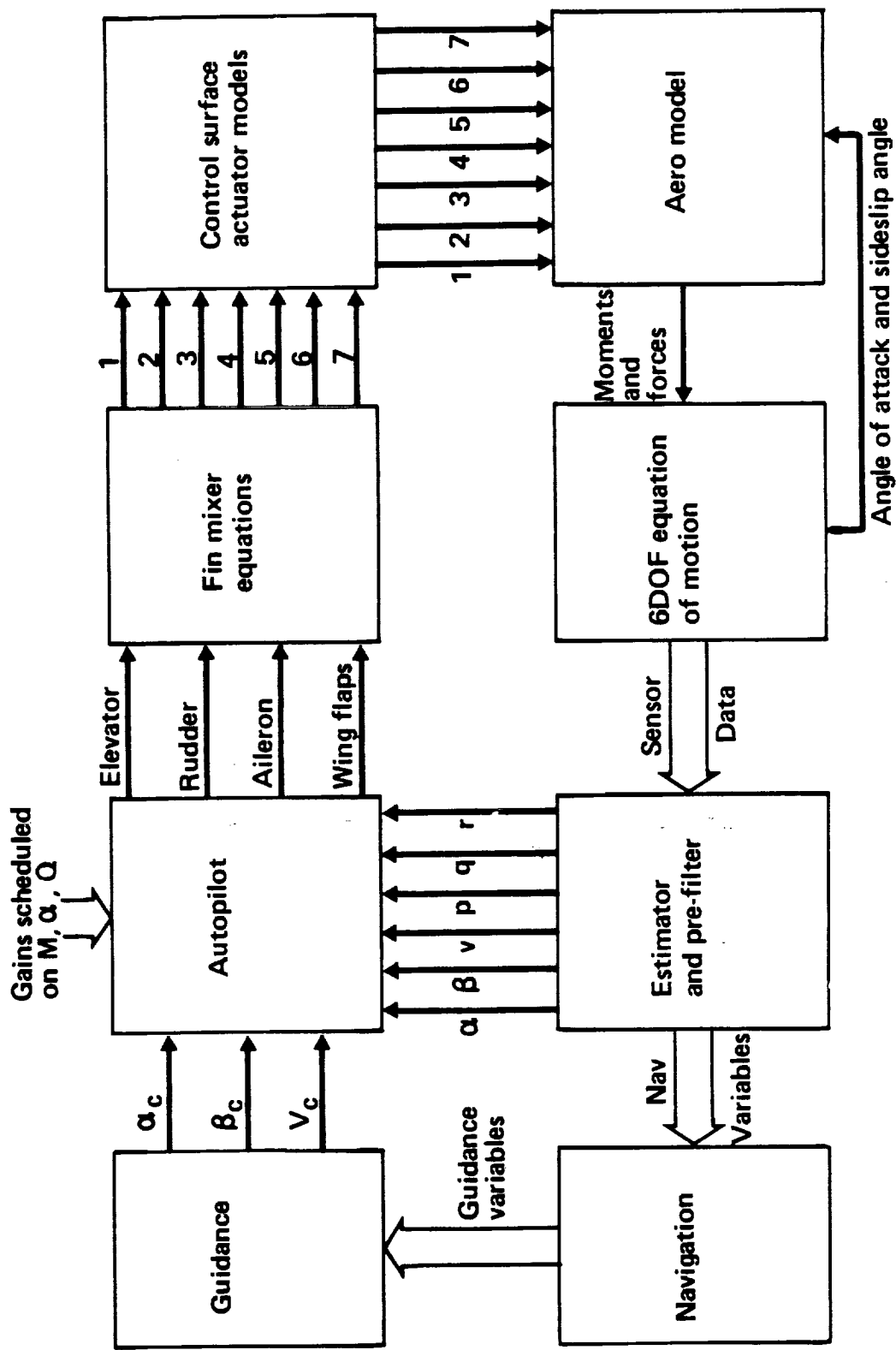
Figure 1-1 Simulation Block Diagram

Baseline Control Surface Configuration

- Pitch control — wing elevon
- Speed control — split body flaps
- Roll control — Differential body flaps + Differential wing elevon
- Yaw control — All movable rudder #2

Right wing elevon

Upper right body flap

Upper left body flap

Left wing elevon

Avionics

Upper body flap

Lower body flap

Rudder

Body
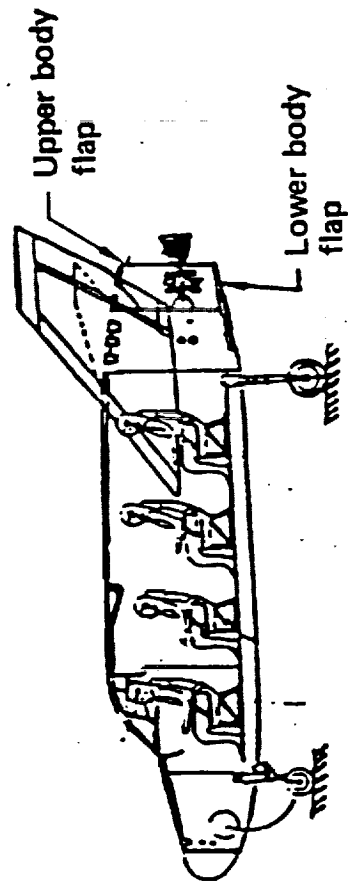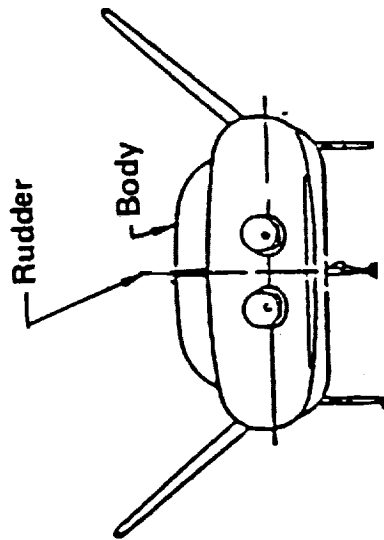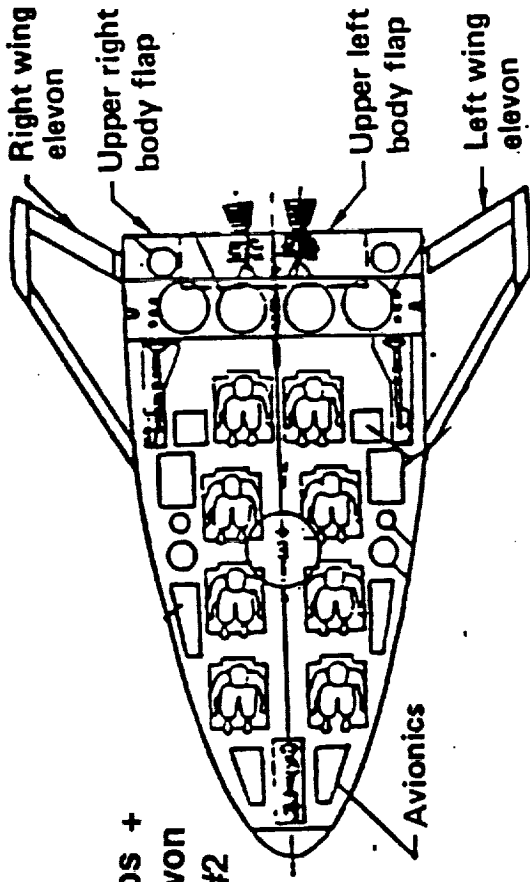
Figure 1-2 Baseline Control Surface Configuration

required for trim during the decrab maneuver in sidewinds. It is recommended for other portions of the flight since it offers additional margin for side wind gusts. A disadvantage is that the additional yaw/roll coupling will require significant rudder usage. The tail configuration recommended is an all-moveable design (No. 2) which is 69% larger than the initial design. The larger rudder is required for trim during the decrab maneuver. The mixing of the control surface commands is performed in the control system mixer logic. Details of the control mixer are discussed in section 2.0.

The baseline control consists of using the integral-LQG autopilot designs with classical guidance laws. An overall block diagram is shown in figure 1-3. Landing reference information for the guidance and control will be received either from a microwave landing system, a global-positioning system, or both supplemented with inertial reference data. The guidance, navigation and control will use a common set of strap-down sensors. The guidance forms angle-of-attack and bank angle commands for the autopilot. The modern control autopilot, together with fin mixer equations, form the control surface actuator commands. The design is an all-digital design; sample times and computational delays selected are shown in figure 1-3. Details of the autoland system are described in section 2.0.

The baseline CERV control configuration and autoland system meets the touchdown accuracy requirements and desired stability margins in the presence of wind disturbances. A summary of the results is shown in figure 1-4. The baseline flare with the altitude control achieves a sink rate of 1 fps. The nominal landing speed is 177 knots. Simulation results demonstrate that the desired landing speed can be achieved using the speed control system for head wind uncertainties and midcourse guidance inaccuracies.

The most difficult part of the autoland mission is landing during a sidewind where a decrab maneuver is required to line-up with the runway. A stable, controllable decrab maneuver has been demonstrated for the worst case 22 knots sidewind. The heading error at touchdown was 1.5° with landing within 15ft of the runway center. Figure 1-5 shows the altitude profile and time histories for the worst case side wind condition. Again, the touchdown condition of sink rate and speed are easily within the requirements. The aileron deflections (both body flaps and wing flaps) and rudder deflections are 28° and 9°, respectively, to trim the 8° sideslip angle due to sidewind. The aircraft attitudes with respect to the runway at touchdown are shown in figure 1-6. The vehicle has a 11.3° roll angle to trim out the side force due to an 8° sideslip angle.

Wind turbulence, discrete gusts, and wind shear conditions have been simulated to analyze the controllability and stability (figure 1-4). Results demonstrated stable, controllable

5

Figure 1-3 Autoland System Block Diagram

Touchdown Accuracy

Parameter	Requirements	Simulation results
Sinkrate	<2 fps	Nominal sink rate, 1 fps
Speed	160-180 knots	Nominal landing speed, 177 knots
Decrab Heading	<3 degree from runway center line	1.5 degree for worst case side wind (22 knots)

Performance & Stability with Winds

Wind conditions	Requirements	Simulation results
Wind Turbulence	1σ = 5 knots	• Demonstrated stable flight • Aileron fin rate Requirements 50-100°/sec
Wind Shears	8 knots/100 ft. • Headwinds = 30 knots • Crosswind = 22 knots	• Demonstrated stable flight • Achieved touchdown accuracy requirements.

Figure 1-4 Autoland Feasibility Study (Summary)

7
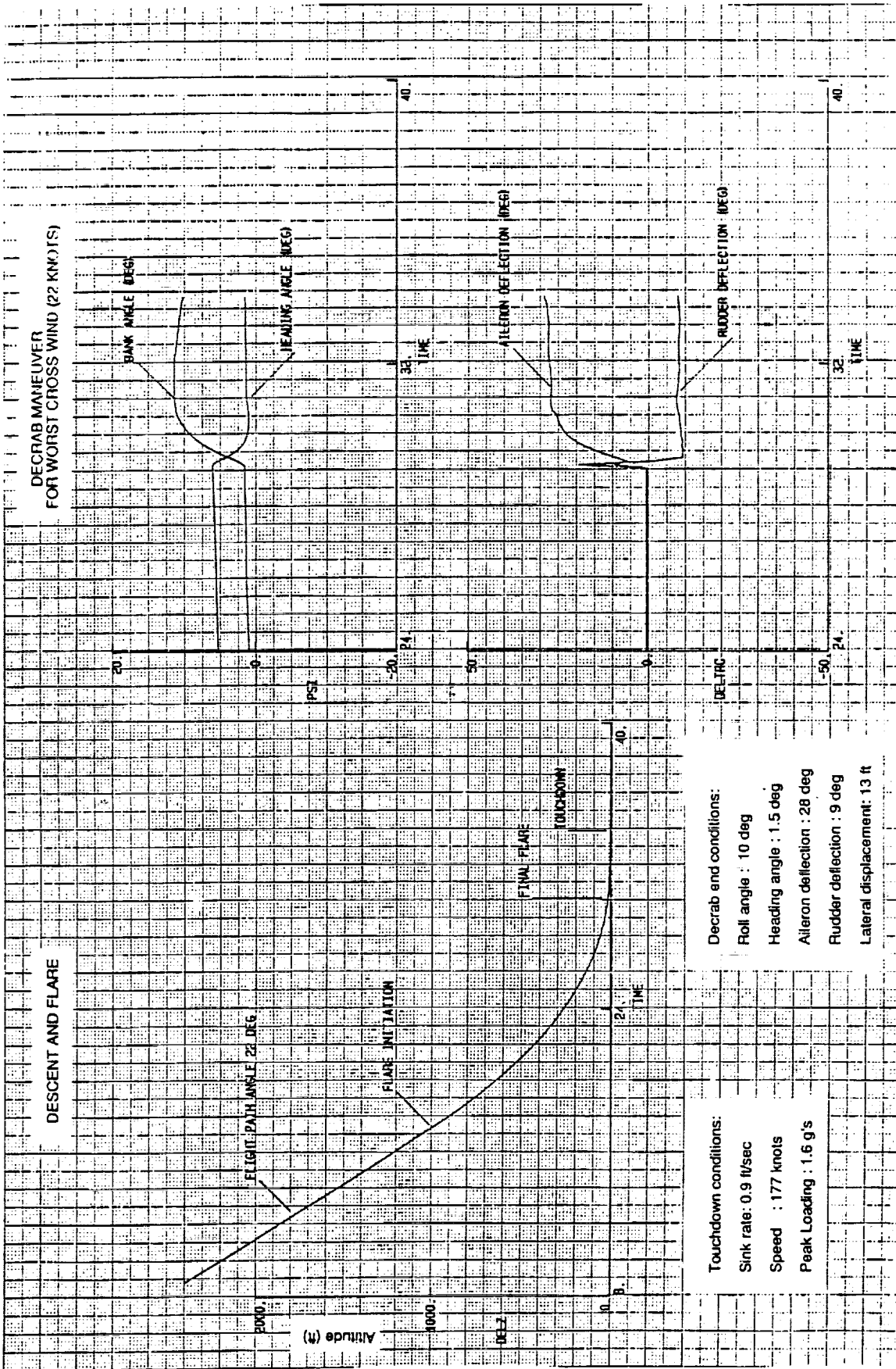
Figure 1-5 6DOF Simulation Results

SIDESLIP ANGLE

$\beta = 8°$

AIR
SPEED

Touch Down Condition
- δ rudder = -10.3°
- δ wf aileron = +27.7
- Dynamic pressure = 105 psf
- Velocity = 295 fps
- Design option #5

ANGLE OF
ATTACK

$\alpha = 15°$

$\phi = 11.3°$

Roll Angle
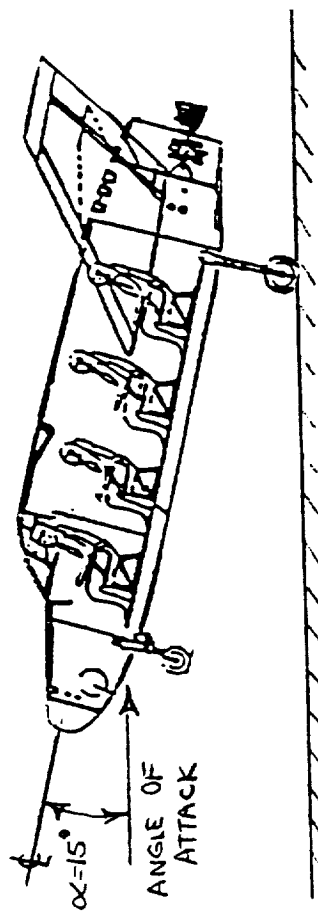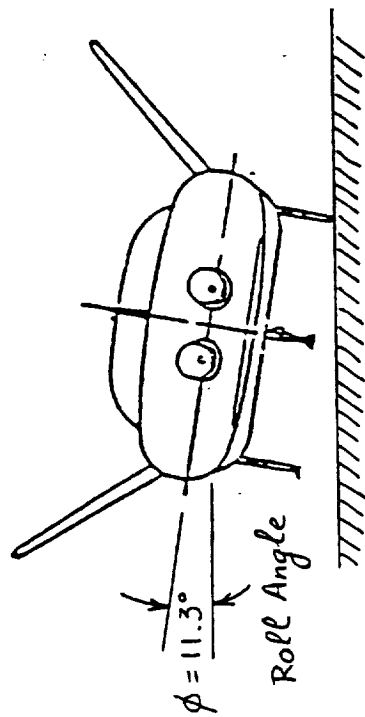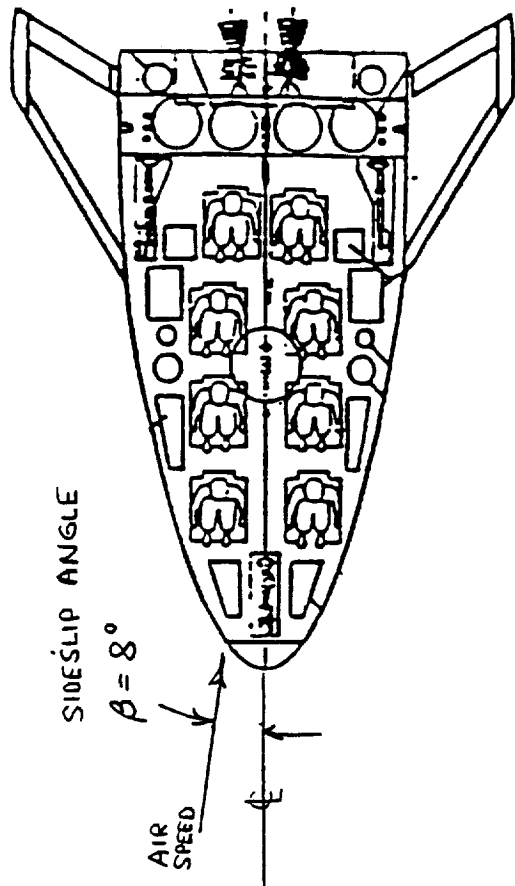
Figure 1-6 Touchdown In Maximum Cross Wind (22 Knots)

performance for all conditions simulated. The 6DOF simulation in section 6.0 contains a description of simulation results.

Preliminary control surface actuator requirements for wind conditions and maneuvers are summarized in figure 1-7. Peak rates are 200 deg/sec, with a 100 deg/sec RMS usage. These results are for the baseline control without pre-filters and internal limiting in the autopilot. Further analysis has demonstrated that, with control system tailoring, the rate can be reduced to the 50-100 deg/sec range. Actuator hardware designs are available to achieve these rates for a range of control surface hinge-moments.

	Body Flap	Rudder	Wing Flap
Wind Turbulence ($\sigma_{x,y}$ = 8.5 ft/sec, σ_z = 6 ft/sec)	100 RMS 200 Peak	60 RMS 200 Peak	100 RMS 200 Peak
1-COS Discrete Gust (@ 700 ft Alt)	1 sec, 70 2 sec, 30 5 sec, 10	60 20 5	70 30 10
Flare Maneuver Final Flare Maneuver	0 0	0 0	30 70
Decrab Maneuver (37 ft/sec side wind) $\beta = 8°$	40	100	80

Figure 1-7 Preliminary Actuator Rate Data (Deg/sec)

* These rates can be reduced to less than wind turbulence requirement by phasing in the decrab autopilot gradually.

11

2.0 Control Concept

The following section describes the autoland mission, the CERV aerospace vehicle, and the control technique used in the autoland. The mission is the landing portion from an 15000 ft approach (section 2.1). The CERV vehicle is the baseline hight lift/drag (3.0) augmented with a 60% larger rudder. Details of the vehicle are contained in section 2.2.

2.1 Autoland Mission

The CERV mission is to return astronauts, generally under emergency conditions, from a spacestation to Earth, landing at a prescribed runway. The mission consists of de-orbit, re-entry, and landing on an available runway. The autoland portion of flight is only considered in this study. Figure 2-1 shows an altitude profile for this portion of the mission. The flight portion is from 15000 ft altitude, Mach 0.6 to the landing site. The mid-course guidance will deliver the CERV vehicle to this prescribed range/altitude/speed starting condition for the autoland.

The autoland trajectory consists of a high flight path angle descent (22°) followed by a flare to the touchdown point. The flare is build-up of two segments, high g flare and low g flare similar to the space shuttle design. A decrab maneuver is performed near touchdown to line the wheels up with the runway. The required conditions at touchdown are 160-180 knots in speed, sink rate less than 2 ft/sec with a decrab to within 3° of runway heading. The autoland system drag modulates to control vehicle speed, since no engine is available.

2.2 Spacecraft Configuration

The CERV configuration is a relatively low lift-to-drag ($L/D_{max}=3$) lifting body configured to perform autoland on available runway. Figure 2-2 shows a drawing of the configuration. The vehicle is 24.5 ft long, 5.7 ft high with 24.5 ft wing span. The wing dihedral is 52°. The maximum L/D for subsonic speed is approximately 3.0.

For control, the vehicle has seven control surfaces, 4 body flaps, 2 wing elevons, and an all-moveable tail for rudder control. Pitch control can be achieved using either the body flaps or wing elevons. Our baseline approach is to use the wing elevons for pitch control and reserve the body flaps for drag modulation. Yaw control is achieved using the rudder. Roll control consists of using differential body flaps together with differential wing elevons.

12

- Altitude 15,000 ft
- Mach 0.6

γ_c

h_0

22° constant glide path

h_1

Range ~ 7.6 miles

Flare

Final flare and decrab

- Speed 160-180 knots
- Sink rate < 2 fps
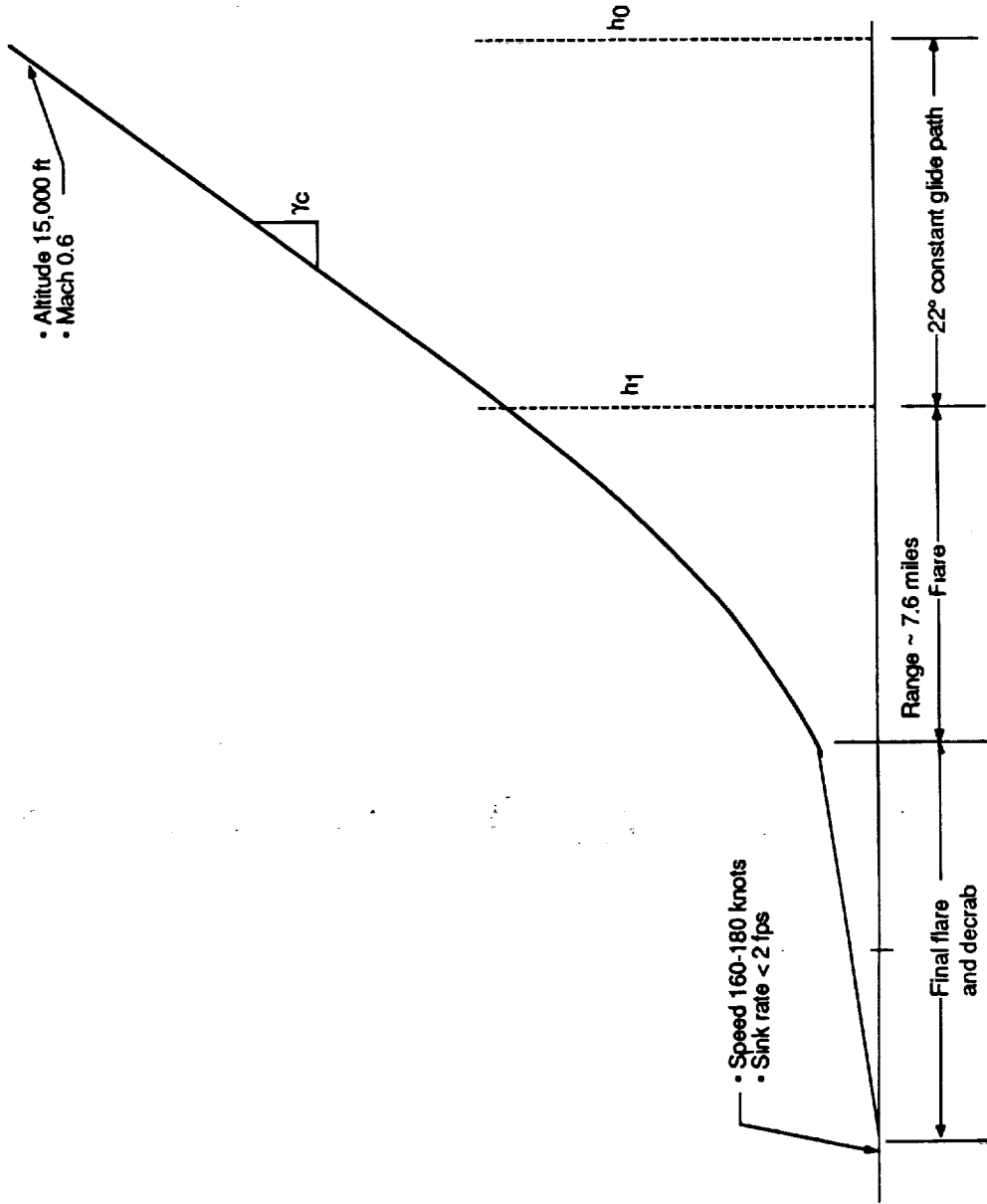
Figure 2-1 Autoland Mission for CERV

FL9-8-89-2a

Right wing elevon

Upper right body flap

Upper left body flap

Left wing elevon

Avionics

Upper body flap

(-)

(+)

Lower body flap

Weight = 11193 lbs

I_x = 6345 slug - ft^2

I_y = 13994 slug - ft^2

I_z = 17123 slug - ft^2

Reference area = 215.61 ft^2

Reference lengths b = 12.132 ft

$\bar{c}$ = 24.583 ft

C.G. location = 13.275 ft from the nose (or at 54% of body length)

Trailing edge

(+)

Rudder

Trailing edge

(+)

Trailing edge

(+)

Trailing edge
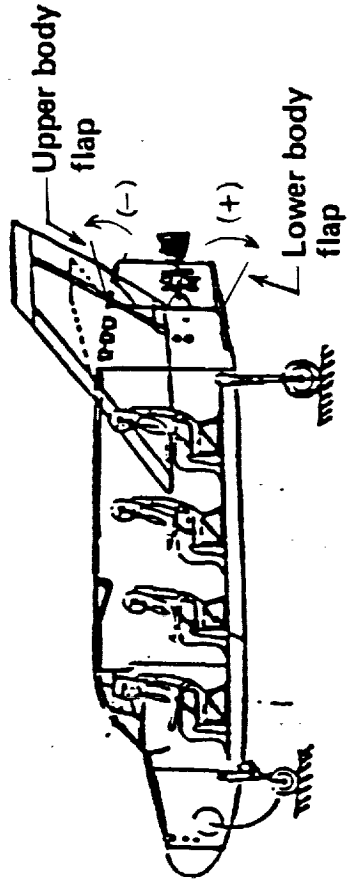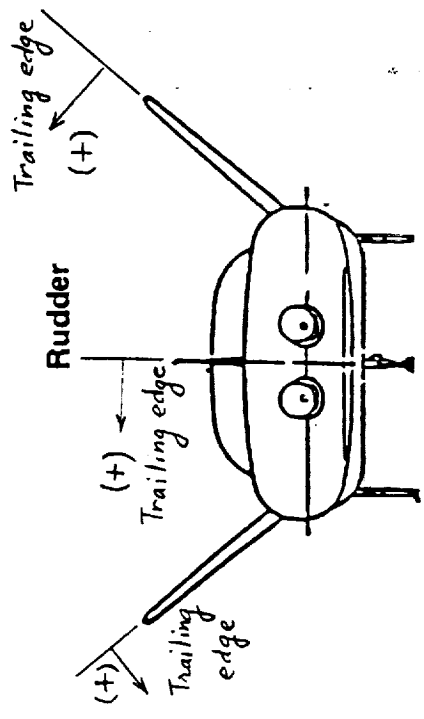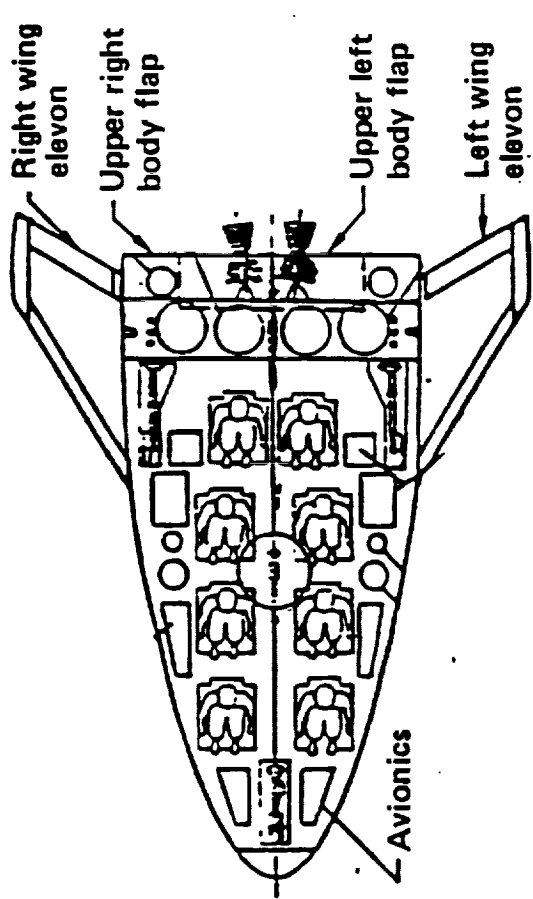
Figure 2-2 Crew Emergency Return Vehicle, CERV

2.3 Control Technique

The autoland system will be an all digital control system consisting of the sensors, flight processor, interfaces and control surface actuators. The algorithms associated with navigation, guidance, and control will be within the flight processor. A functional block diagram for the system is shown in figure 2-3. The navigation will use velocity and altitude information from a strap-down inertial sensors augmented with altitude information from a radar altimeter and inertial measurement updates based on Global Positioning System (GPS). Vehicle information with respect to the runway will be received from the Microwave Landing System

A block diagram for the guidance law is shown in figure 2-4. The longitudinal guidance is an altitude/altitude rate system using feedback information from the Microwave Landing System and augmented with Navigation information. Output of the longitudinal guidance is angle-of-attack command for the pitch autopilot. An angle-of-attack command limit is included along with an angle-of-attack trim function based on level flight.

The lateral guidance is cross track/cross track rate system using information derived off the Microwave Landing System. The output of the lateral guidance is bank angle command.

An integral plus proportional air speed control loop is also included. Air speed feedback information is derived per the air data system. The speed loop commands all four body flaps, splitting them to produce a drag force with no resulting pitching moment. The nominal setting selected was 7.5° (the upper body flaps deflected 7.5° and the lower deflected down 7.5°).

A block diagram for the autopilots is shown in figure 2-5. The design was developed using integral LQG technique. The pitch autopilot is an angle-of-attack autopilot with integral control and pitch rate damping. Angle-of-attack is calculated using an estimator complemented with air data information. Elevator command feedback (δec) is used to compensate for the computer computational delay. The yaw/roll autopilot is a coupled design controlling bank angle. Other feedback variables are sideslip angle, yaw rate, bank angle, and roll rate. δrc and δac feedback again are used to compensate for the computer computational delays. A control surface mixer is included to change the elevator, speedbrake, and aileron commands to individual surface commands. Elevator, speedbrake, rudder, and aileron command limiters are also included. A block diagram of the control surface mixer is shown in figure 2-6.

15

Figure 2-3 Autoland System Block Diagram
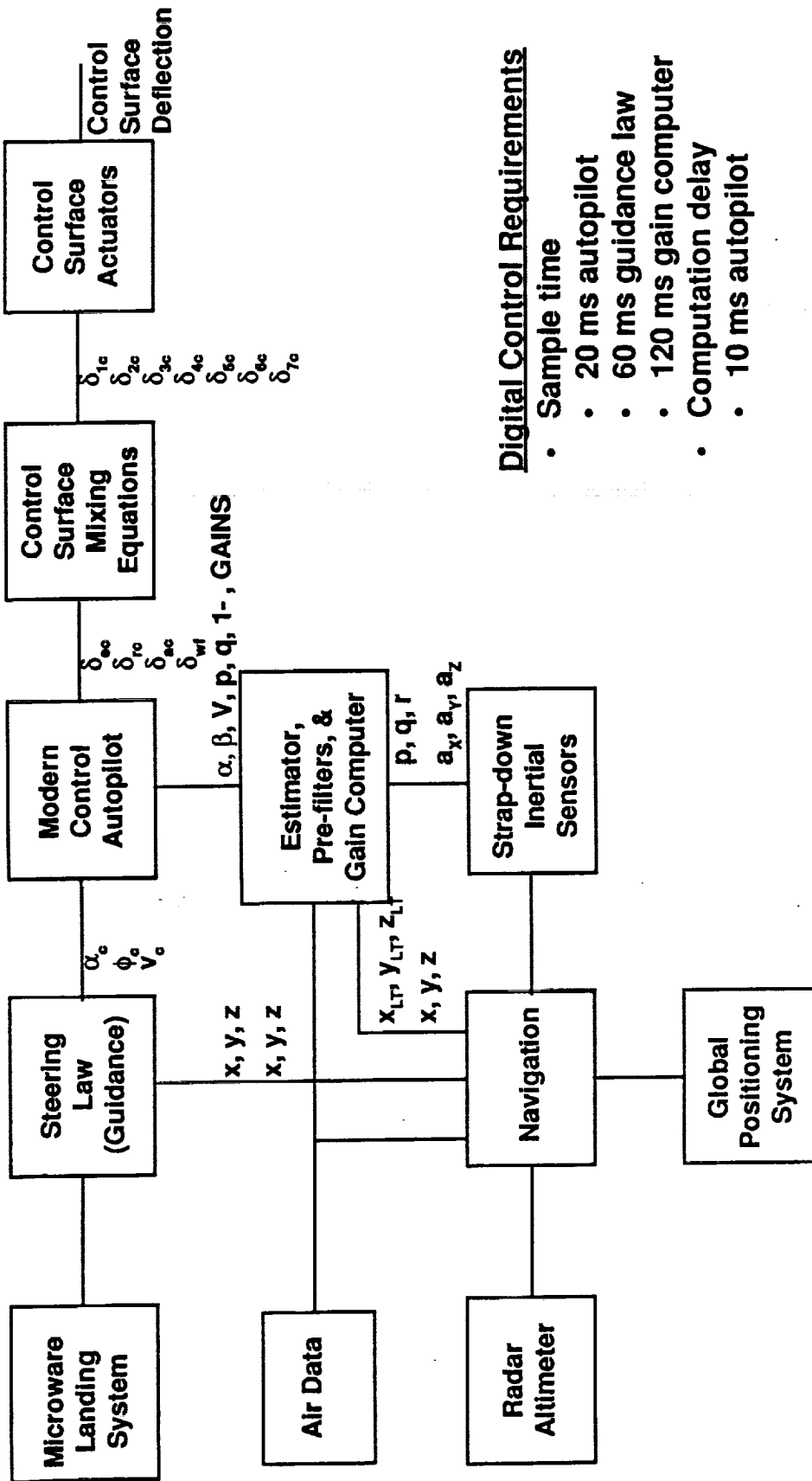
Digital Control Requirements

- Sample time
  - 20 ms autopilot
  - 60 ms guidance law
  - 120 ms gain computer
- Computation delay
  - 10 ms autopilot

16
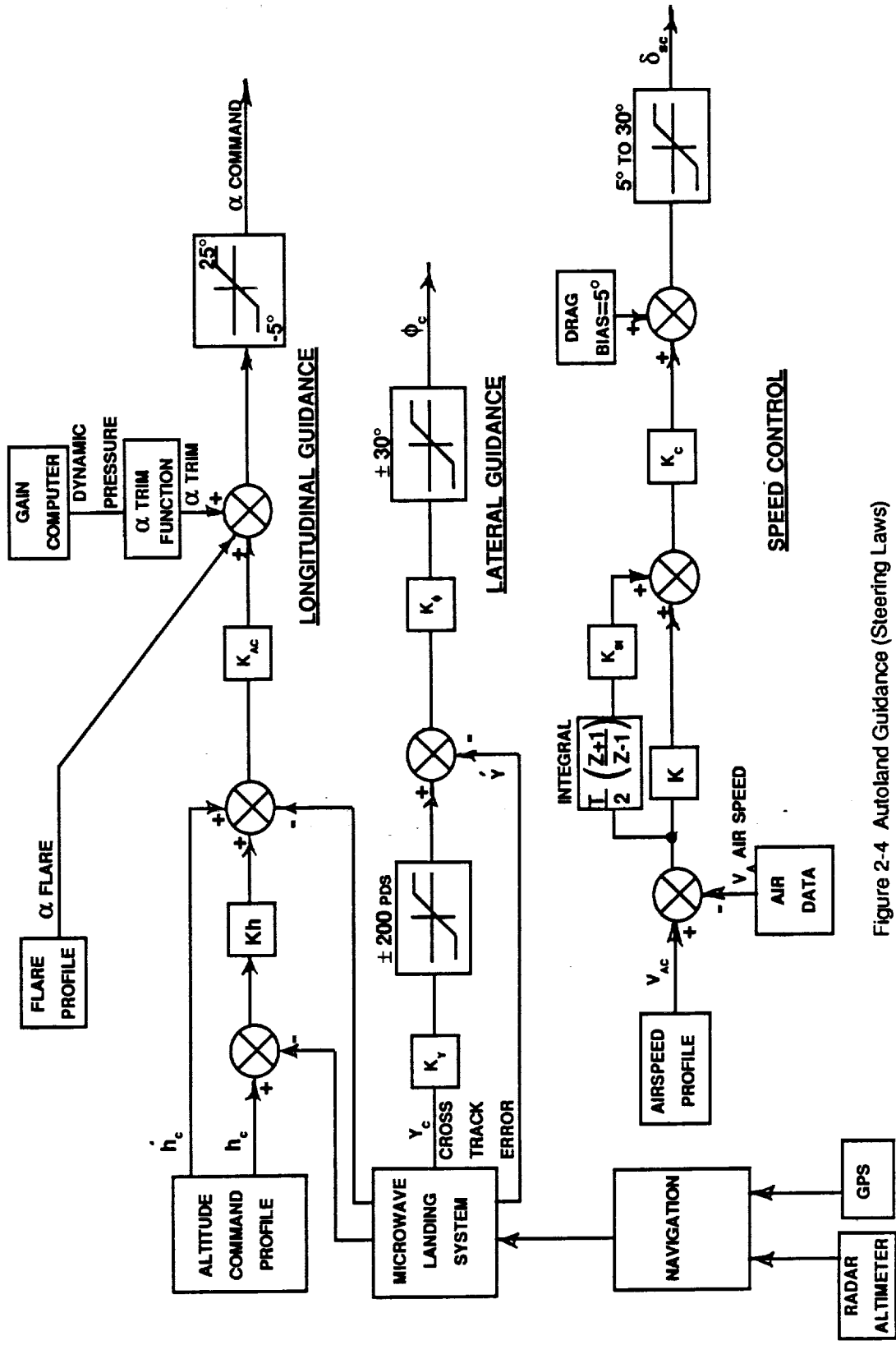
Figure 2-4 Autoland Guidance (Steering Laws)

17
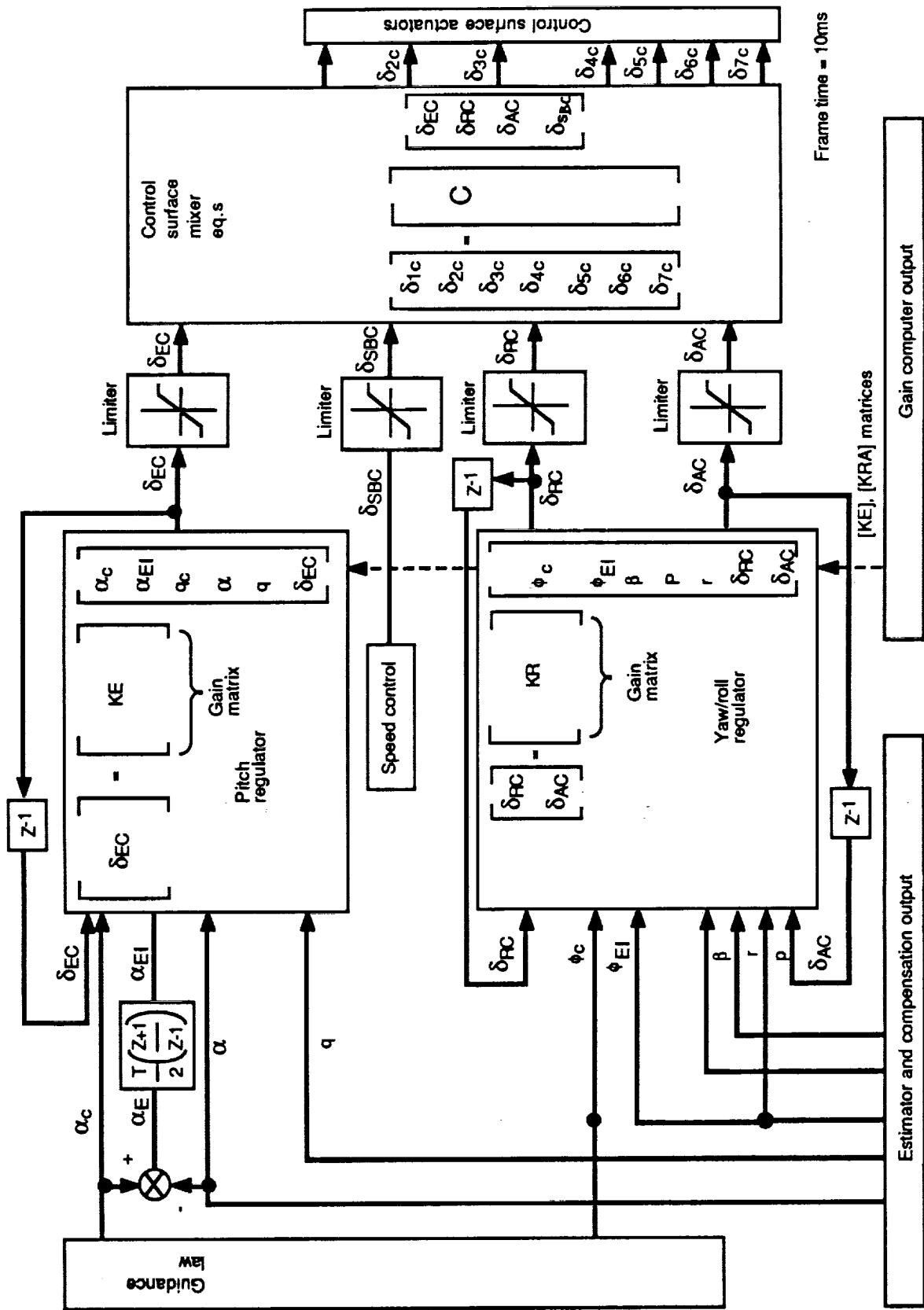
Figure 2-5 Block Diagram of Pitch and Yaw/Roll Autopilots

18
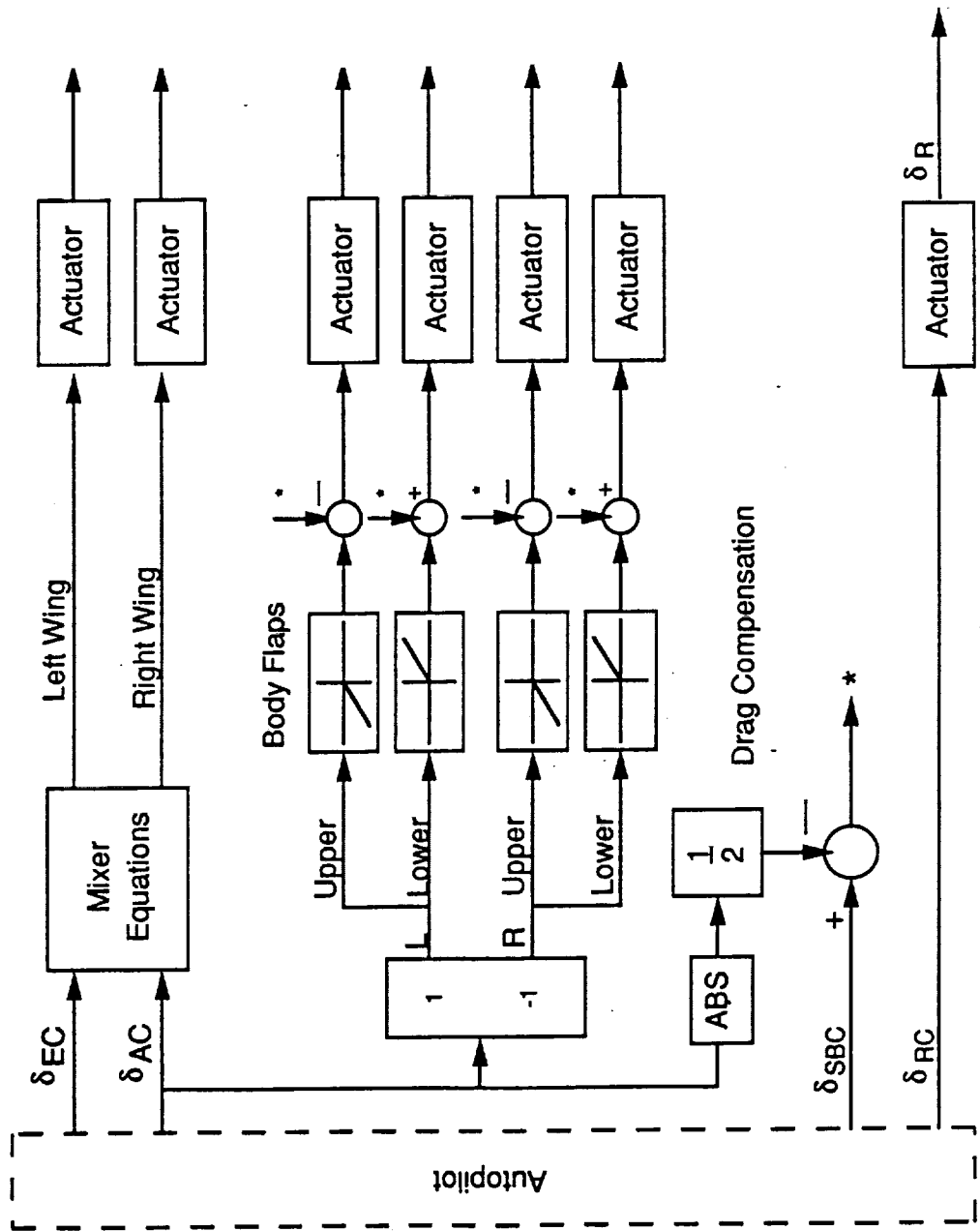
Figure 2-6 Control Surface Mixer Equations

3.0 Design Criteria

The following section presents the design criteria used in developing the CERV autoland system. Included are the flare and decrab performance requirements in terms of touchdown accuracy, control system stability requirements, and the off nominal wind conditions for the 6DOF simulation.

3.1 Flare and Decrab Performance Requirements

Table 3-1 lists the touchdown accuracy requirements for the CERV autoland system. These requirements are related to control algorithm error and flight vehicle performance error and do not include the effect of instrument error associated with the Microwave Landing System, air data or navigation information. These additional errors are independent of the algorithm error and therefore can be combined statistically.

The flare maneuver shall be designed such as to achieve sinkrates at touchdown less than 2 fps at an air speed between 160-180 knots. For the decrab maneuver, the vehicle attitude heading shall be within 3° of the runway centerline. Our design goal also is to keep the CERV vehicle within 50 ft off the centerline of the runway.

3.2 Stability Margins

The autopilot are required to be stable for all the modes throughout the mission. Our design goal for gain and phase margin is shown in figure 3-1. These margins are calculated by opening each loop of the autopilot and analyzing the stability margins. The design goal for the rigid mode for each autopilot loop open at the control surface actuator channel command is 6db gain margin and 30 deg phase margin. 4 db gain margin is reserved for scheduling the autopilot loop gains.

The structural modes were not avialable for the CERV vehicle therefore no analysis has been conducted. The autopilot design does however include high frequency attenuation which could produce the desired structural mode margins.

3.3 Wind Conditions

Table 3-2 presents the wind requirement used in developing the CERV control system. Included are wind requirements for touchdown winds, wind shear and wind turbulence. These requirements have been implemented into 6DOF simulation models as described in the design approach column.

20

	Requirement	Design Goal
Sinkrate	<2 fps	—
Speed	160–180 knots	—
Decrab Heading	3° off Runway Centerline	±50 ft. of Center Line (Runway width)

Table 3-1 Touchdown Accuracy Requirements
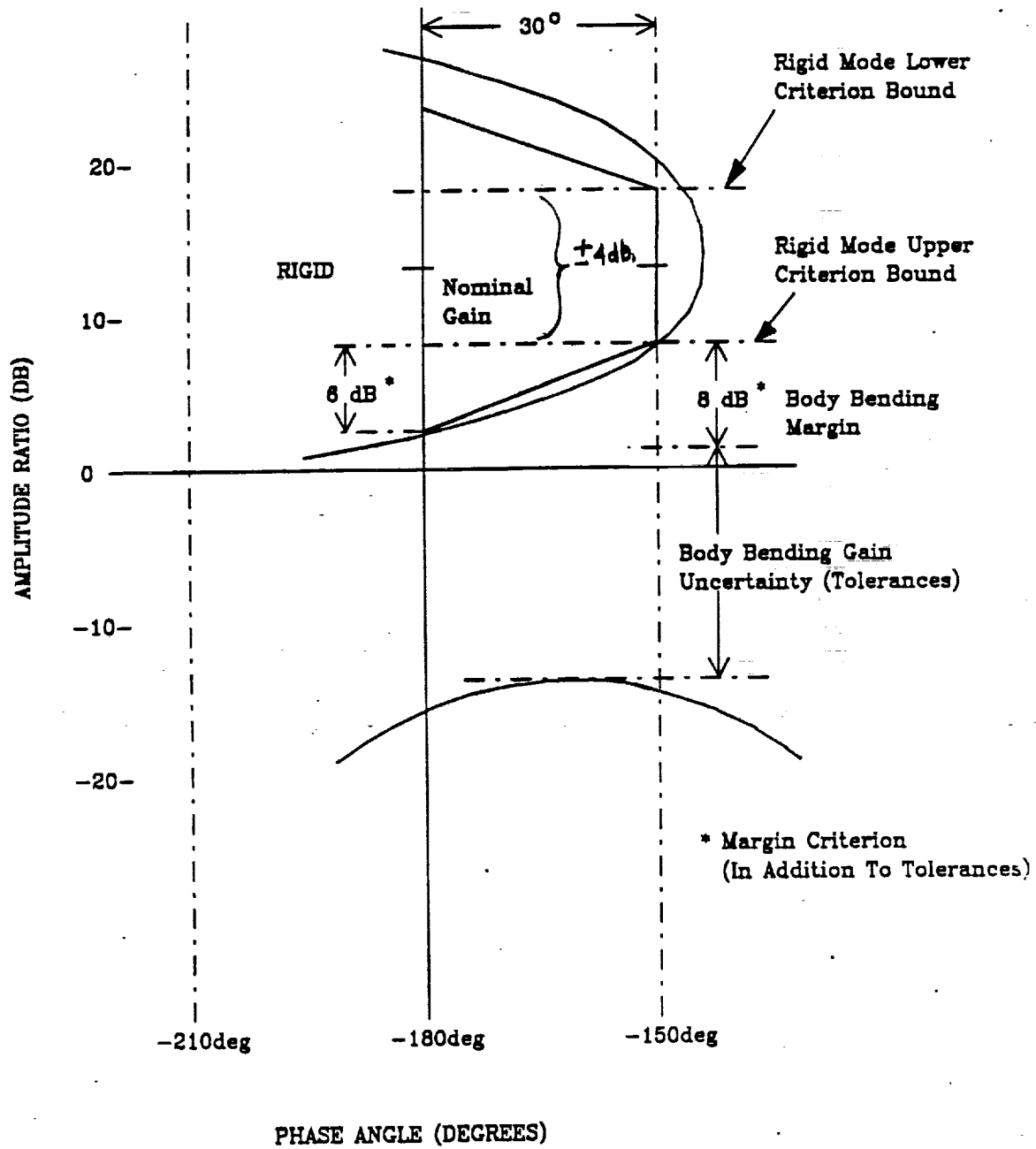
Figure 3-1 Autopilot Stability Criteria

Wind Type	Requirements	Design Approach
Touchdown Wind	Maximum headwind = 30 knots Maximum crosswind = 22 knots	• Maximum value constant with altitude • 1-COS gust (peak value @ maximum condition per requirement)
Wind Shear	8 knots/100 ft.	• Shear profiles as shown in figure 3-2.
Wind Turbulence	1σ = 5 knots	*• Von Karman approximation • Turbulence Scale Factor x= 69 ft y= 36 ft z= 16 ft

* Complete model described in Appendix C.

Table 3-2 Wind Conditions Requirements

The maximum wind requirements are 30 knots headwind and 22 knots crosswind. The CERV runway approach direction will be selected so that only headwind or sidewind conditions will occur. The maximum winds are used as constant with altitude and also in 1-cos discrete wind gust model.

The requirements for windshear are 8 knots per 100 ft of altitude. Figure 3-2 shows the wind profiles used in the design studies. The model is represented by 8 knots per 100 ft shear until the maximum values are reached. The shear nose (maximum wind value) is used at altitude 375ft and at runway elevation.

The wind turbulence requirement is for a 1σ value equal to 5 knots. An approximation of the Von Karman model has been used in the simulation to model turbulence. The turbulence scale factor has been adjusted such as to produce results with similar frequency to the model use in the space shuttle design. Details of the model are described in Appendix C.
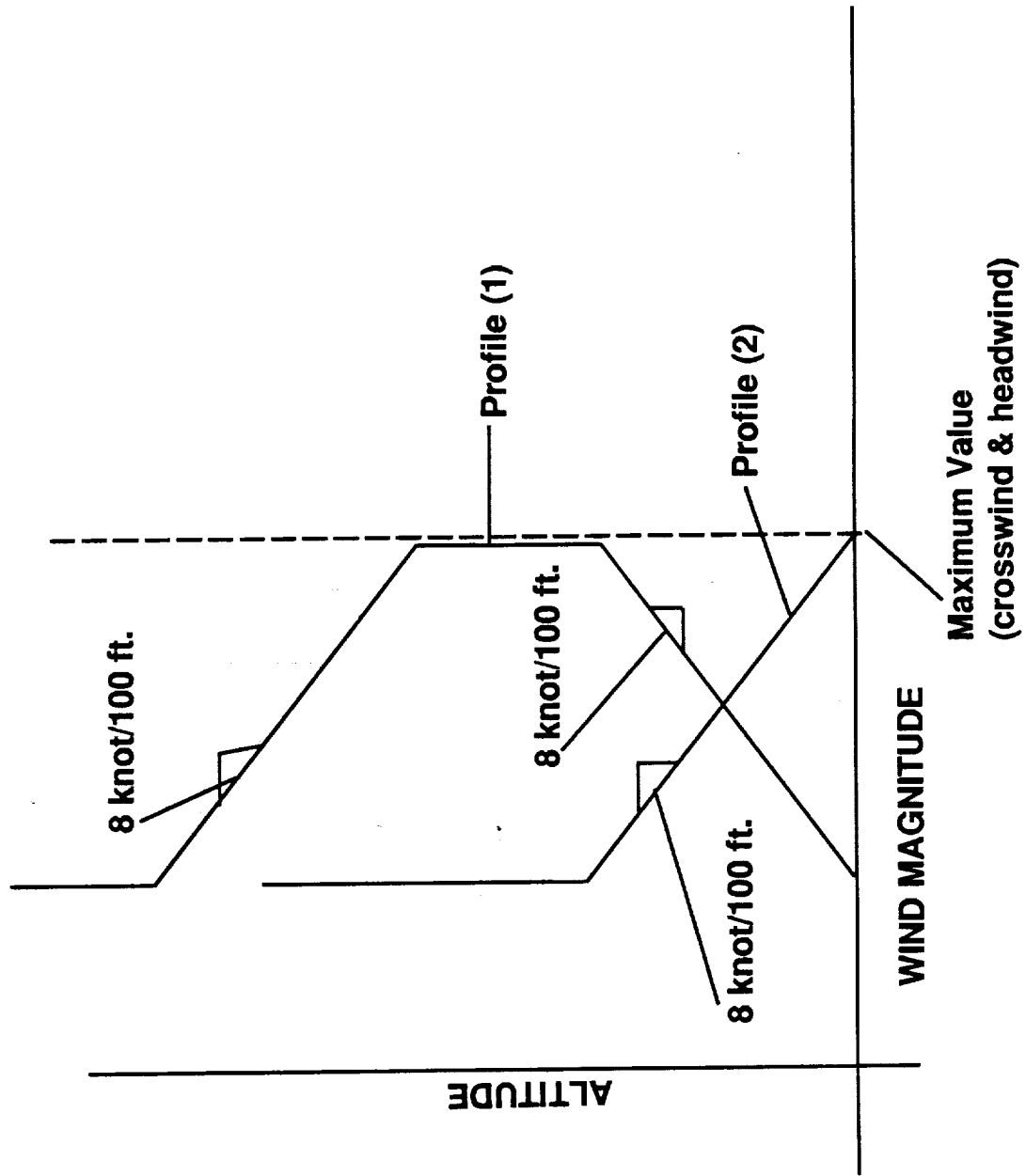
Figure 3-2 Wind Profiles Used in Design Studies

4.0 Control Configuration Trades and Requirements

The CERV vehicle has seven aerodynamic control surfaces as shown in figure 2-2 of section 2.2. The control surfaces have multiple axis capability for control. The four body flaps can be used for elevators, ailerons or drag modulation; two wing flaps can be used for elevators, ailerons, rudder and/or drag modulation. The rudder is mainly for yaw control, but does introduce some roll moment. This section address the trade of which control surface or combination are best applicable to each axis, pitch, yaw, roll, and drag modulation. Controllability issues are addressed along with resizing considerations. The control surface requirement have been analyzed for the three portions of the autoland missions, initial constant glide path portion, flare maneuvers, and the decrab maneuver. Section 4.1, 4.2, 4.3 discuss these requirements for the elevators and drag modulation, ailerons and rudder, respectively.

4.1 Elevators and Drag Modulation Requirements

Two sources of pitch control and drag modulation are available on the CERV vehicle, upper and lower body flaps and wing flaps. These two sets are also to be shared with the roll control functions. A trade study has been conducted on two options:

(1) Body flap elevators for pitch control and wing flaps for drag modulation.

(2) Wing flaps elevators for pitch control and splitting body flaps for drag modulation.

Three aspects were considered in this trade study, pitch trim, pitch control effectiveness and speed control efficiency. Figure 4-1 summarizes the trade study results. The CERV vehicle is designed to trim with zero elevator deflection at approximately 14 degrees angle of attack. At lower angle of attack, a pitch down moment is required from the elevator to trim the vehicle, at 5 degrees angle-of-attack, 15 degrees elevator deflection is required for trim.

Figure 4-2 shows for option 1 the drag coefficient for various wing flap deflection. Body flap trim deflections are noted on the plot. To achieve the speed control efficiency, the wing flap nominal setting needs to be selected such that positive control can be achieve to increase the vehicle speed and decrease vehicle speed. The operating region selected for the wing flaps is shown in figure 4-2 (0 degree nominal with +2 degree variation for control). The body flaps for pitch trim would then operate in the region of 15-20 degrees. There is only minimum deflection capability left for roll control. In this design, option 1, there is coupling of the pitch controller and speed control loop which will have to be compensated for in the control design.

26

Control Surfaces Options / Trade Factors	Pitch Trim	Pitch Fin Effectiveness	Speed Control Efficiency	
Option 1 • Body flap elevators for pitch control • Wing flap for drag modulation	• Higher trim deflection than option 2 δ body flap 20-25° max δ wing flap=±2.5° max • Less flap deflection available for roll control	• Satisfactory fin effectiveness	• Higher drag configuration than option 2 • Pitch/drag coupling required in control design • Less margin for roll control	
		⇑ Same ⇓ Capability		
Option 2 • Wing flap elevators for pitch control • Splitting body flaps for drag modulation	• Lower trim deflection than option 1 δ body flap=5-10° max δ wing flap=16° max • More roll control capability with body flap	• Satisfactory fin effectiveness	• Lower drag configuration than option 1 • Decoupled design	⇐ RECOMMENDED APPROACH

Figure 4-1 Elevators & Drag Modulation Trade Study
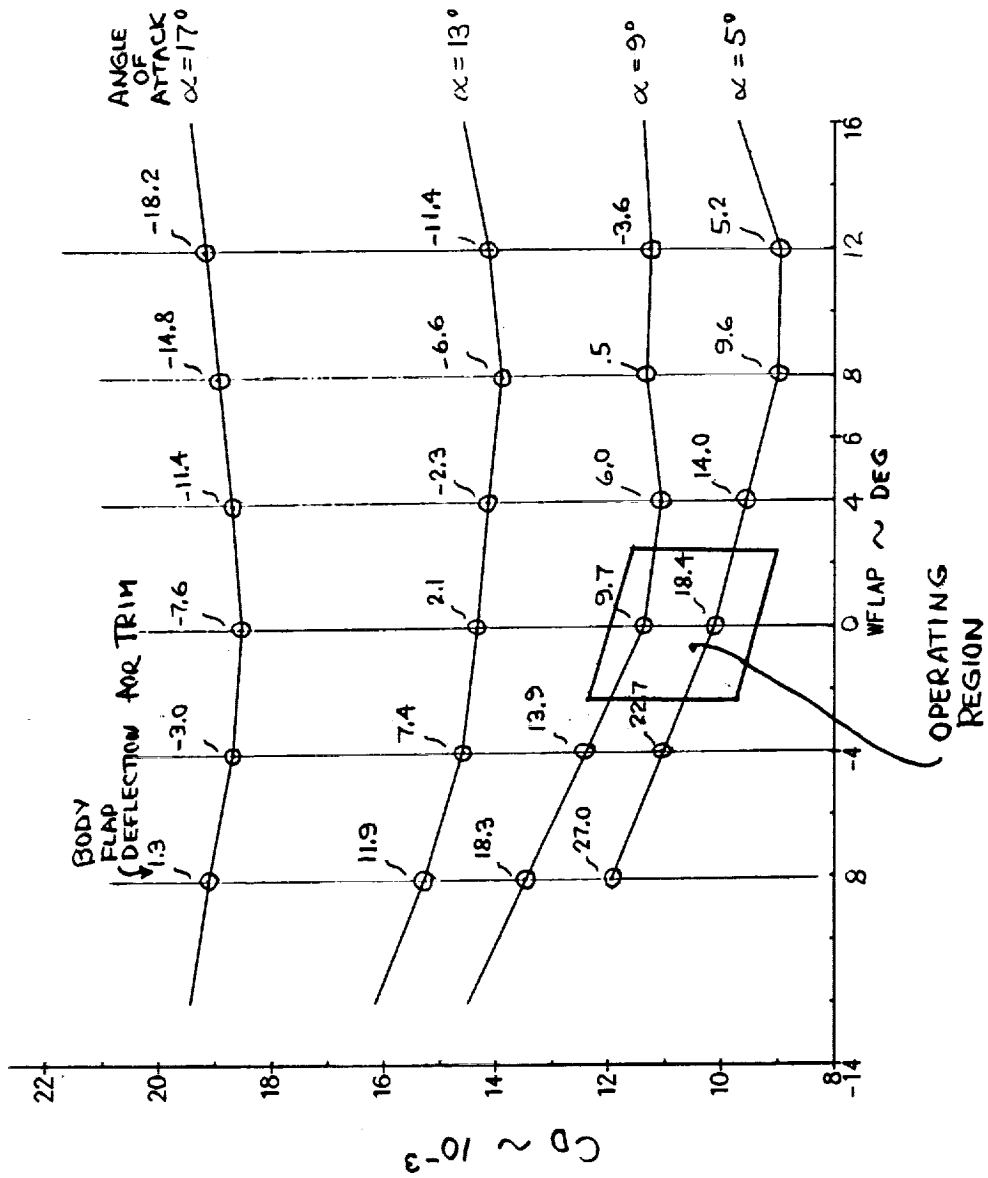
Figure 4-2 Drag & Trim Capability for Option 1

28

Figure 4-3 shows for option 2, the drag coefficient for various split body flap deflection. The wing flap deflections for pitch trim are noted on the plot. For this option 2, the body flaps would operate in region between 5-10 degrees for speed control (figure 4-3); 20 degrees deflection would be left for roll control. The wing flap deflection for pitch trim would be between 7-15 degrees depending on the angle-of-attack. This option has very little pitch/speed control cross coupling since splitting the body flaps introduce very little pitching moment.

Option 2, body flap for speed control and roll control and wing flaps for pitch control, is the recommended design due to its advantages in pitch trim and speed control efficiency.
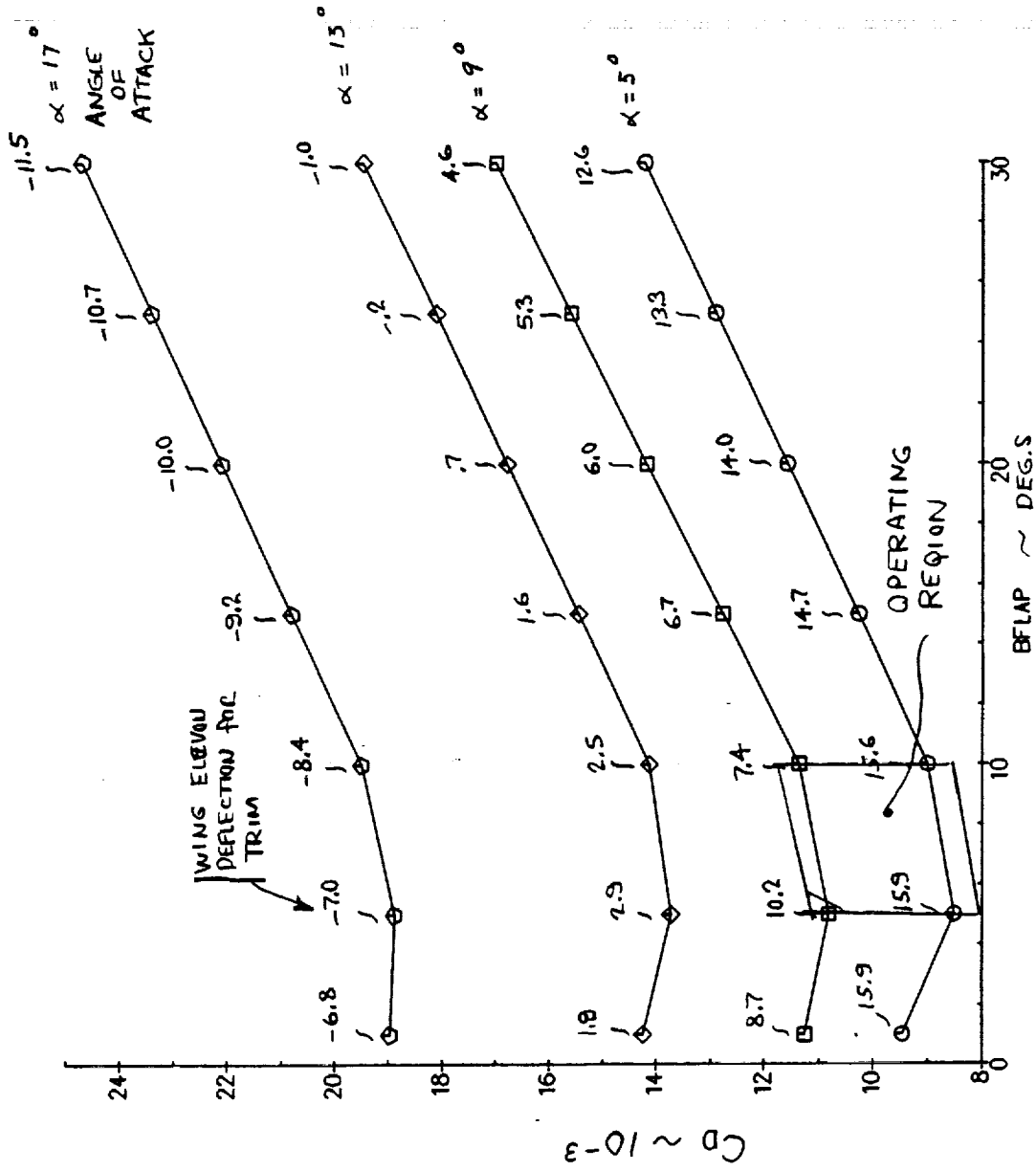
Figure 4-3 Drag & Trim Capability for Option 2

30

4.2 Ailerons and Rudder Requirements

The options for roll control are either to use differential body flap, differential wing flap or some combination of both. The yaw control is achieved by using the center vertical rudder. For the constant glide path and flare portion of the flight, the vehicle flies bank-to-turn, zero sideslip angle. The requirement for roll and yaw control are minimum with only the requirement to control during wind gust or shears. Both options could be used for roll control for these phase of flight, but the option using differential wing flaps is perferred since it has more roll control authority and it is the same control configuration used in the decrab maneuver. The following sections 6.3 and 6.4 show the yaw/roll control performance during wind gust for these portions of flight. Depending on the gust frequency, large aileron correction can occur as shown in section 6.4.

The critical portion of flight for the yaw/roll control is during the decrab maneuver with side wind. In this condition, the vehicle approaches the runway crabbed into the wind ($\beta = 0$ degree). The vehicle rotates to line up with the runway and rolls to null the side force and eliminate the side translation. Large sideslip condition (6^0-8^0) can occur which need to be trimmed by the ailerons and rudder. Figure 4-4 shows the touchdown conditions. The most critical design requirement is for a 22 knot sidewind. At this condition the yaw and roll moments need to be balanced along with side force due to the sideslip angle.

A trade study was conducted on the aileron and rudder requirement to trim the decrab condition. Figure 4-5 summarizes the configuration considered, the resulting touchdown condition for 22 knots sidewind, and the side wind capability as limited by 30 degrees control surface deflection. Option 1 consists of using only the differential body flap for roll with the nominal rudder no. 1 (moving trailing edge). This design has insufficient roll authority. The maximum sidewind capability is only 8.2 knots. Option 2 using the wing flap instead of body flap also is short of roll authorithy and yaw authority, surface deflection far beyond the 30 degree limit. The maximum sidewind capability of only 7.5 knots. The differential wing elevons introduce large yaw/roll cross coupling which cause the large rudder deflection requirements. Option 3 consisting of adding an all movable rudder improves design 2 only slightly. Option 4, which consists of increasing the size of the all movable rudder, is also short of roll authorithy. Option 5, a combination of using both the differentiated wing flap and body flap plus a larger all movable rudder does furnish the required trim capability for the maximum side wind condition. In this case both the wing flaps and body flaps are differentiated 27.7^0 to achieve the roll trim. The larger rudder was used to trim the yaw. Configuration 1 is short of yaw authority to trim this condition, but configuration 2 is sized larger than required. A rudder deflection of only 10.3 is used to trim the maximum side wind condition. Option 5 has been implemented on the 6DOF simulation and

31

Touch Down Condition (option #5)

- δ rudder = -10.3°
- δ wf aileron = +27.7
- Dynamic pressure = 105 psf
- Velocity = 295 fps
- Design option #5

Steady State Condition @ Touchdown

Roll: $Cl_\beta*\beta + Cl_{\delta a}*\delta a + Cl_{\delta r}*\delta r = 0.$

Yaw: $Cn_\beta*\beta + Cn_{\delta a}*\delta a + Cn_{\delta r}*\delta r = 0$

Side Force: $Q*S*[Cy_\beta*\beta + Cy_{\delta a}*\delta a + Cy_{\delta r}*\delta r] + m*g*\phi = 0$

where $\beta = Vw/u$

Vw = cross wind velocity (22 knots)

u = Nominal forward velocity (180 knots)

SIDESLIP ANGLE

$\beta = 8°$

AIR SPEED

α = 15°

ANGLE OF ATTACK

$\phi = 11.5°$

Roll Angle
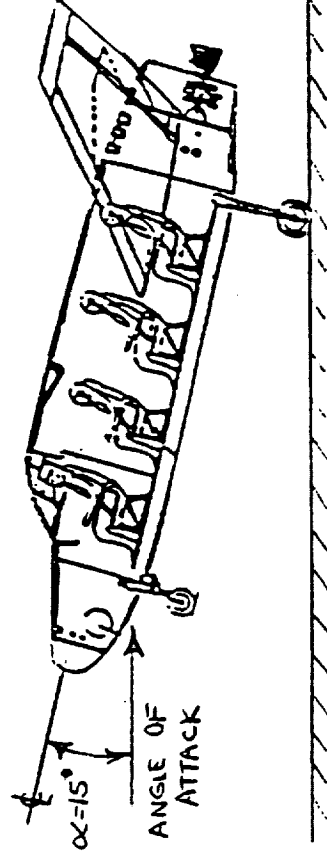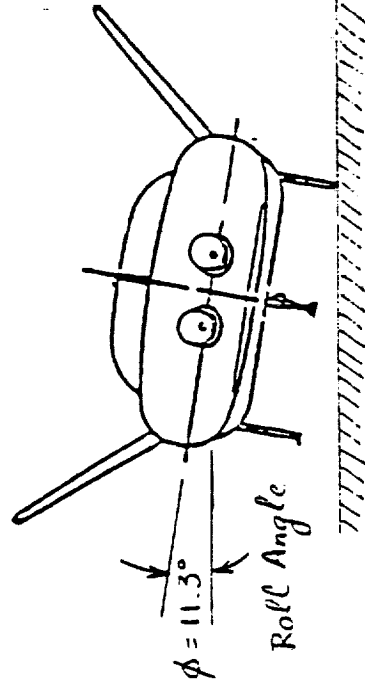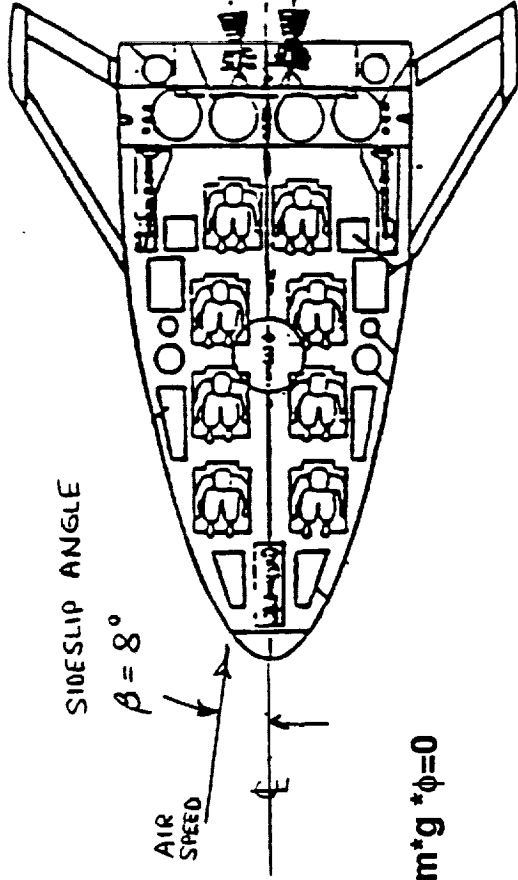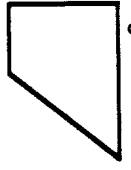
Figure 4-4 Touchdown in Maximum Cross Wind (22 Knots)

32

Options	Control configuration		Touch down conditions for 22 knot side wind			Maxium sidewind (knots) capability (30° deflection limit)
	Ailerons	Rudder	Aileron deflection (deg)	Rudder deflection (deg)	Roll angle (deg)	
1	Differential body flap	Configuration #1	80.4	-18.5	7.0	8.2
2	Differential wing flap	Configuration #1	42.4	-87.6	18.9	7.5
3	Differential wing flap	All movable Configuration #1	37.9	-66.2	12.1	10.6
4	Differential wing flap	All movable Configuration #2	36.4	-19.0	11.2	18.1
5	Differential* wing flap + body flap	All movable Configuration #2	27.7	-10.3	11.3	22.0

Req. 22 knots

* 1:1 relationship between wing flap and body flap deflection

Rudder sizes

Configuration #2	Configuration #1
S = 15.0 ft²	S = 8.70 ft²

Touchdown condition
- Dynamic pressure = 105 psf
- Velocity = 295 fps (173 knots)
- Sideslip angle = 8°
- Angle of attack = 15°

Figure 4-5 Ailerons & Rudder Trade Study (Decrab Maneuver)

the decrab maneuver has been demonstrated (section 6.2). This is the recommended configuration for the descent flight.

In the above analysis, the aerodynamic effect of landing gear was not included in the analysis. This effect will decrease the roll moment due to sideslip which will decrease the roll authority requirements slightly. One potential solution would be to put large door along the side of the gear to reduce the large Cl_β introduced by the vehicle wings. This would be good for control but adds complexity to the design.

4.3 Control Surface Actuator Requirement

The following section summarizes the preliminary control surface actuator requirements. The requirements have been developed through 6DOF simulation studies discussed in section 6.

The previous two sections have addressed the elevator, rudder, and aileron deflection ranges. The wing flaps and body flaps will require the +30 degrees range for the decrab maneuver. Surface deflections larger than 30 degrees are not considered due to the aerodynamic non-linearity associated with large deflection. The rudder deflection requirements using the larger all movable rudder could be less than +30 degrees. There is a trade on size versus the deflection requirement.

A summary of preliminary actuator rate requirements for wind disturbances and worst case maneuvers is shown in figure 4-6. The critical condition occurs with worst case wind turbulence where the wing flap and body flap usage is 100 deg/sec RMS and with peak value of 200 deg/sec. Simulation runs with limited actuator rate capability at 50 deg/sec show stable flight characteristics with only slight degradation in autopilot regulation. There is trade between how well the control system tracks the commands verse the actuator rate requirements. Our results demonstrate actuator rate between 50-100 deg/sec are adequate.

	Body Flap	Rudder	Wing Flap
Wind Turbulence ($\sigma_{x,y}$ = 8.5 ft/sec, σ_z = 6 ft/sec)	100 RMS 200 Peak	60 RMS 200 Peak	100 RMS 200 Peak
1-COS Discrete Gust (@ 700 ft Alt)	1 sec, 70 2 sec, 30 5 sec, 10	60 20 5	70 30 10
Flare Maneuver Final Flare Maneuver	0 0	0 0	30 70
Decrab Maneuver (37 ft/sec side wind) β = 8°	40	100	80

* **These rates can be reduced to less than wind turbulence requirement by phasing in the decrab autopilot gradually.**

Figure 4-6 Preliminary Actuator Rate Data

5.0 Design Synthesis

This section discusses the design synthesis for the autopilot, guidance, and speed control. The designs are not intended to be optimum, but are adequate to conduct trade studies, and to investigate the flyability of the CERV.

5.1 Autopilot Design

Linear models were constructed from the aerodynamic derivative data at various trim conditions. During the descent flight path trajectory, the dynamic pressure varies from approximately 300 lb/ft^2 at 15,000 ft at Mach=0.6 to about 90 lb/ft^2 at sea level at landing speed (160 knots). Design points at dynamic pressure (Qpres) of 300, 200 and 100 lb/ft^2 were selected for our analysis. It is estimated that the angle-of-attack varies from 5° at 15,000 ft to 17° at landing (without wind). In this study , the autopilots were designed around the trim conditions α=5° for Qpres=300 and 200 lb/ft^2, and α=11° for Qpres=100 lb/ft^2. The point designs were evaluated at other angles-of-attack to verify gain and phase margins.

The autopilot was synthesized on the MATRIXx program using a modern control Linear Quadratic Regulator (LQR) design technique. The pitch and yaw-roll autopilots were designed separately, since there was little aerodynamic cross coupling between the pitch and yaw/roll axes. The following sections present a short description of the design methodology, the structure and the resulting gains of the autopilots.

5.1.1 Pitch Autopilot

The pitch linear model data are shown in figure 5-1. The control surfaces used are the wing flaps. A trade study on the use of body flaps or the wing flaps as pitch control devices is presented in section 4. The pitch LQ regulator design was done for a state vector that included angle-of-attack, pitch rate and integral of angle-of-attack, using the transmission zero output weighting technique (Reference 1). This technique helps the designer to form a desired state weighting matrix methodically and quickly, instead of by trial and error. The method involves defining output variables, equal in number to the inputs, for output weighting. For the pitch autopilot, there is one input, so one output equation is used. An integral is included in the output variable to improve command following and robustness to parameter variations. Keeping the number of output variables equal to the number of inputs allows specification of transmission zero locations in the LQ regulator design process; thus the designer can control the position to which the closed loop poles will migrate due to the LQ weighting.

37

State Vector: $x^T = [\alpha \quad q \quad \int \alpha dt]$,

Units: Degrees, Degrees/sec

Control Vector: $u = \delta$elev (wing flaps),

Units: Degrees

$\alpha = 5$ degree,   Qpres = 300 psf,   Mach=0.6

$$A = \begin{bmatrix} -0.763 & 1 & 0 \\ -9.764 & 0 & 0 \\ 1 & 0 & 0 \end{bmatrix}, \quad B = \begin{bmatrix} -0.0386 \\ -5.89 \\ 0 \end{bmatrix}$$

Eigenvalues: 0, $-0.381 \pm 3.101i$

$\alpha = 5$ degrees,   Qpres = 200 psf,   Mach=0.45

$$A = \begin{bmatrix} -0.684 & 1 & 0 \\ -6.69 & 0 & 0 \\ 1 & 0 & 0 \end{bmatrix}, \quad B = \begin{bmatrix} -0.0346 \\ -4.035 \\ 0 \end{bmatrix}$$

Eigenvalues: 0, $-0.342 \pm 2.564i$

$\alpha = 11$ degrees,   Qpres = 100 psf,   Mach=0.3

$$A = \begin{bmatrix} -0.458 & 1 & 0 \\ -2.69 & 0 & 0 \\ 1 & 0 & 0 \end{bmatrix}, \quad B = \begin{bmatrix} -0.0291 \\ -2.50 \\ 0 \end{bmatrix}$$

Eigenvalues: 0, $-0.229 \pm 1.624i$

Figure 5-1   Pitch Linear Models

An analog autopilot was first designed. Then the same LQ weighting was used to do a direct digital design. In our case, a 20ms autopilot frame time is used, with a 10ms computational delay. The digital autopilot structure is shown in figure 5-2. The associated gains are tabulated in table 5-1. Nichols plots for the discrete designs at Qpres=300, 200 and 100 lb/ft^2 with the loop open at the actuator are shown in figures 5-3 to 5-5. The actuator is modeled as a second order filter with a 10Hz bandwidth and a 0.5 damping ratio. Angle-of-attack step response at those conditions are shown in figures 5-6 to 5-8. The autopilot bandwidth is designed to decrease as the dynamic pressure reduces, to avoid actuator rate limiting effects.
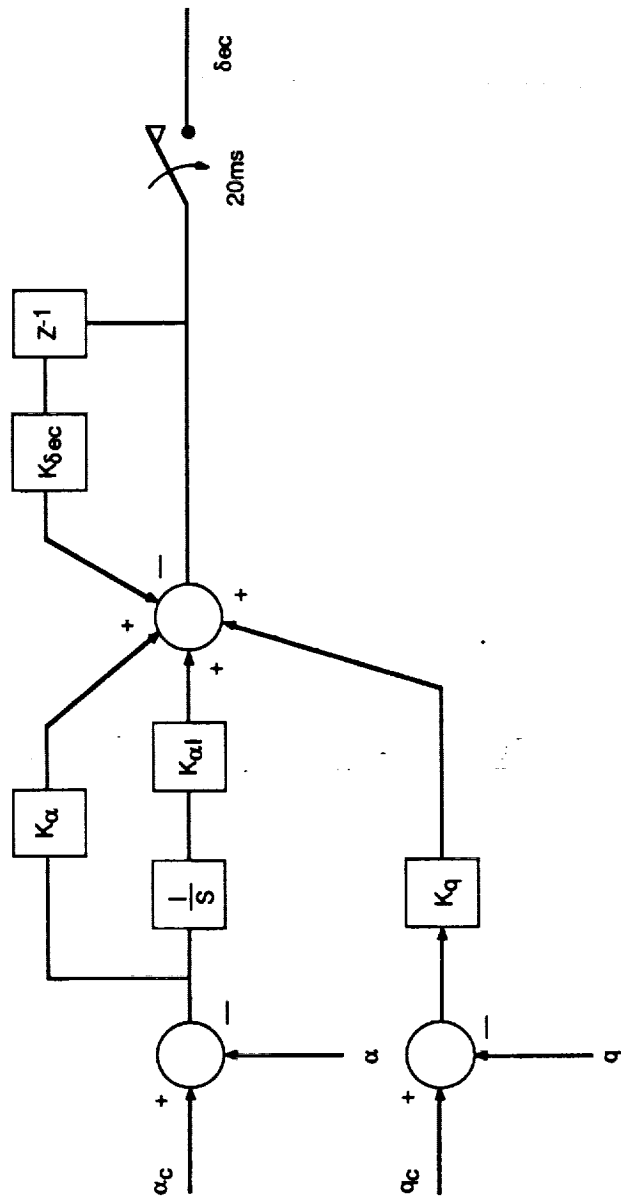
Figure 5-2 Pitch Autopilot

40

Q (lbft²)	K_α	K_q	$K_{\alpha I}$	$K_{\delta ec}$	Closed Loop Poles (Continuous System)
301	-2.596	-1.206	-5.292	0.182	-1.483 -3.43 ± 3.37 i
206	-2.845	-1.380	-5.403	0.143	-1.467 -2.532 ± 3.096 i
110	-5.255	-2.564	-9.421	0.130	-3.394 -1.901 ± 1.952

Table 5-1 Pitch Digital Autopilot Gains
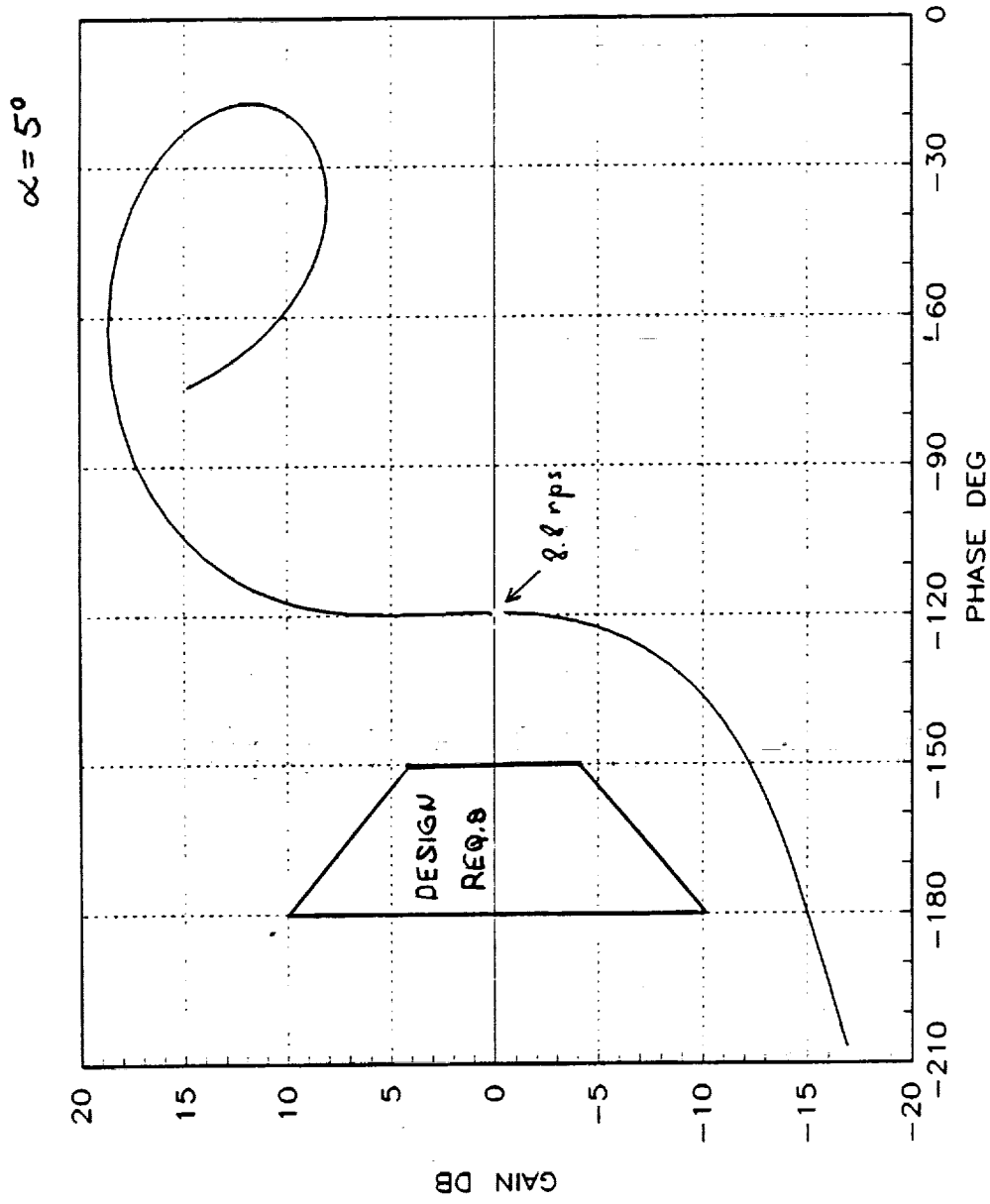
Figure 5-3 Nichols Plot (Pitch, α=5°, Qpres=300psf)
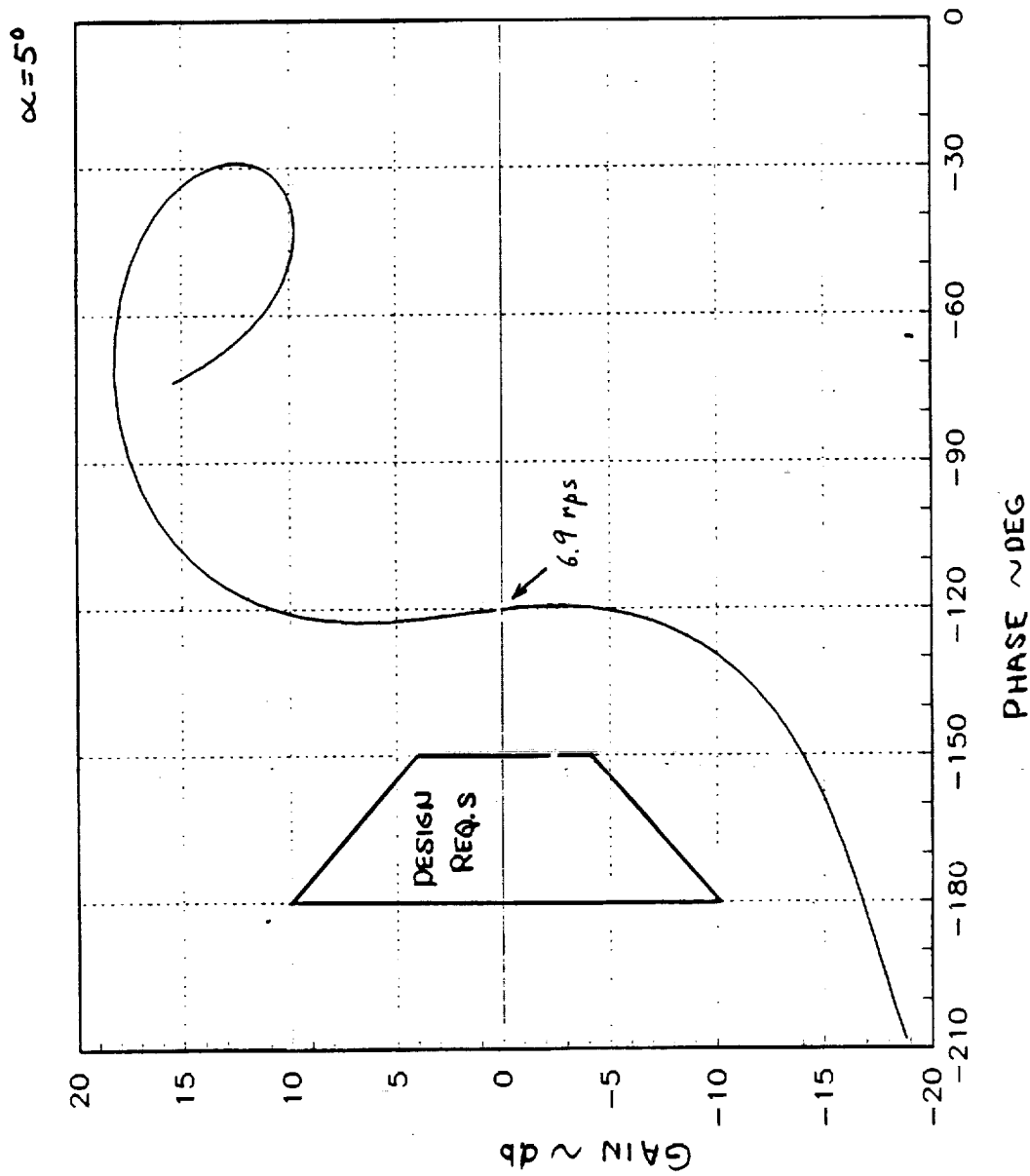
Figure 5-4 Nichols Plot (Pitch, α=5°, Qpres=206psf)

43

$\alpha = 11°$
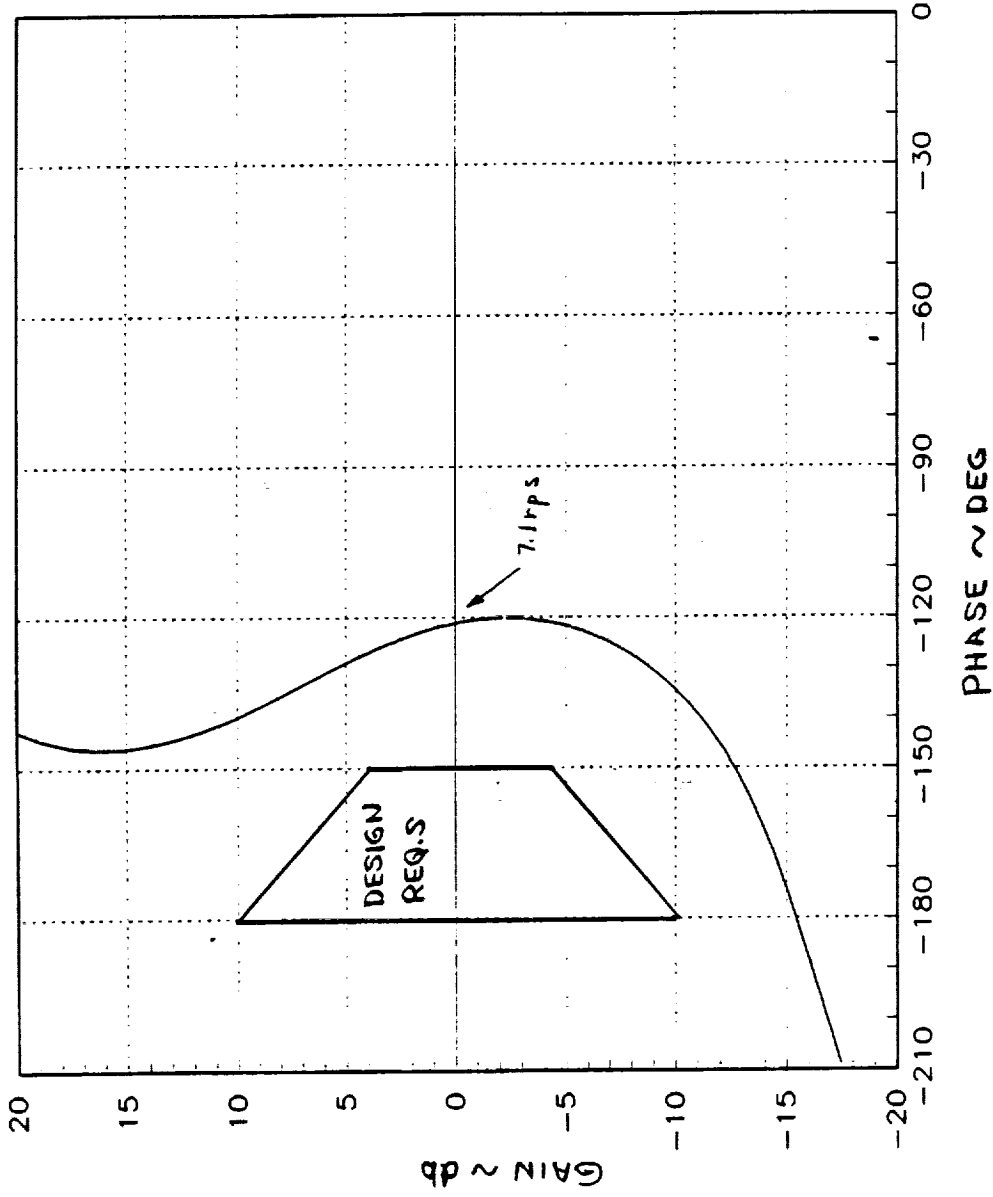
Figure 5-5 Nichols Plot (Pitch, α=11°, Qpres=100psf)
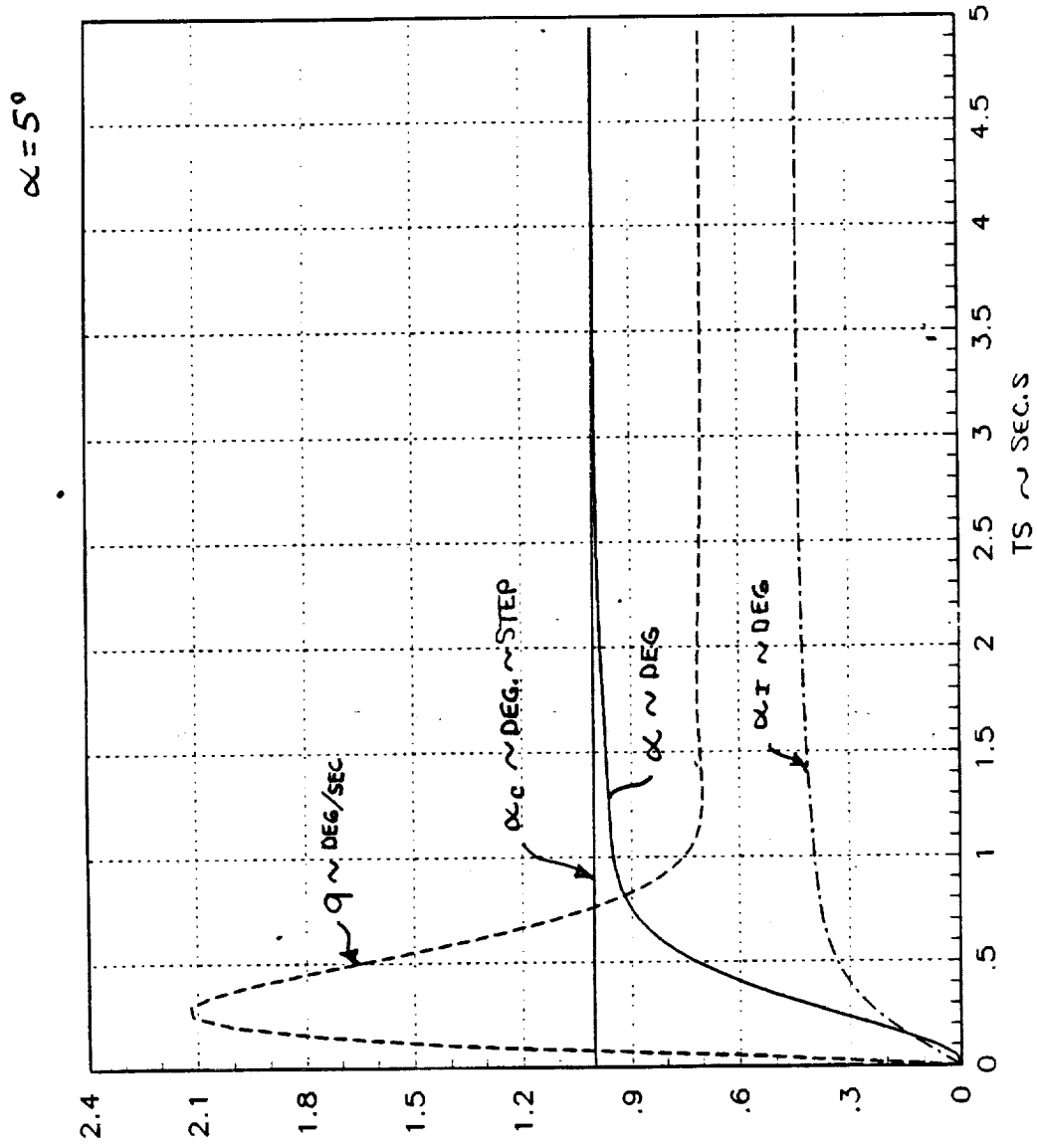
44

$\alpha = 5°$

Figure 5-6 Angle-of-Attack Step Response (α=5°, Qpres=300psf)

45

$\alpha = 5^o$

$\dot{\delta}e \sim DEG/SEC$

$\delta e \sim DEG$

TS $\sim$ SEC.

Figure 5-6 Angle-of-Attack Step Response ($\alpha=5^o$, Qpres=300psf)

(Continued)

46

$\alpha = 5°$
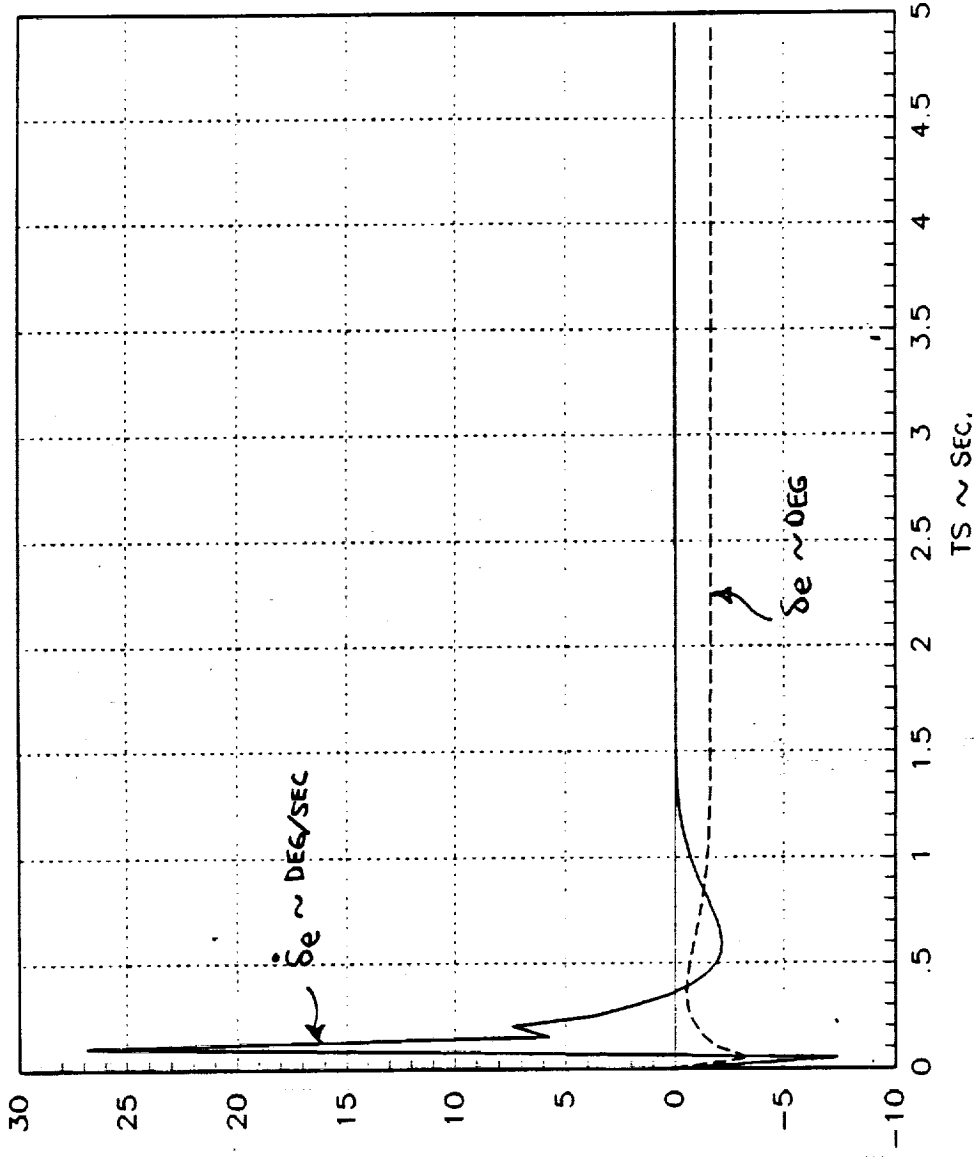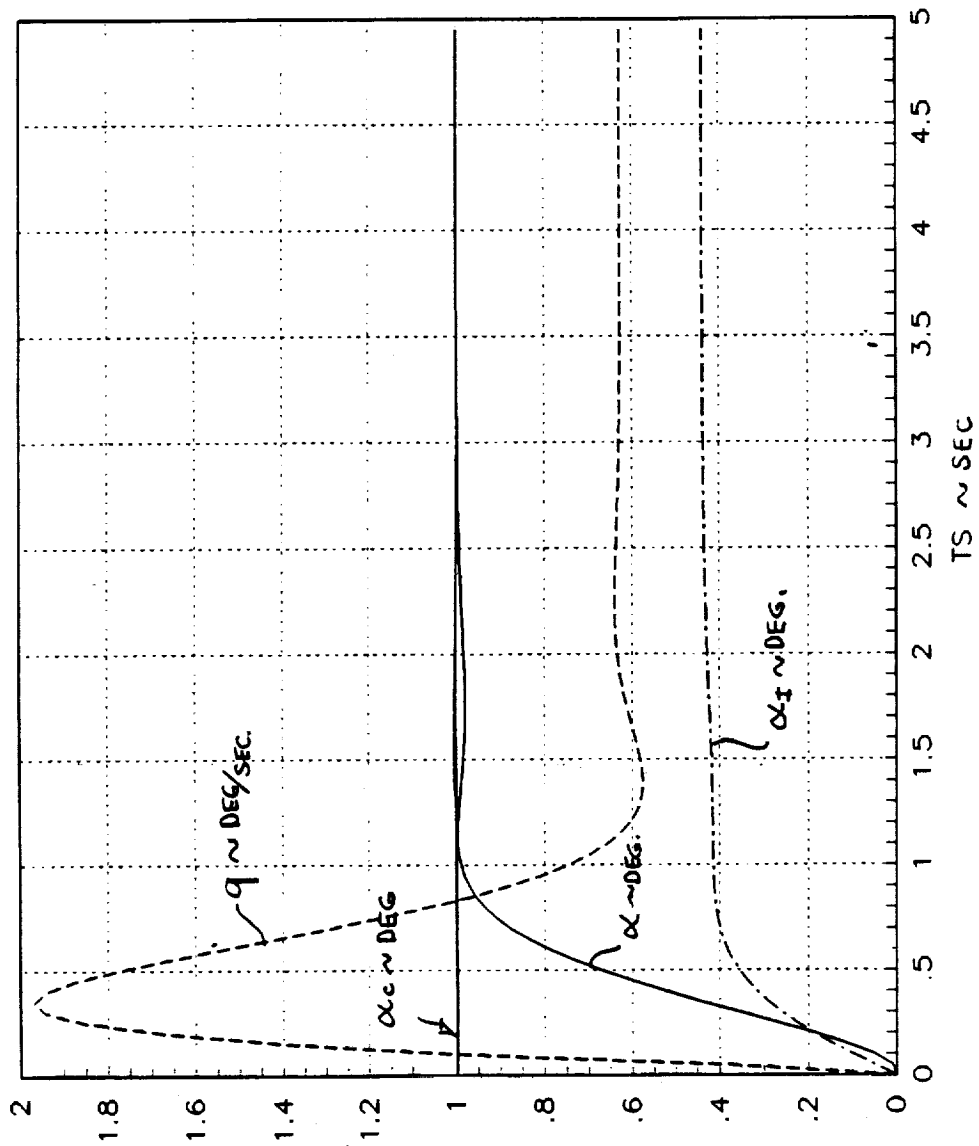
Figure 5-7 Angle-of-Attack Step Response ($\alpha=5°$, Qpres=206psf)

47
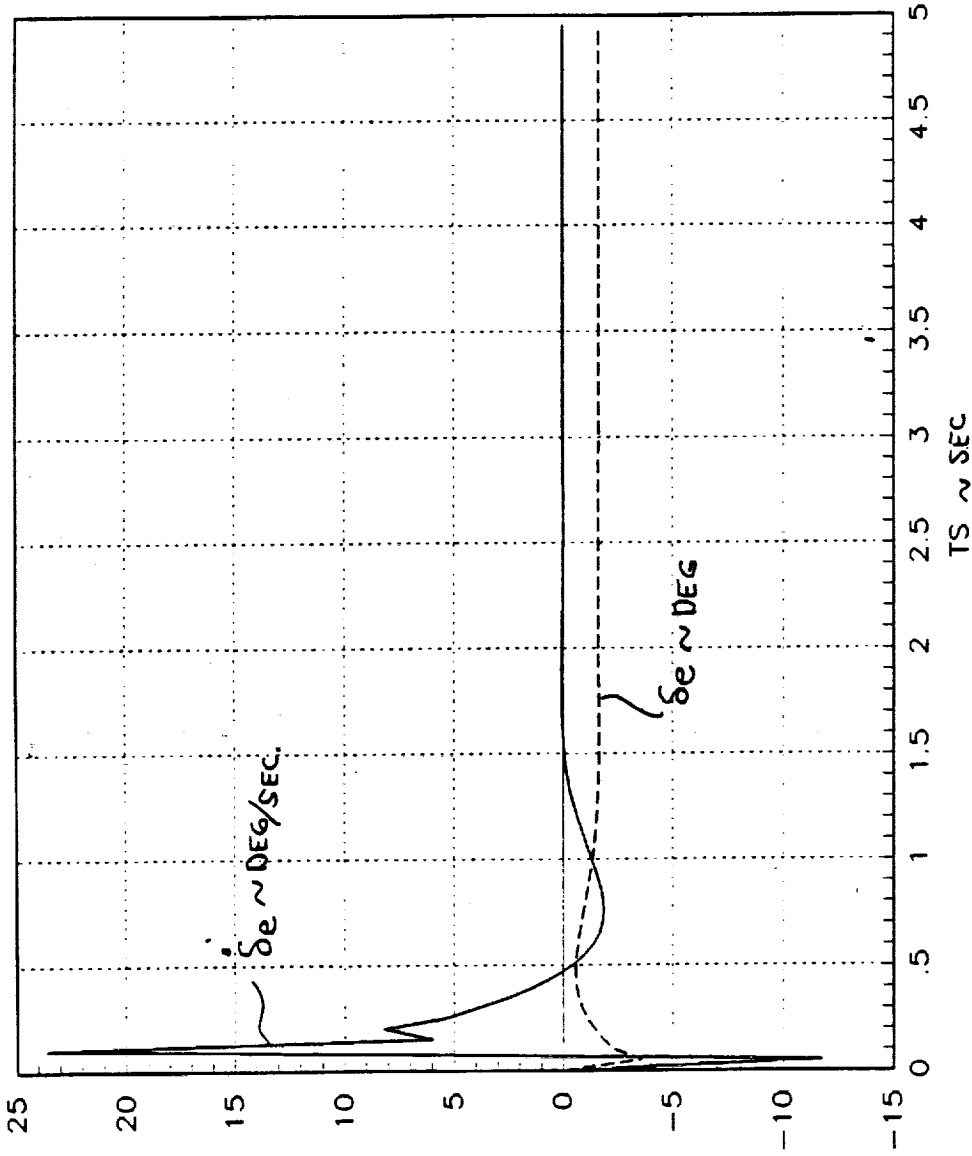
Figure 5-7 Angle-of-Attack Step Response (α=5°, Qpres=206psf)

(Continued)
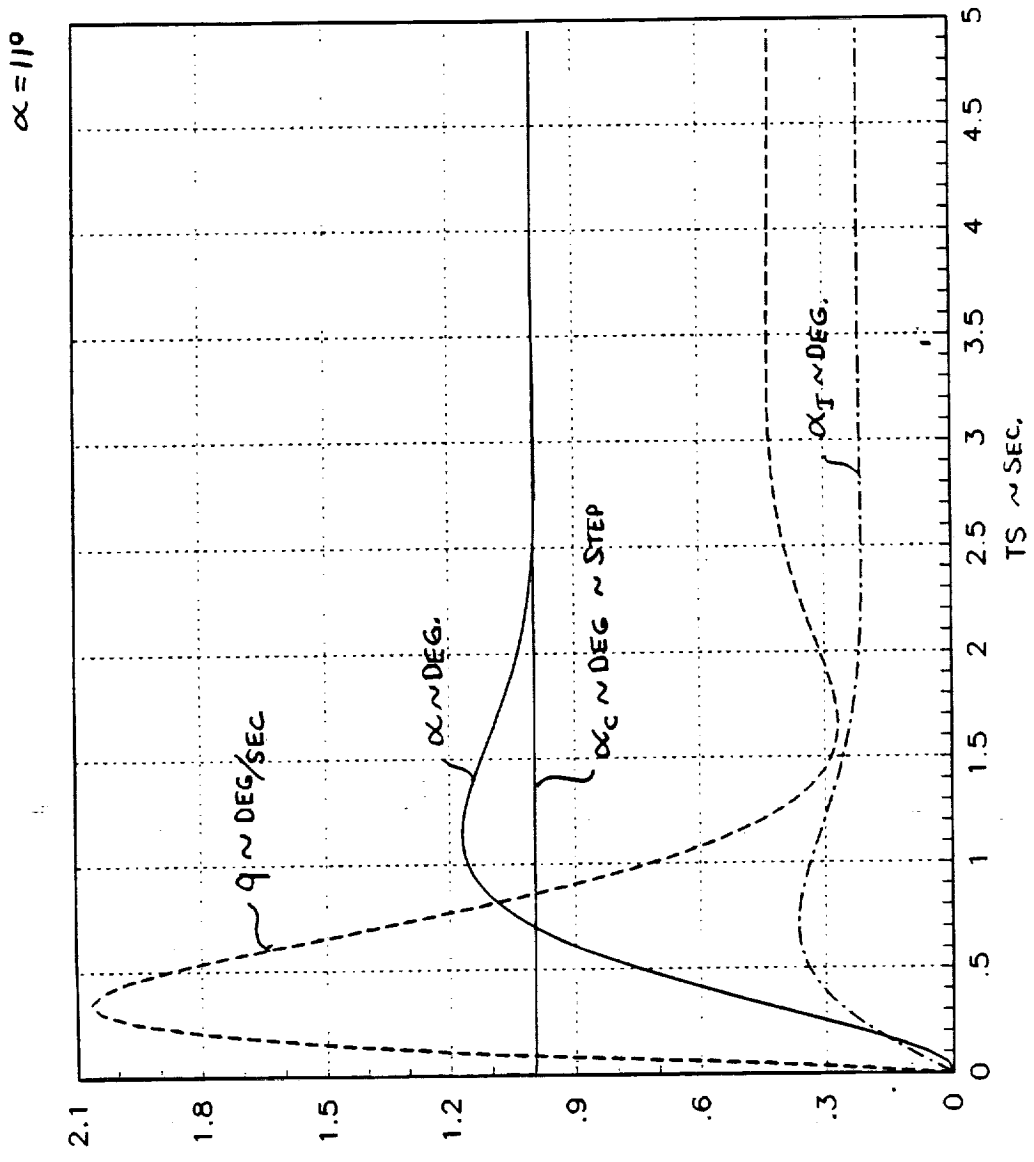
Figure 5-8 Angle-of-Attack Step Response (α=11°, Qpres=100psf)

49

$\alpha = 11°$

$\dot{\delta}e \sim DEG/SEC.$

$\delta e \sim DEG.$

$TS \sim SEC.$

Figure 5-8 Angle-of-Attack Step Response ($\alpha=11°$, Qpres=100psf)

(Continued)

50

5.1.2 Yaw-Roll Autopilot

The yaw-roll linear model data are shown in figure 5-9. The control surfaces used are the all-movable vertical tail as rudder, and both the body flaps and wing flap as ailerons. It was found in the trade study discussed in section 4 that the body flaps alone lack the roll control authority to decrab the vehicle for a side wind more than 15 knots. From the static equilibrium calculations, it was also noted that by using both the wing and body flaps in a 1:1 ratio, and a larger rudder for yaw roll control, it is possible to decrab the vehicle in a 22 knots side wind. A yaw-roll autopilot is designed for the descent and parabolic flare phase. At about 30 ft altitude, a decrab autopilot is engaged. The following paragraphs describe the two autopilots in detail.

The yaw-roll LQ regulator design was done for a state vector that included sideslip angle, yaw rate, roll rate and roll angle. As in the pitch autopilot, an analog autopilot is first designed. Then the same LQ weighting is used to obtain a corresponding discrete design with computational delay compensation included. Figure 5-10 shows the structure of the digital yaw-roll autopilot. The associated gains are tabulated in table 5-2. Nichols plots for the yaw and roll loop (with one of the loops closed) at Qpres=200 and 100 lb/ft^2 are shown in figures 5-11 to 5-14. Roll angle step responses at those conditions are shown in figures 5-15 to 5-18.

Initially, the decrab maneuver was attempted with the yaw-roll autopilot of figure 5-10 by commanding an offset in sideslip. However, the resulting transients and drifts in heading angle and lateral position made this approach unacceptable. Thus, the autopilot had to be re-designed with an expanded state vector to regulate all the necessary variables.

A block diagram of the decrab autopilot is shown in figure 5-19. The autopilot is designed with the lateral guidance integrated. The linear model used in shown figure 5-20. The state vector selected included lateral displacement from the runway centerline, inertial sideslip angle, yaw rate, roll rate, roll angle, and heading angle. The LQ weights on these states for design of the state feedback gains were determined by the integral-LQ method, augmented with small weights (0.01) on two integral states (lateral displacement and heading angle). Since there are two controls (rudder and aileron), two outputs were chosen for weighting,

$$Y1 = \beta + 0.51 \dot{\beta} \quad \text{and} \quad Y2 = p + 0.5 \phi$$

which provide transmission zeros at about 0.5 rad/sec. The controls were given unity weighting. The resulting autopilot gains are provided in table 5-3.

51

State Vector: $x^T = [\beta \ r \ p \ \int pdt]$,

Units: Degrees, Degrees/sec

Control Vector: $u^T = [\delta rud \ \delta ail]$,

Units: Degrees

$\alpha = 5$ degree,   Qpres=300 psf, Mach=0.6

$$A = \begin{bmatrix} -0.2625 & -1 & 0.0873 & 0 \\ 12.0 & 0 & 0 & 0 \\ -54.47 & 0 & 0 & 0 \\ 0 & 0 & 1 & 0 \end{bmatrix} \qquad B = \begin{bmatrix} 0.047 & 0.0536 \\ -6.35 & -7.568 \\ -0.221 & 23.10 \\ 0 & 0 \end{bmatrix}$$

Eigenvalues: 0, 0, $-0.1312 \pm 4.09i$

$\alpha = 5$ degree,   Qpres=200 psf, Mach=0.45

$$A = \begin{bmatrix} -0.2354 & -1 & 0.0873 & 0 \\ 8.225 & 0 & 0 & 0 \\ -37.33 & 0 & 0 & 0 \\ 0 & 0 & 1 & 0 \end{bmatrix} \qquad B = \begin{bmatrix} 0.042 & 0.0481 \\ -4.353 & -5.1854 \\ -0.151 & 15.83 \\ 0 & 0 \end{bmatrix}$$

Eigenvalues: 0, 0, $-0.1177 \pm 3.387i$

$\alpha = 11$ degrees,   Qpres=100 psf, Mach=0.3

$$A = \begin{bmatrix} -0.1802 & -1 & 0.192 & 0 \\ 4.3194 & 0 & 0 & 0 \\ -23.9 & 0 & 0 & 0 \\ 0 & 0 & 1 & 0 \end{bmatrix} \qquad B = \begin{bmatrix} 0.046 & 0.0348 \\ -2.577 & -2.569 \\ 0.736 & 8.402 \\ 0 & 0 \end{bmatrix}$$

Eigenvalues: 0, 0, $-0.0901 \pm 2.983i$

Figure 5-9   Yaw/Roll Linear Models
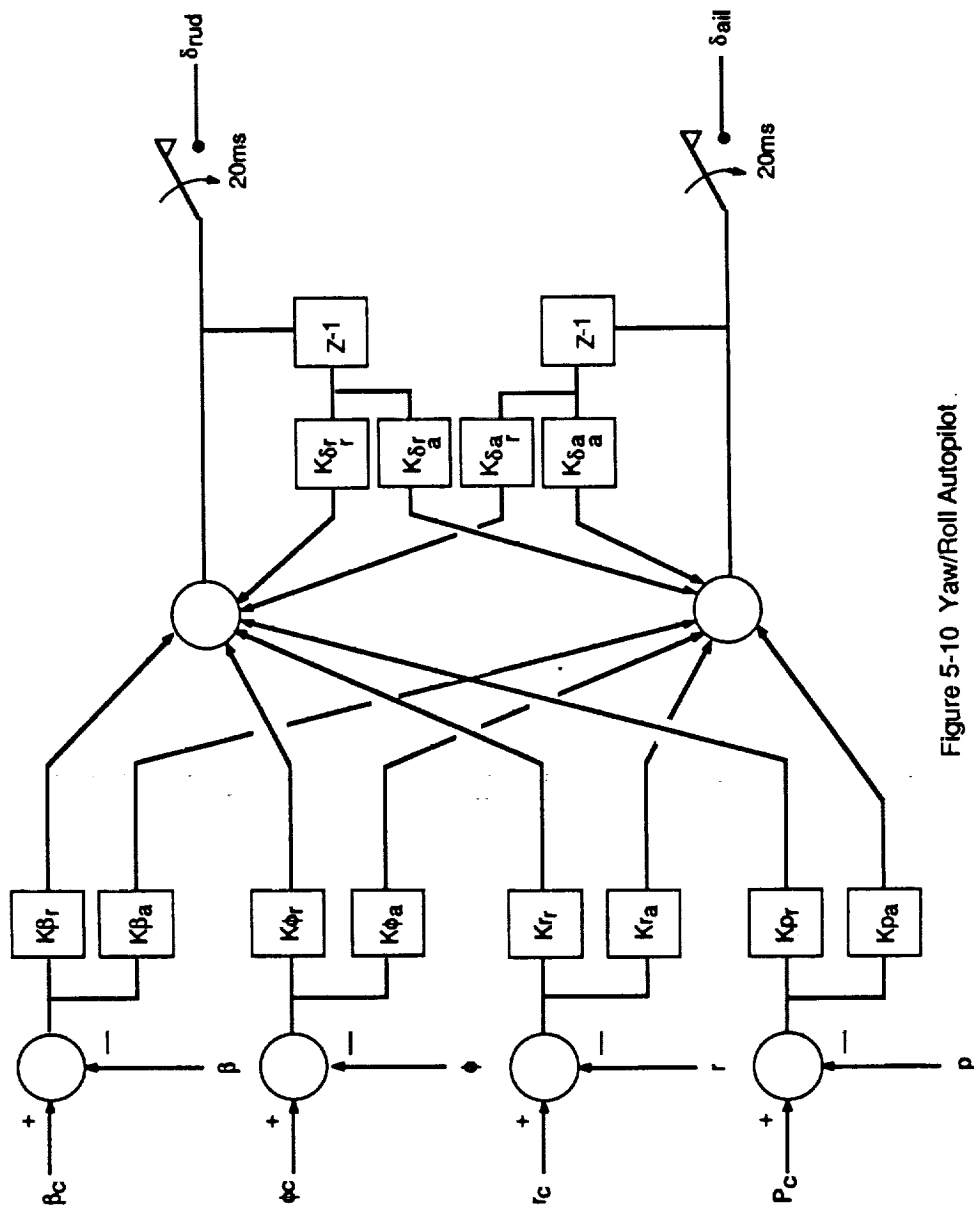
Figure 5-10 Yaw/Roll Autopilot

53

K rudder

Q (lb/ft²)	$K_{\beta r}$	K_{rr}	K_{pr}	$K_{\phi r}$	$K_{\delta RCr}$	$K_{\delta acr}$
301	2.484	-0.960	-0.253	-0.383	0.041	0.010
206	2.484	-0.960	-0.253	-0.383	0.041	0.010
110	1.972	-1.310	-0.231	-0.378	0.026	0.016

K aileron

Q (lb/ft²)	$K_{\beta a}$	K_{ra}	K_{pa}	$K_{\phi a}$	$K_{\delta rca}$	$K_{\delta aca}$
301	-1.507	0.042	0.427	0.838	0.002	0.065
206	-1.507	0.042	0.427	0.838	0.002	0.065
110	0.414	-0.646	0.315	0.416	0.018	0.044

Table 5-2 Yaw/Roll Digital Autopilot Gains
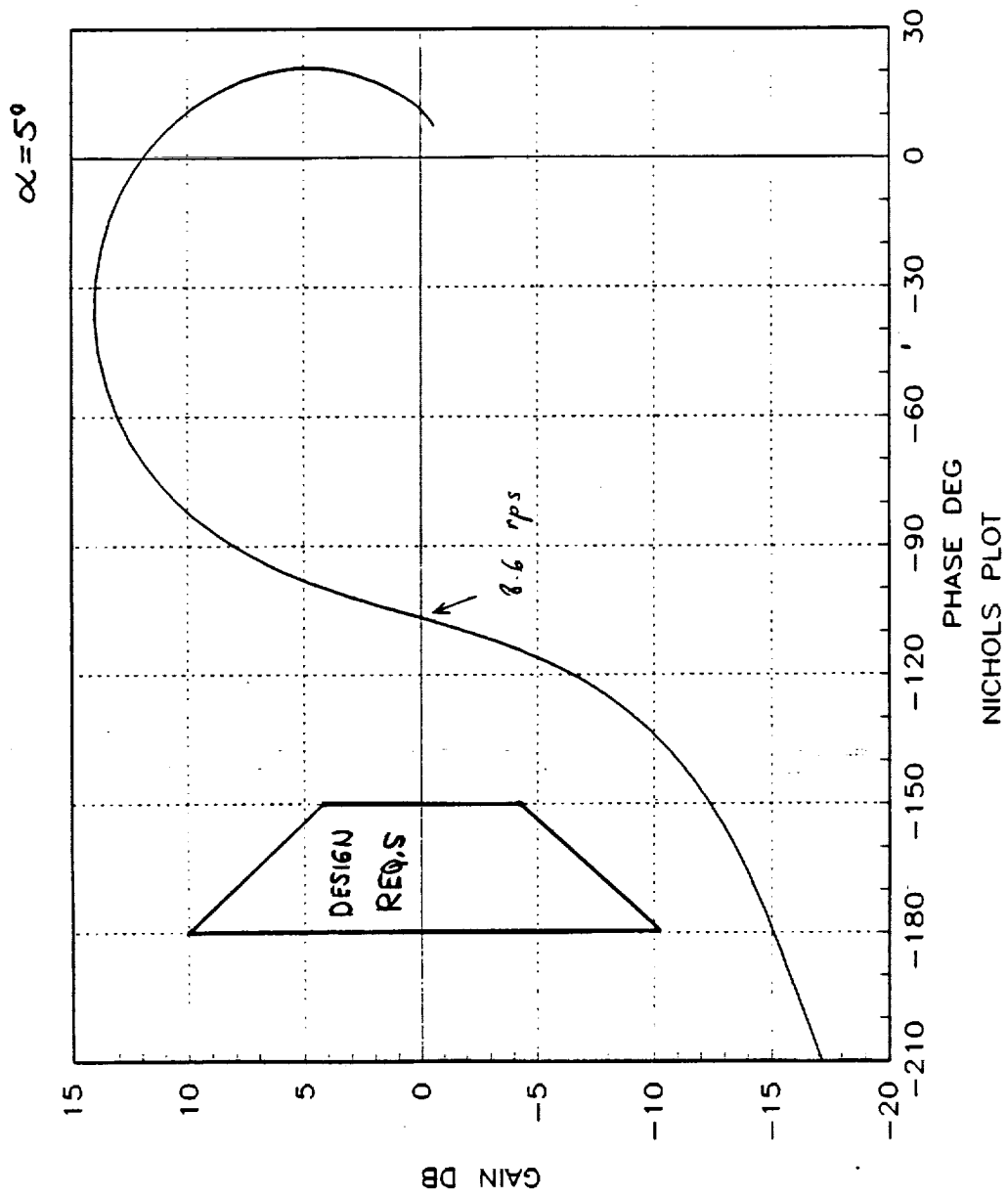
Figure 5-11 Nichols Plot (Roll Loop, $\alpha=5^0$, Qpres=206psf)
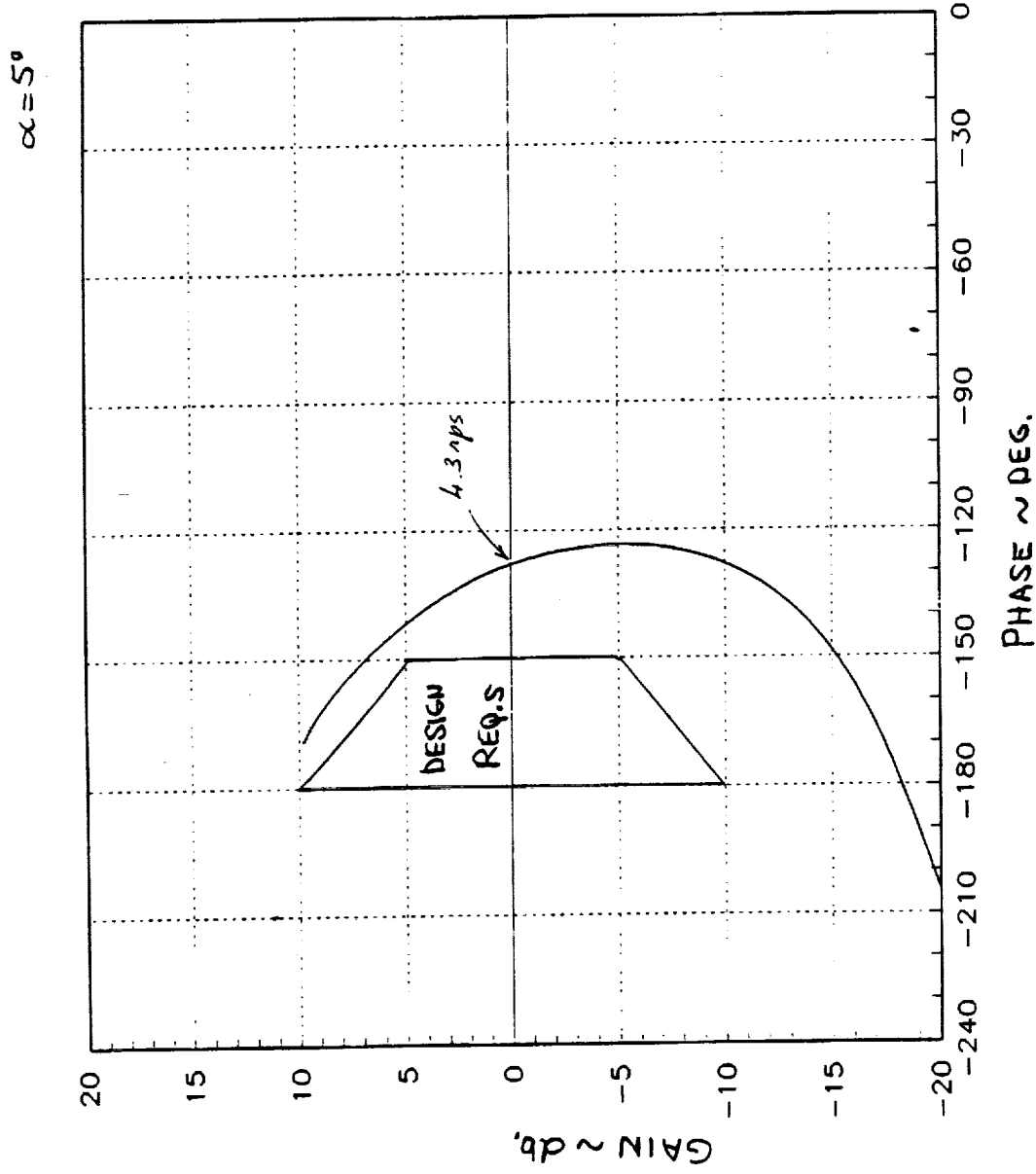
Figure 5-12 Nichols Plot (Yaw Loop, α=5°, Qpres=206psf)
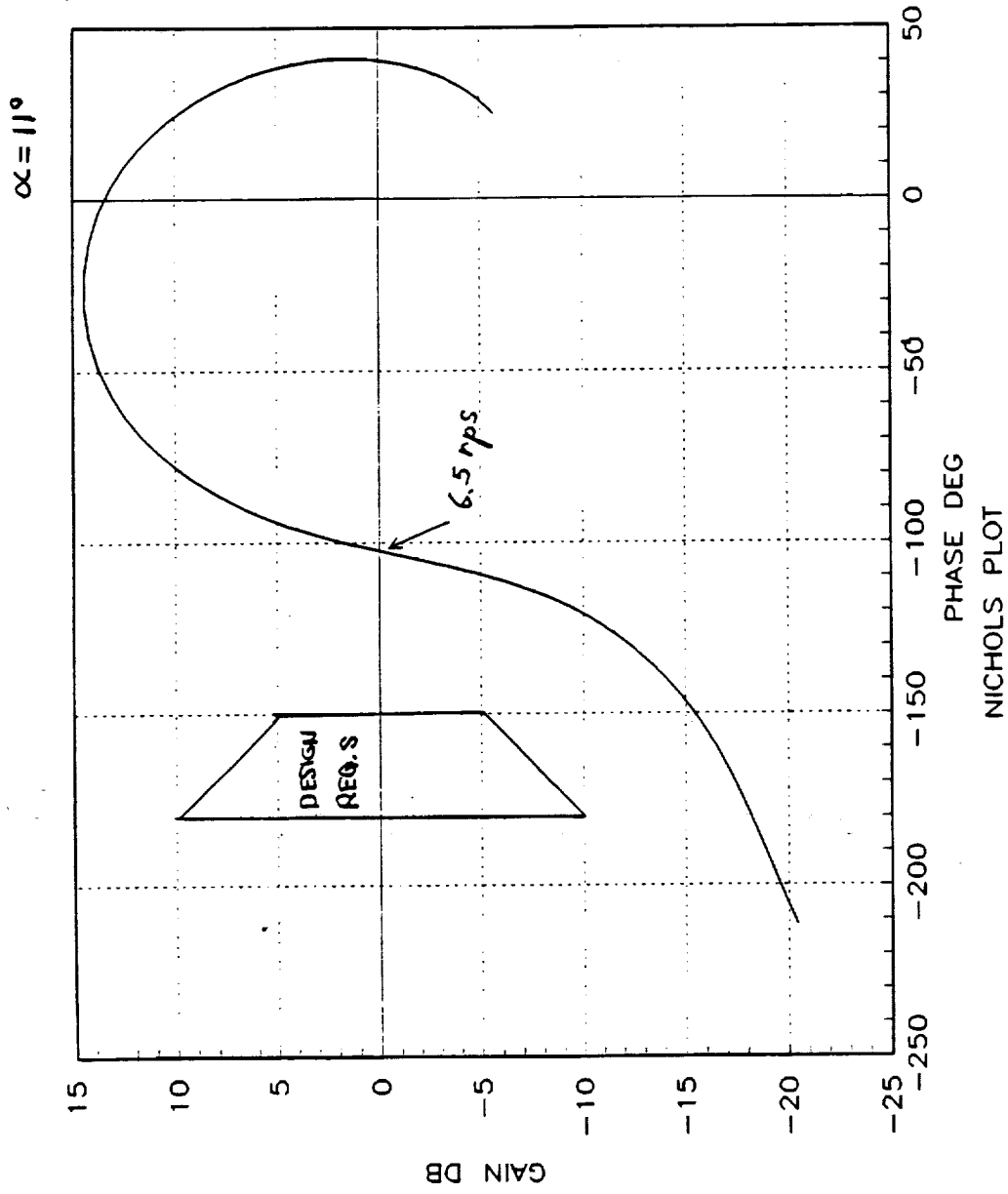
Figure 5-13 Nichols Plot (Roll Loop, α=11°, Qpres=100psf)
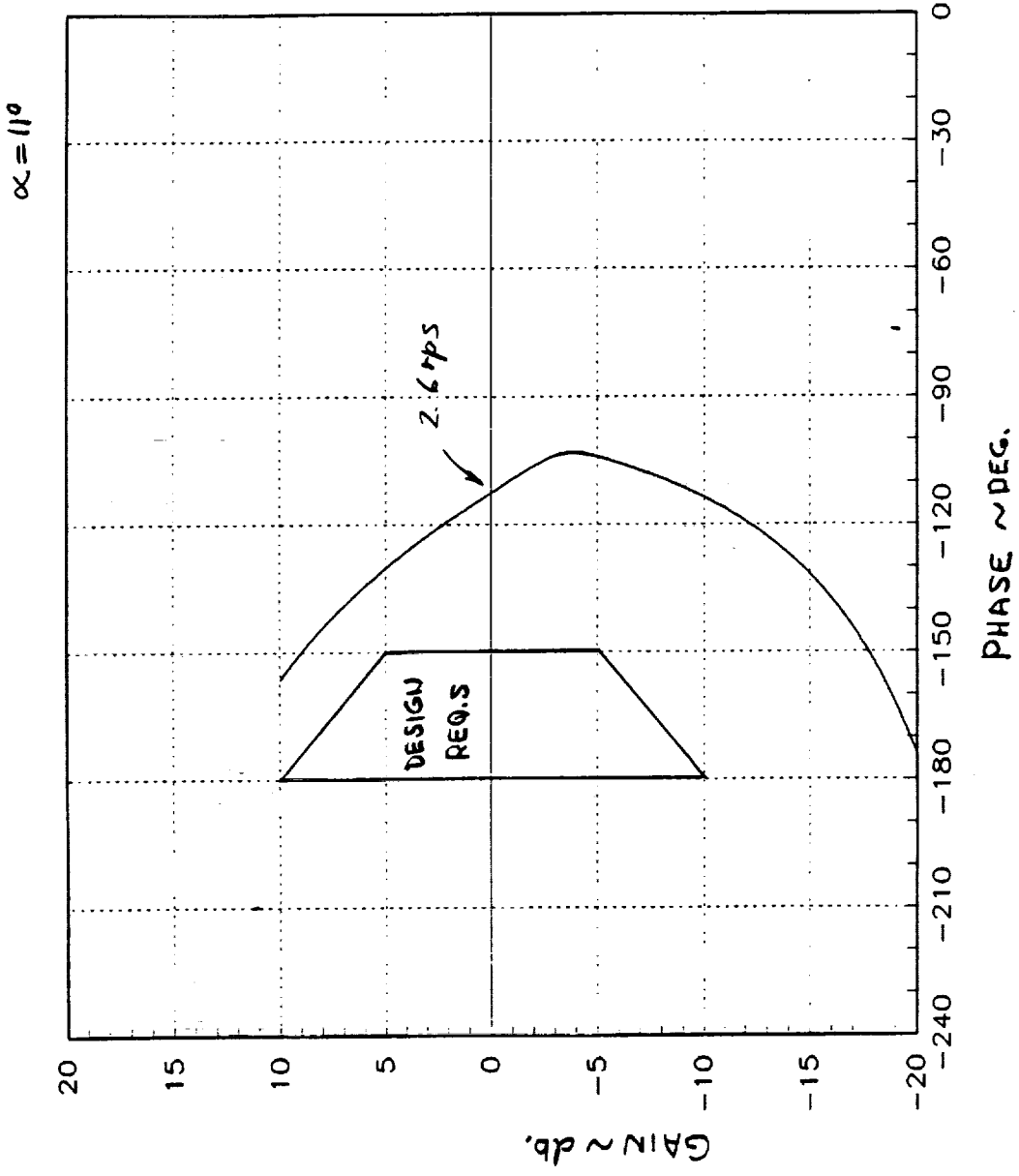
Figure 5-14 Nichols Plot (Yaw Loop, α=11°, Qpres=100psf)
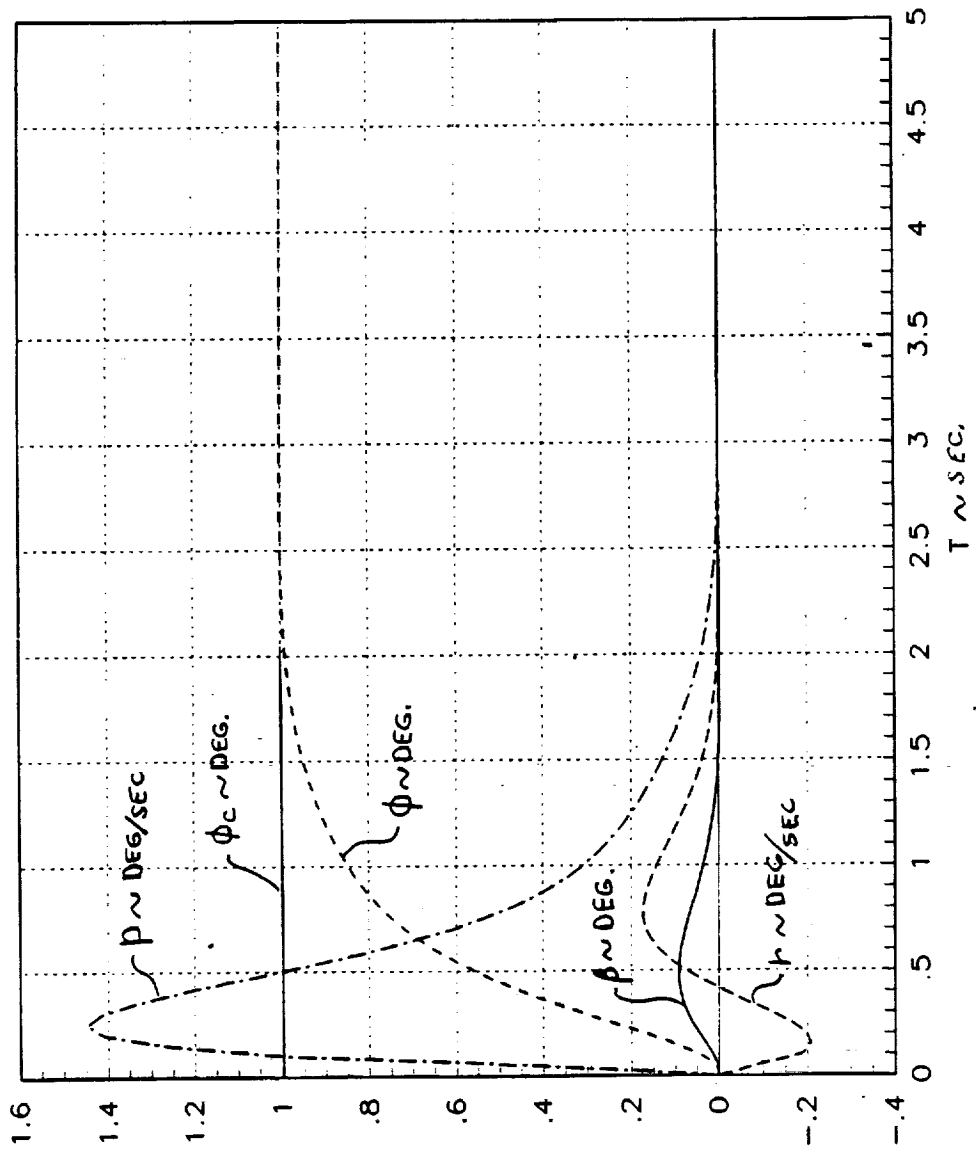
Figure 5-15 Roll Angle Step Response ($\alpha=5^0$, Qpres=206psf)
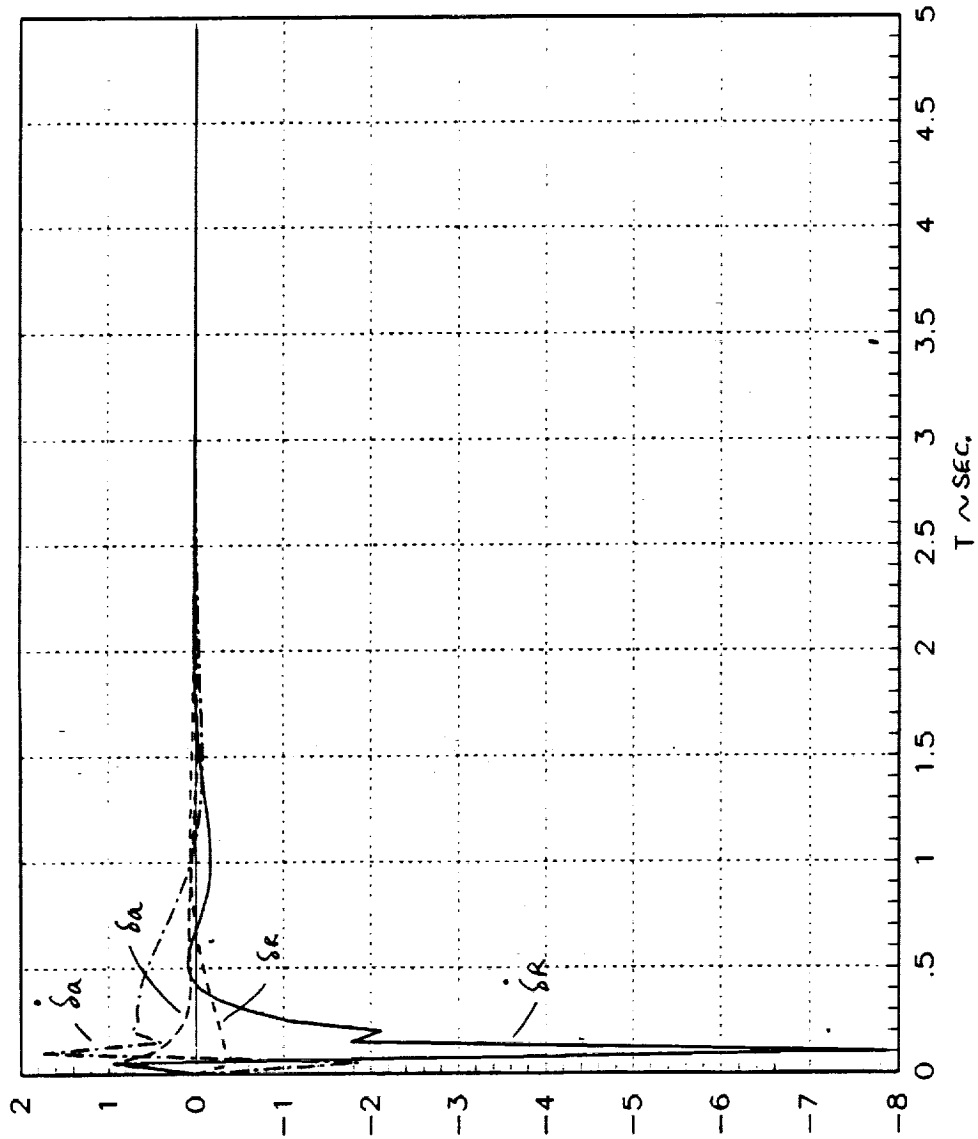
Figure 5-16 Roll Angle Step Actuator Response (α=5°, Qpres=206psf)
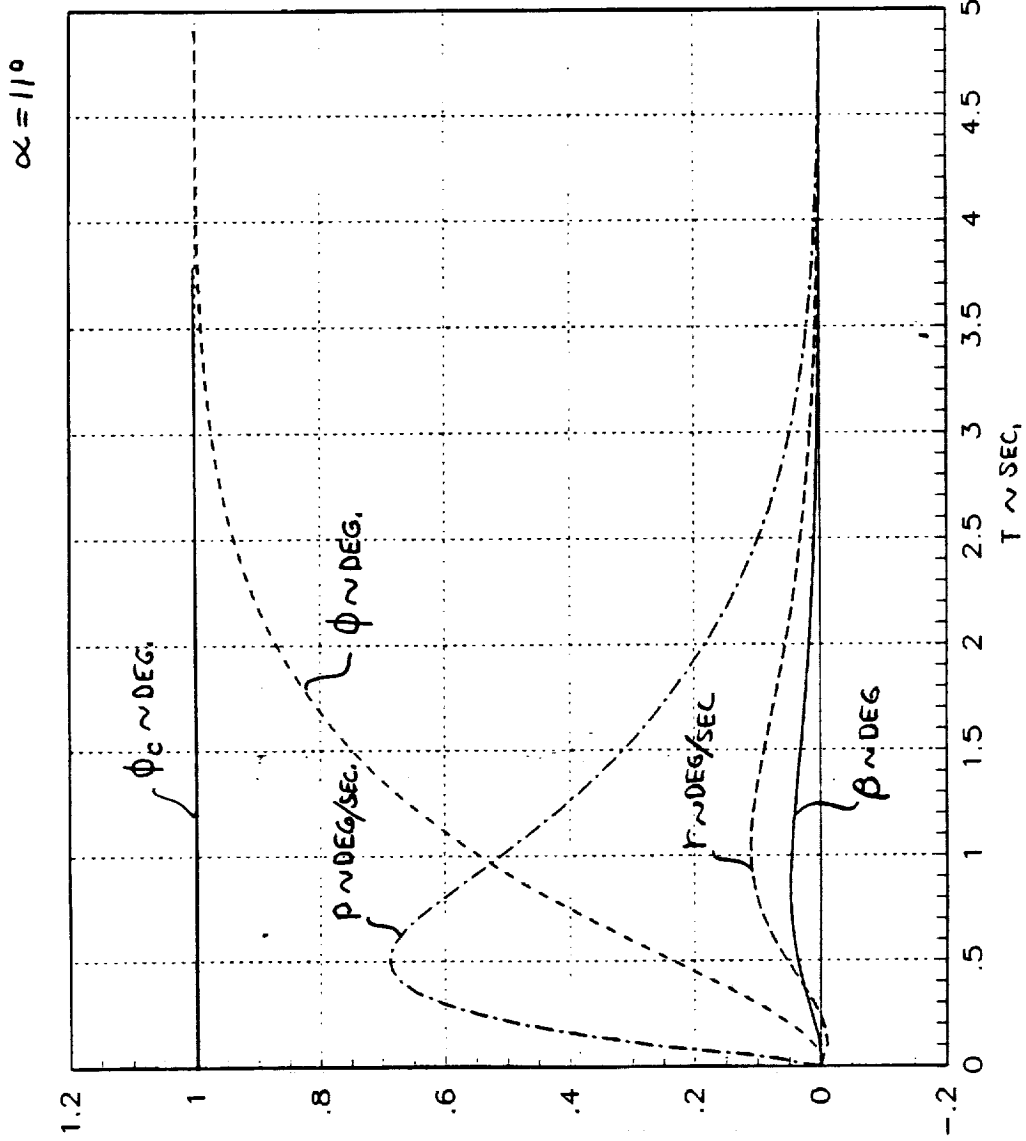
Figure 5-17 Roll Angle Step Response (α=11°, Qpres=100psf)
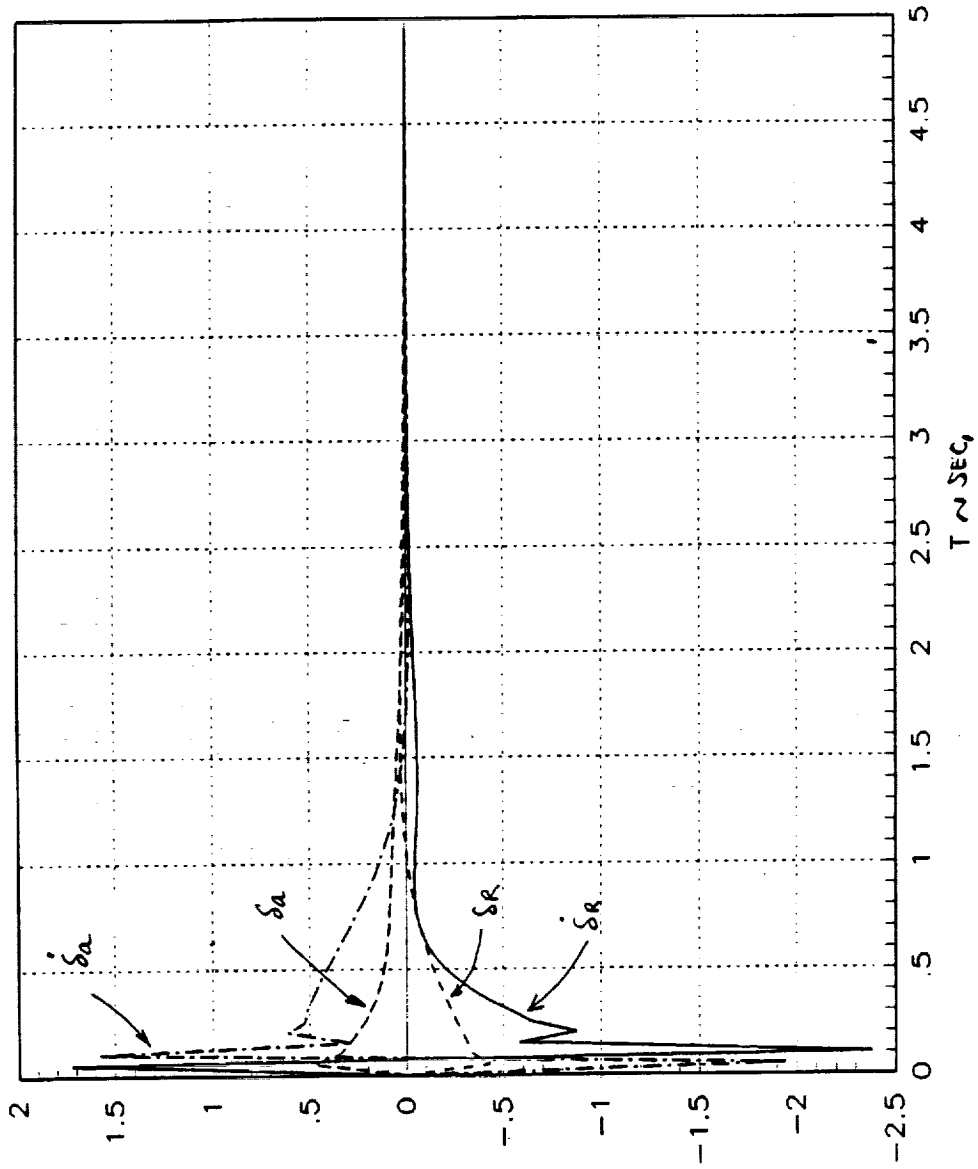
Figure 5-18 Roll Angle Step Actuator Response (α=11°, Qpres=100psf)

62
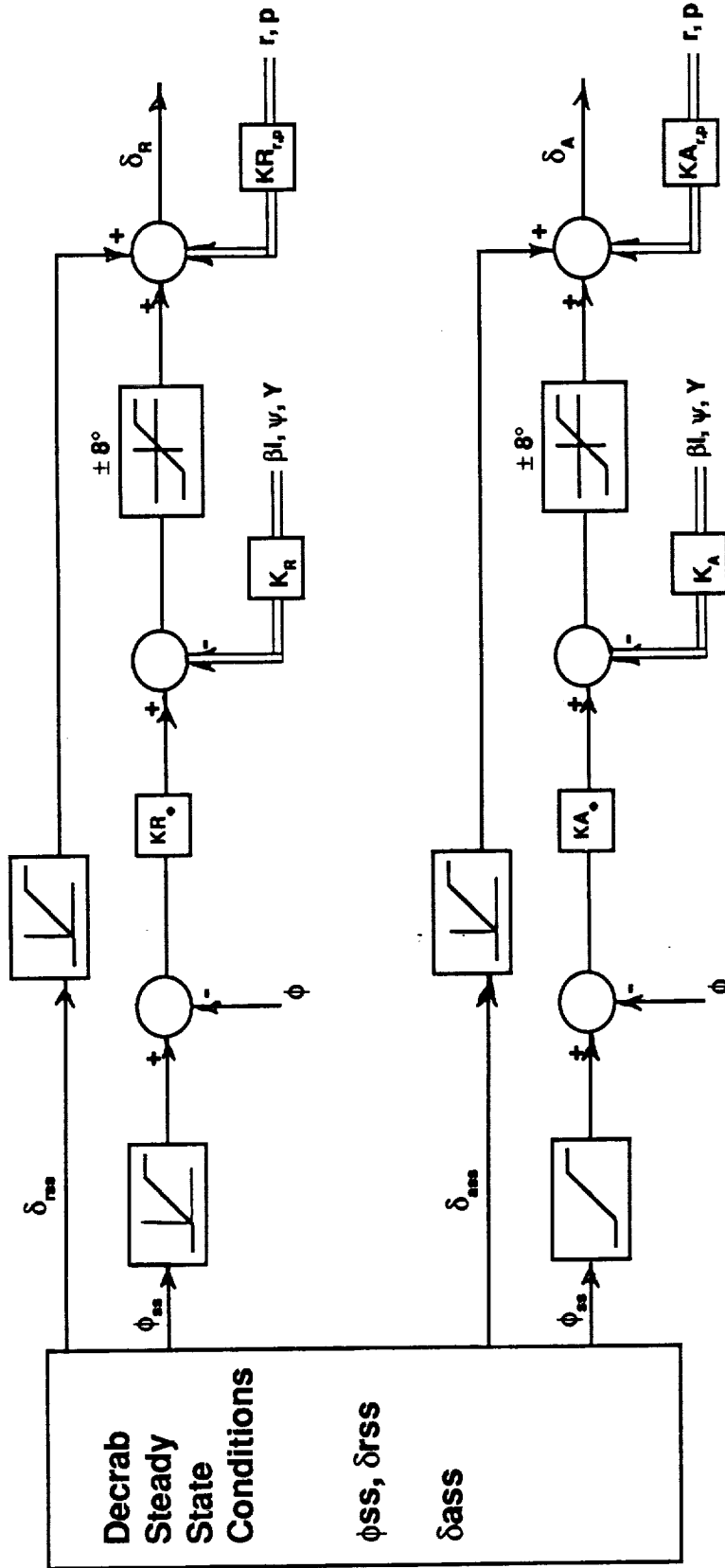
Figure 5-19 Decrab Autopilot Block Diagram

63

State Vector: $x^T = [Y \quad \beta_t \ r \quad p \quad \phi \ \psi]$,

Units: Foot, Degrees, Degrees/sec

Control Vector: $u^T = [\delta rud \quad \delta ail]$,

Units: Degrees

$\alpha = 11$ degree, Qpres=100 psf

$$A = \begin{bmatrix} 0 & 5.66 & 0 & 0 & -1.08 & 5.66 \\ 0 & -0.18 & -1 & 0.192 & 0.099 & 0 \\ 0 & 4.32 & 0 & 0 & 0 & 0 \\ 0 & -23.9 & 0 & 0 & 0 & 0 \\ 0 & 0 & 0 & 1 & 0 & 0 \\ 0 & 0 & 1 & 0 & 0 & 0 \end{bmatrix}$$

$$B = \begin{bmatrix} 0 & 0 \\ 0.046 & 0.035 \\ -2.577 & -2.659 \\ 0.736 & 8.402 \\ 0 & 0 \\ 0 & 0 \end{bmatrix}$$

Eigenvalues: 0, 0, 0, -0.266, 0.0429 ±2.988

Figure 5-20 Linear Model Used in Decrab Autopilot Design

64

Krudder

Q (lb/ft²)	K_{YR}	$K_{\beta IR}$	K_{rR}	K_{PR}	$K_{\phi R}$	$K_{\psi R}$
100	-0.081	1.420	-2.091	-0.444	-0.014	-2.722

Kaileron

Q (lb/ft²)	K_{YA}	$K_{\beta IA}$	K_{rA}	K_{PA}	$K_{\phi A}$	$K_{\psi A}$
100	0.059	0.740	-0.442	0.955	0.364	2.048

Table 5-3 Decrab Autopilot Gains

65

The added state vector elements of the decrab autopilot allow regulation of the lateral flight path, including heading and displacement from the centerline. However, to decrab the vehicle in a steady cross wind (i.e. to hold the inertial sideslip angle at zero), the roll angle must be held at an offset value and this requires steady, non-zero values for the controls. These steady state values can be calculated from the static equilibrium equations discussed in section 4, by introducing a constant cross wind value and setting the derivatives of sideslip, yaw rate, and roll rate to zero.

5.2 Longitudinal Guidance System

The longitudinal guidance system consists of two major modules: the flight profile generator and the altitude steering module. The profile generator determines the desired altitude and descent rate from the vehicle current position relative to the runway. The altitude steering loop translates these signals into appropriate angle-of-attack command to the flight control laws. A block diagram of the signal flow is shown in figure 2-4. The guidance system operates in a 60 ms time frame. The following paragraphs discuss in detail the formulation of these modules.

5.2.1 Flight Profile Generator

The CERV nominal trajectory consists of three phases: a steep constant angle glide path, a parabolic flare profile, and a final shallow constant angle glide path to touchdown.

(1) The steep glide path angle is strongly dependent of the L/D characteristics of the vehicle. Simulation shows a glide path angle of 21° or higher can maintain enough speed to carry the CERV through the flare and touchdown maneuvers. A 22° glide path angle is selected for this study. This value is comparable to the space shuttle glide path angle which varies between 19 and 22 degrees depending on the energy level conditions (Reference 2).

(2) The parabolic flare maneuver is initiated at an altitude of approximately 1200 ft. This altitude is selected such that the normal acceleration does not exceed 1.6 g's during the flare maneuver. The maneuver extends from the initiation altitude to about 10 ft above the ground when a final flare maneuver is performed. The parabolic flare profile is used because it is easy to formulate. For comparison, the space shuttle uses a circular flare profile followed by an exponential decay to a shallow glide slope of 1.5deg. The shuttle maneuver is initiated at an altitude of 2000 ft (Reference 2).

(3) A final touchdown maneuver is executed at about 10 ft above the ground to stabilize the sink rate as the vehicle approaches to the runway. A fixed glide path of 0.2^o is commanded. The corresponding sink rate of the fixed glide path for a forward speed of 180 knots is 1.0 ft/sec. For comparison, the space shuttle initiates its final flare at an altitude of between 80 to 30 ft depending on the enery level conditions (Reference 2). CERV can be designed to start the final flare at these similar altitudes by allowing higher initial speed.

Figure 5.21 shows the general shape of the flight trajectory along with the equations that describe the profile. The derivatives of these equations with respect to range-to-go (or distance traveled) are the glide path slope desired at that instant. Given the desired flare range (S-S$_2$),

.67
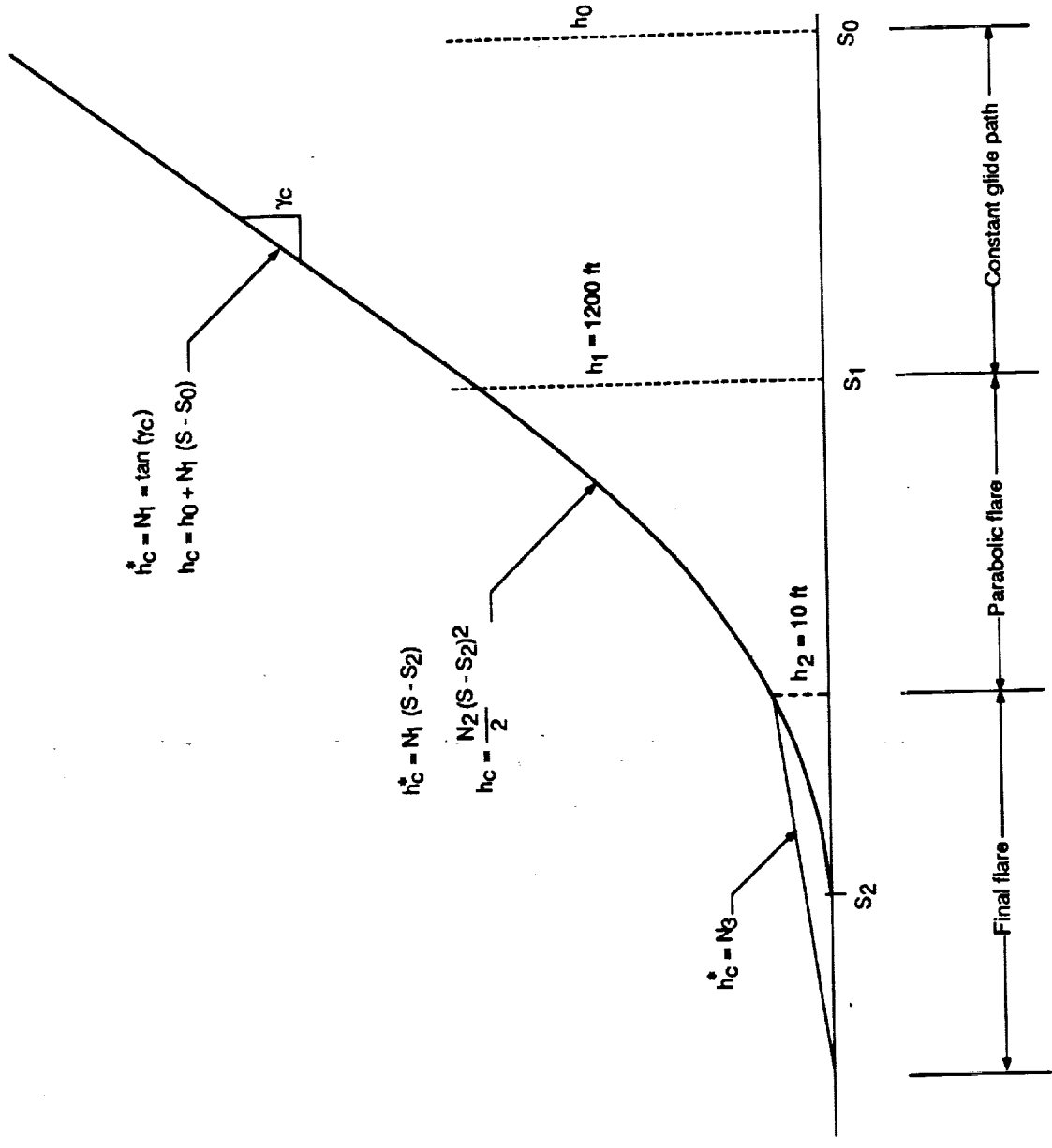
Figure 5-21 Flight Trajectory Profile

$\dot{h}_c^* = M_1 = \tan(\gamma_c)$
$h_c = h_0 + M_1(S - S_0)$

$\dot{h}_c^* = M_1(S - S_2)$
$h_c = \dfrac{N_2(S - S_2)^2}{2}$

$\dot{h}_c^* = N_3$

γ_c

h_0

$h_1 = 1200\ \text{ft}$

$h_2 = 10\ \text{ft}$

S_0

S_1

S_2

Constant glide path

Parabolic flare

Final flare

68

the parabolic constant N2 can be computed by equating the glide path slope at the flare initiation point. Knowing N2, the flare initiation altitude h1 is also computed. Figure 5-22 shows a block diagram of the implementation of the flare maneuver in the simulation. The command sink rate is obtained by multiplying the forward speed to the desired glide slope. The sink rate command is in turn integrated to generate an altitude command. The altitude and sink rate commands are then fed to the longitudinal guidance law described in the previous report.

An exponential flare algorithm was also investigated as an alternative. Figures 5-23 and 5-24 show the flare trajectory and the flight path angle history. The exponential flare has the characteristic of reducing the sink rate early in the flare, and having a shallow glide slope to touchdown. This is demonstrated in the flight path angle profile. The flight path angle decreases linearly in the parabolic flare method while it decreases exponentially in the other. However, this method has the disadvantage of losing speed quickly, because of the longer time spent in the shallow glide slope. Figure 5-24 shows the vehicle did not maintain enough speed to hold the angle-of-attack within limits, and sank to the ground. Unlike the previous method, the exponential flare algorithm is generated using model following linear quadratic optimal design technique. A block diagram of the algorithm is shown in figure 5-25. This method generates an angle-of-attack command that feeds directly to the autopilot, by-passing the longitudinal guidance law described in the previous report. Clearly, more analysis are needed to arrive to a successful design. But the exponential flare posseses unique characteristics that merit additional investigation.

5.2.2 Altitude Steering Module

The function of the altitude steering loop is to translate the altitude and sink rate command from the flight profile generator into appropriate angle-of-attack signals for the flight control. A block diagram of the longitudinal guidance loop is shown in figure 5-26. The guidance loop is designed classically, and consists of an altitude and altitude rate feedbacks. The gain KH associated with the altitude error forms a zero in the root locus plot. Gain KAC is the guidance loop gain. The nominal value for KH and KAC are 0.3 and 0.3 respectively. The steering loop stability is analyzed. A root locus plot of the guidane, autopilot and plant system is shown in figure 5-27. Altitude step response is also performed on the simulator, and is shown in figure 5-28.

Trimmed angle-of-attack generated from the lift curve as function of dynamic pressure is summed with the altitude steering command to form a total angle-of-attack command. Due to the lack of an integrator in the altitude loop, an altitude error bias is observed when the calculated trimmed angle-of-attack is not exactly matched with the real trim angle. However, this error bias

69

is small (less than 10 ft) and does not affect the landing performance. An altitude error integrator will eliminate this bias, but it may pose stability problem in the steering loop due to the presence of an additional pole at the origin.
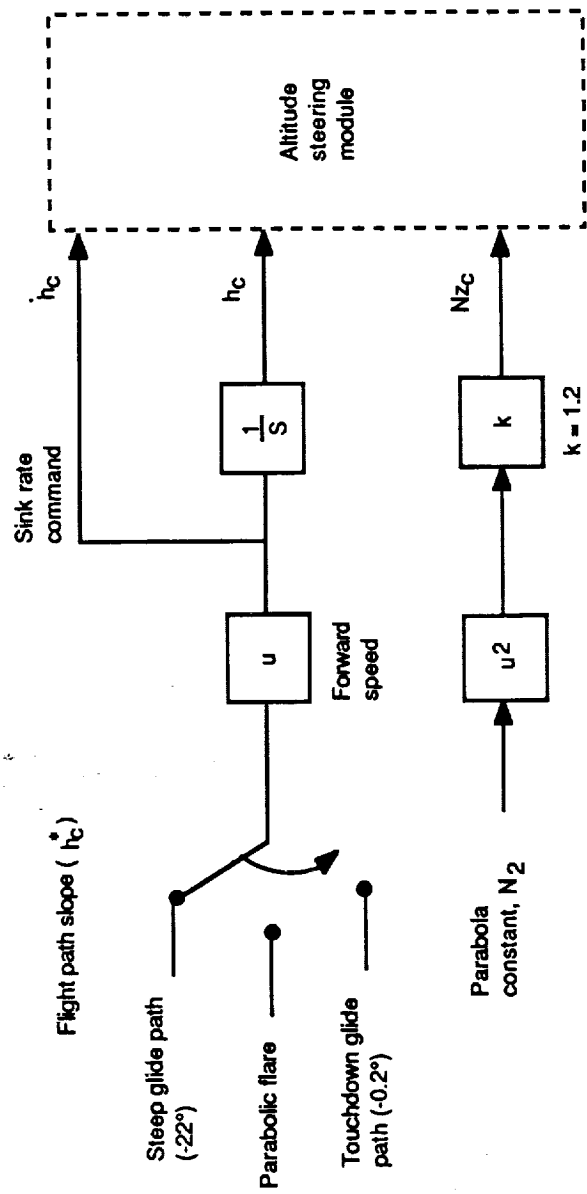
Figure 5-22 Flare Algorithm Implementation
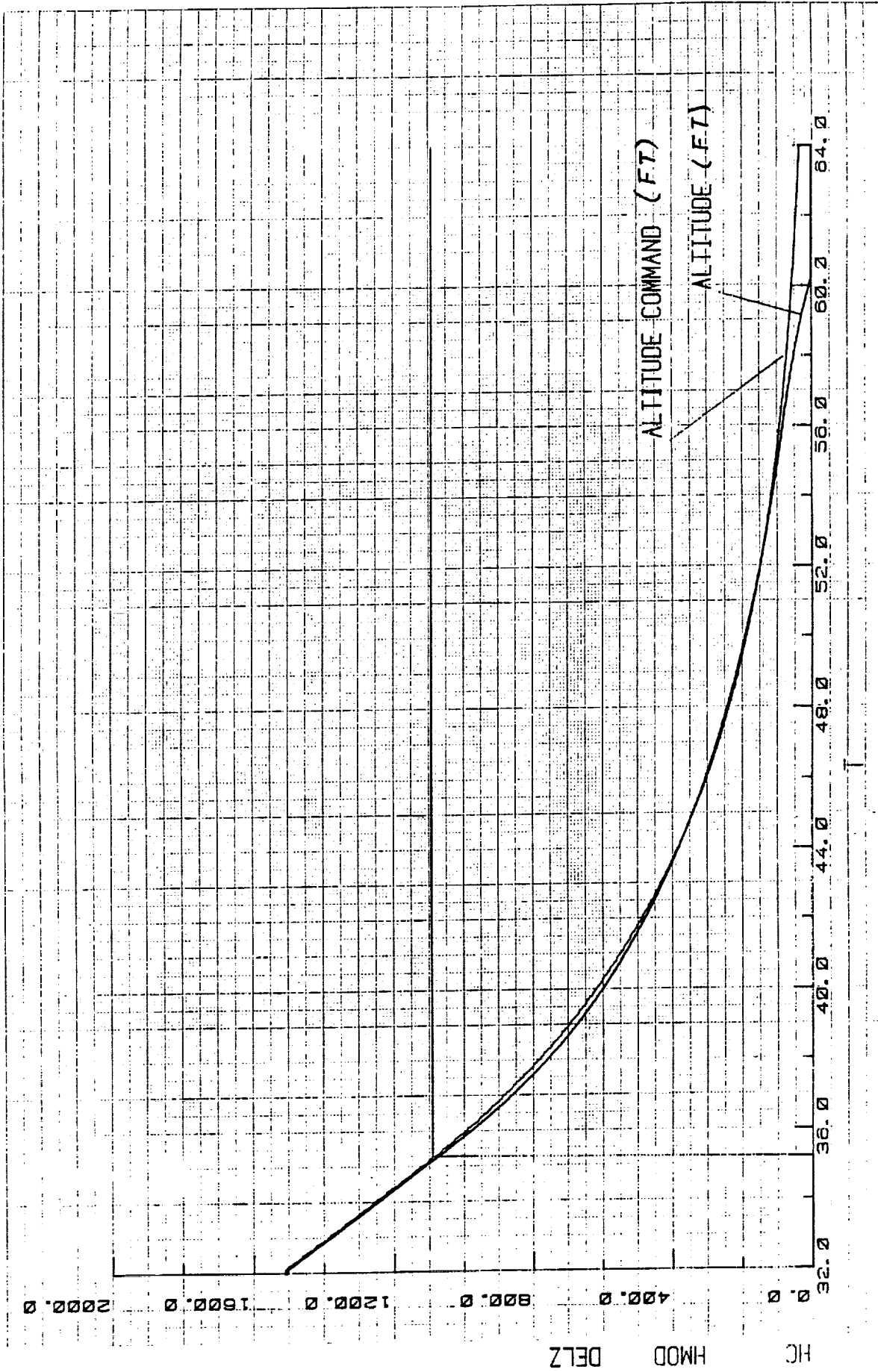
Figure 5-23 Exponential Flare Altitude Profile
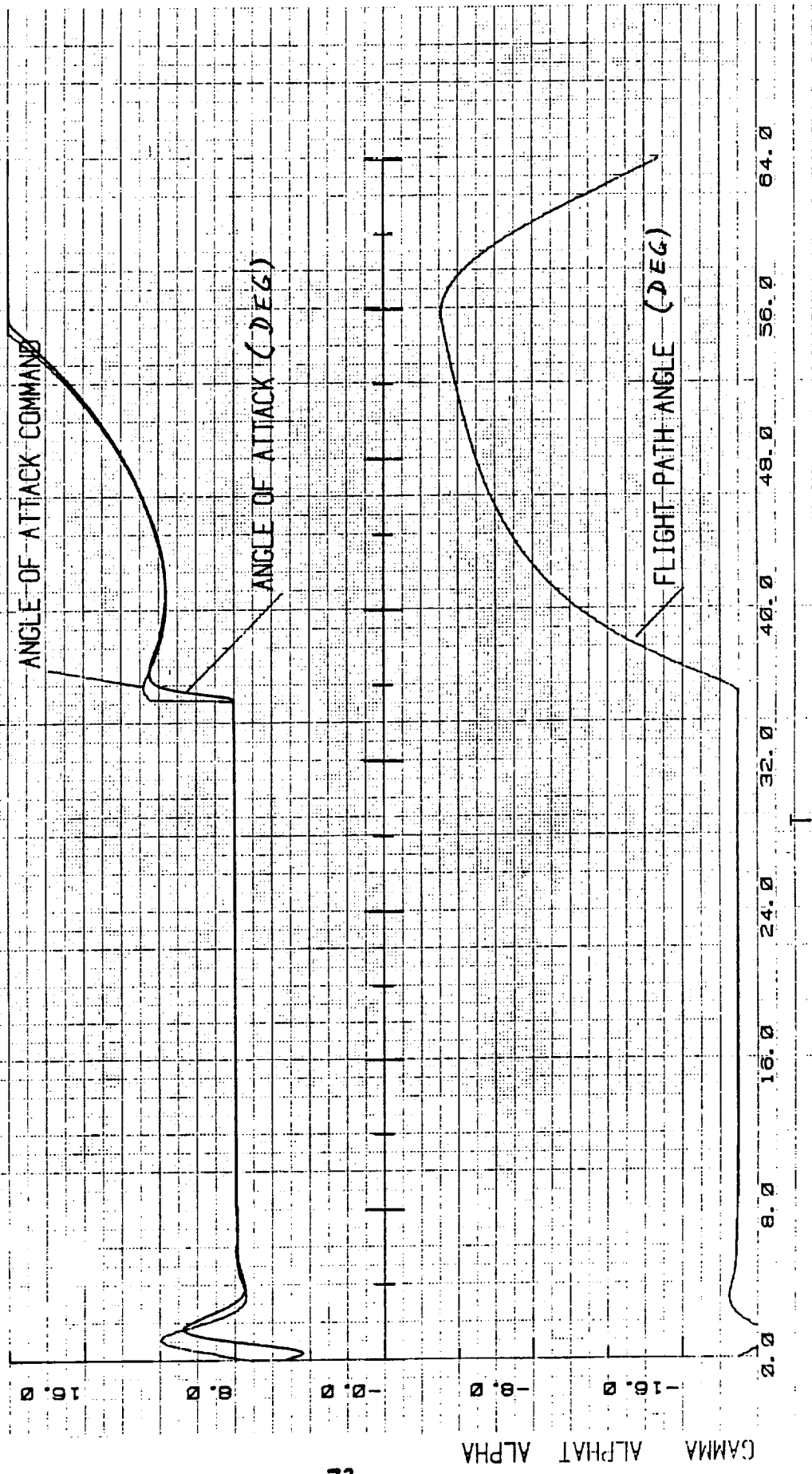
Figure 5-24 Exponential Flare Angle-of-Attack and Flight Path Angle Histories

73
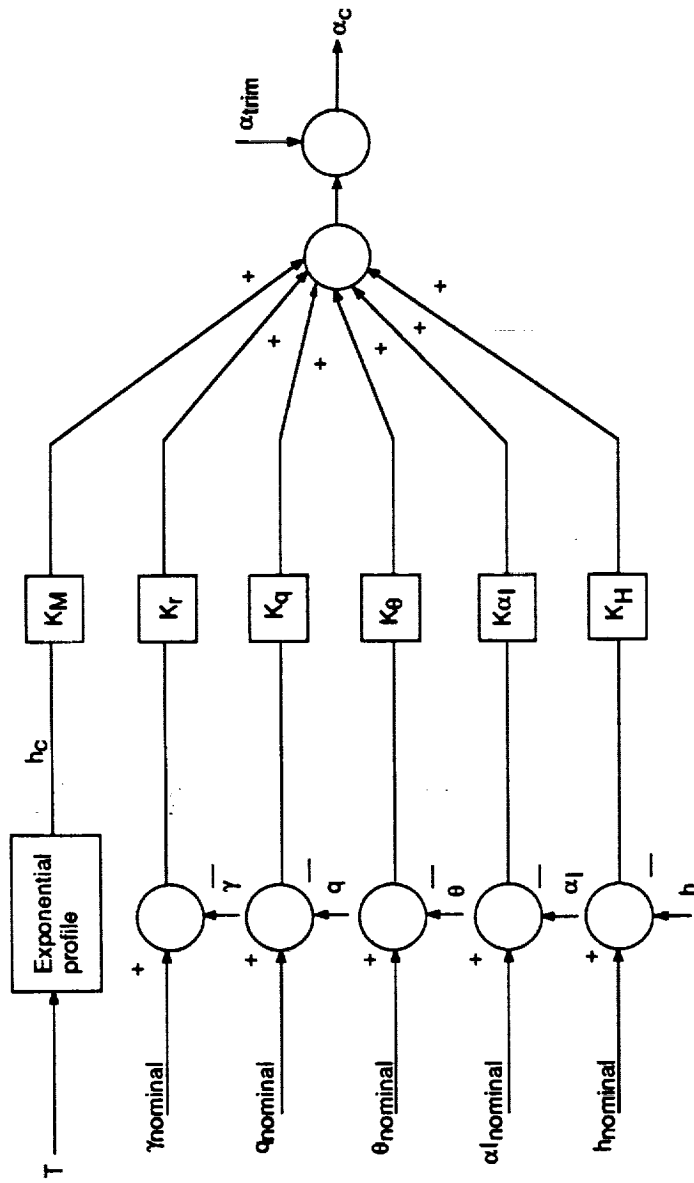
Figure 5-25 Exponential Flare Algorithm

74
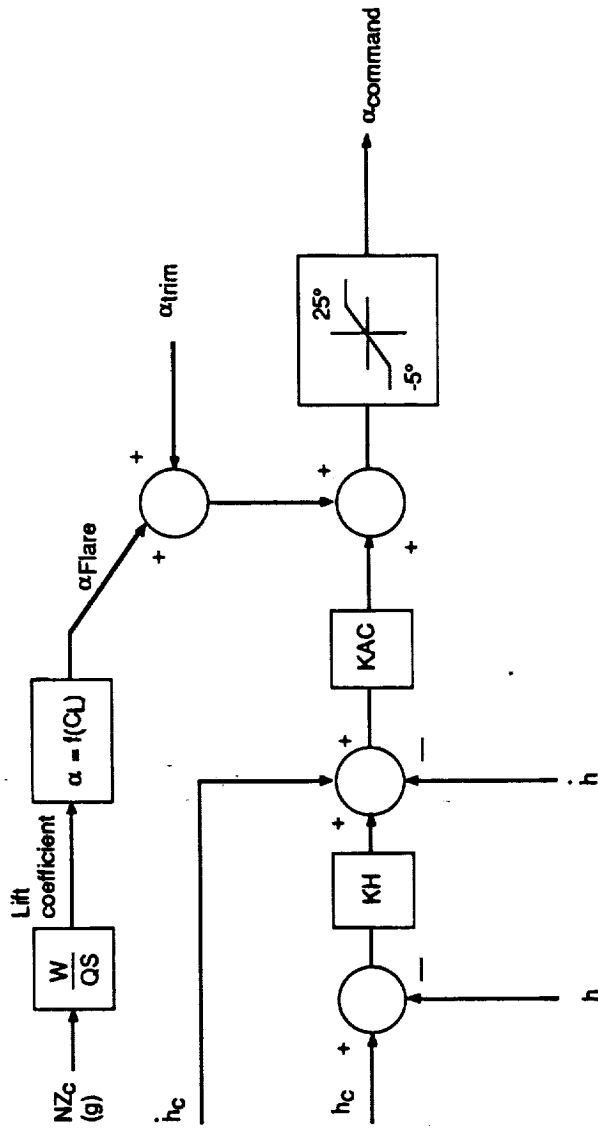
Figure 5-26 Longitudinal Guidance Design

75

Autopilot & Plant Poles

Roots at Nominal Gains:

-0.376

$-0.546 \pm 0.418 j$

$-3.085 \pm 2.36 j$
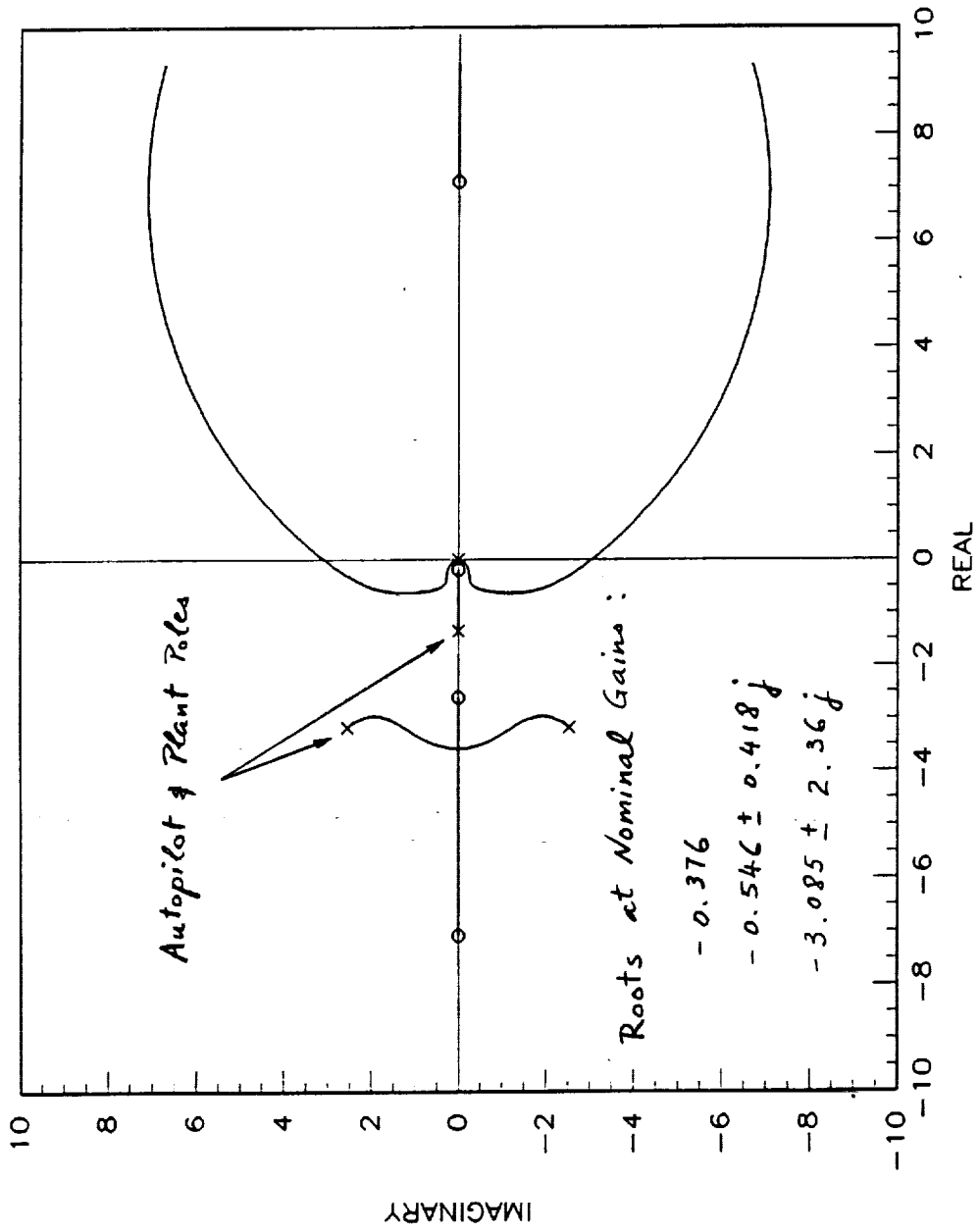
Figure 5-27 Guidance, Autopilot and Plant Root Locus
(Longitudinal, $\alpha=5°$, Qpres=300psf)

76
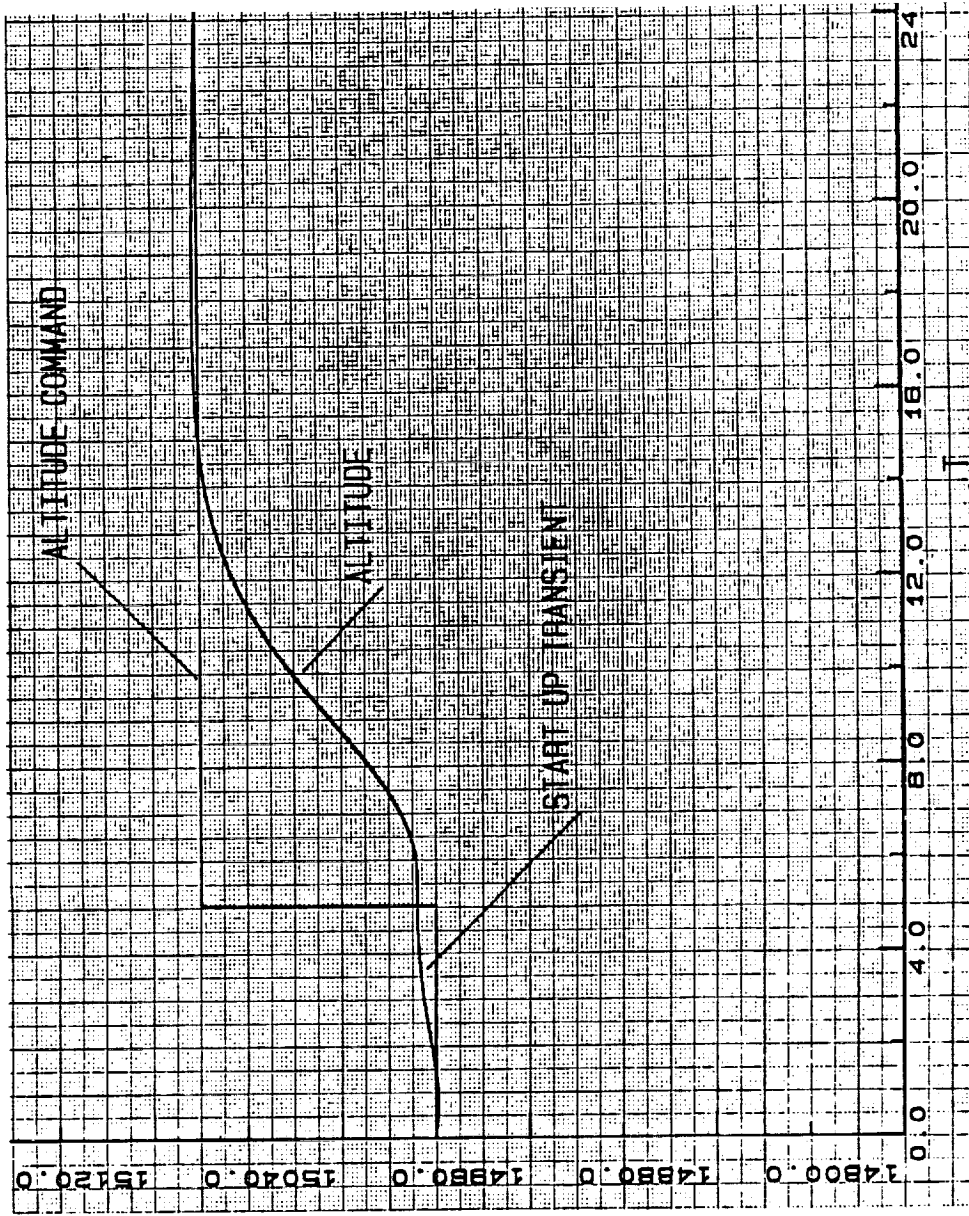
Figure 5-28 Altitude Step Response (Qpres=300psf)

77

5.3 Lateral Guidance

The lateral guidance system tracks the runway centerline during the descent trajectory. It generates the appropriate bank angle command to roll the vehicle toward the centerline. A block diagram of the lateral guidance loop is shown in figure 5-29. The feedback signals are the lateral offset from the fixed runway center line (Y) and the lateral velocity normal to the fixed center line. Similar to the gain KH in the longitudinal guidance law, KY forms a zero in the root locus plot, and KPHI is the lateral loop gain. The nominal values for KY and KPHI are 0.2 and 1.0 respectively. A root locus plot of the guidance, autopilot and plant system is shown in figure 5-30. Lateral step response performed on the simulator is shown in figure 5-31.

The lateral guidance is turned off when the decrab maneuver is engaged.
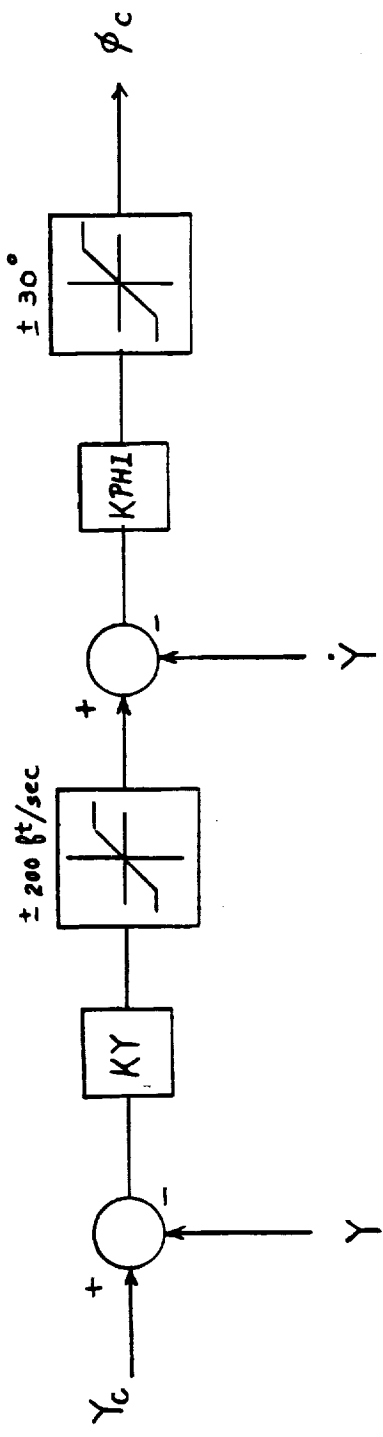
Figure 5-29 Lateral Guidance Design
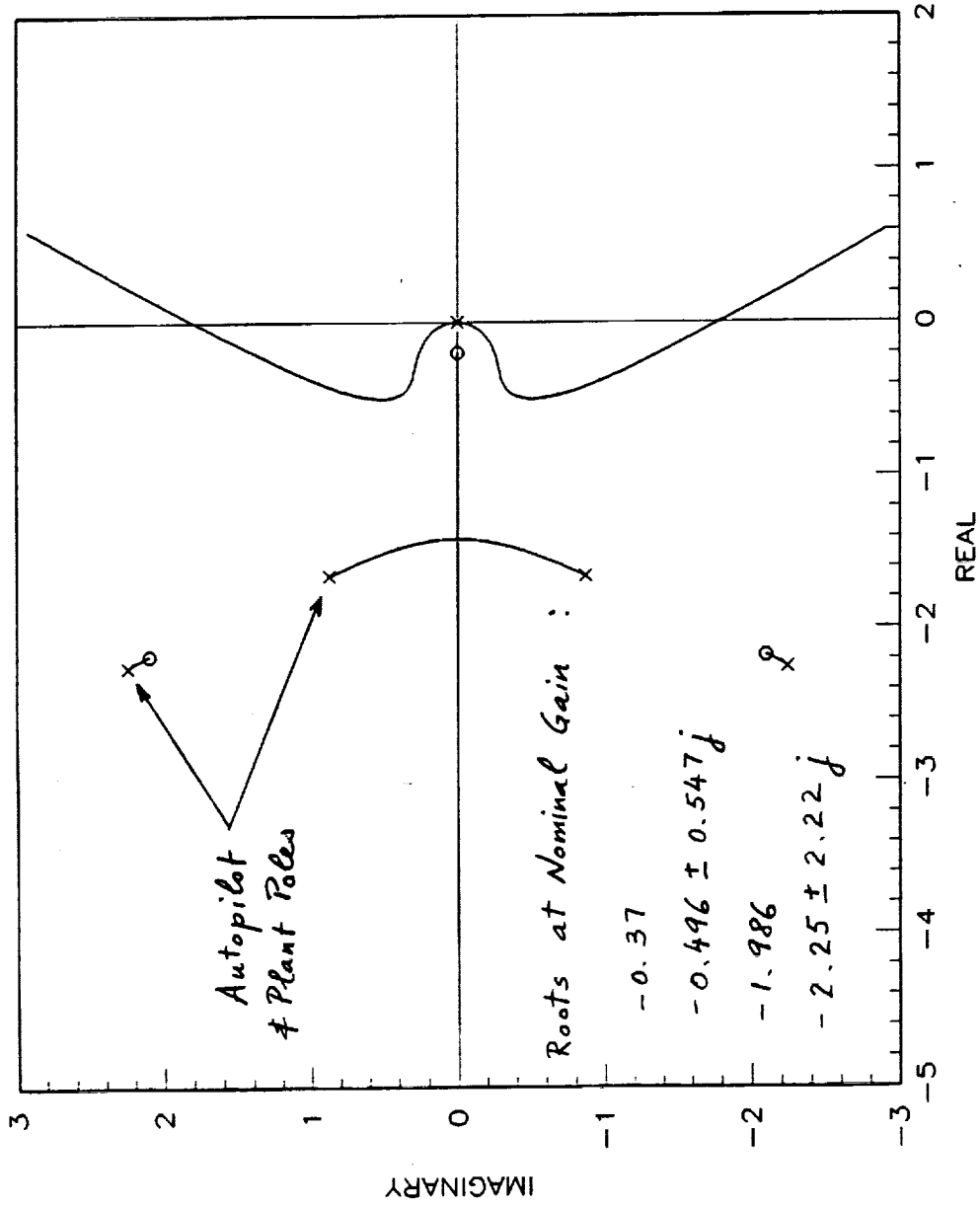
Figure 5-30 Guidance, Autopilot and Plant Root Locus
(Lateral, α=5°, Qpres=200psf)

Autopilot
+ Plant Poles

Roots at Nominal Gain :

-0.37

$-0.496 \pm 0.547j$

-1.986

$-2.25 \pm 2.22j$
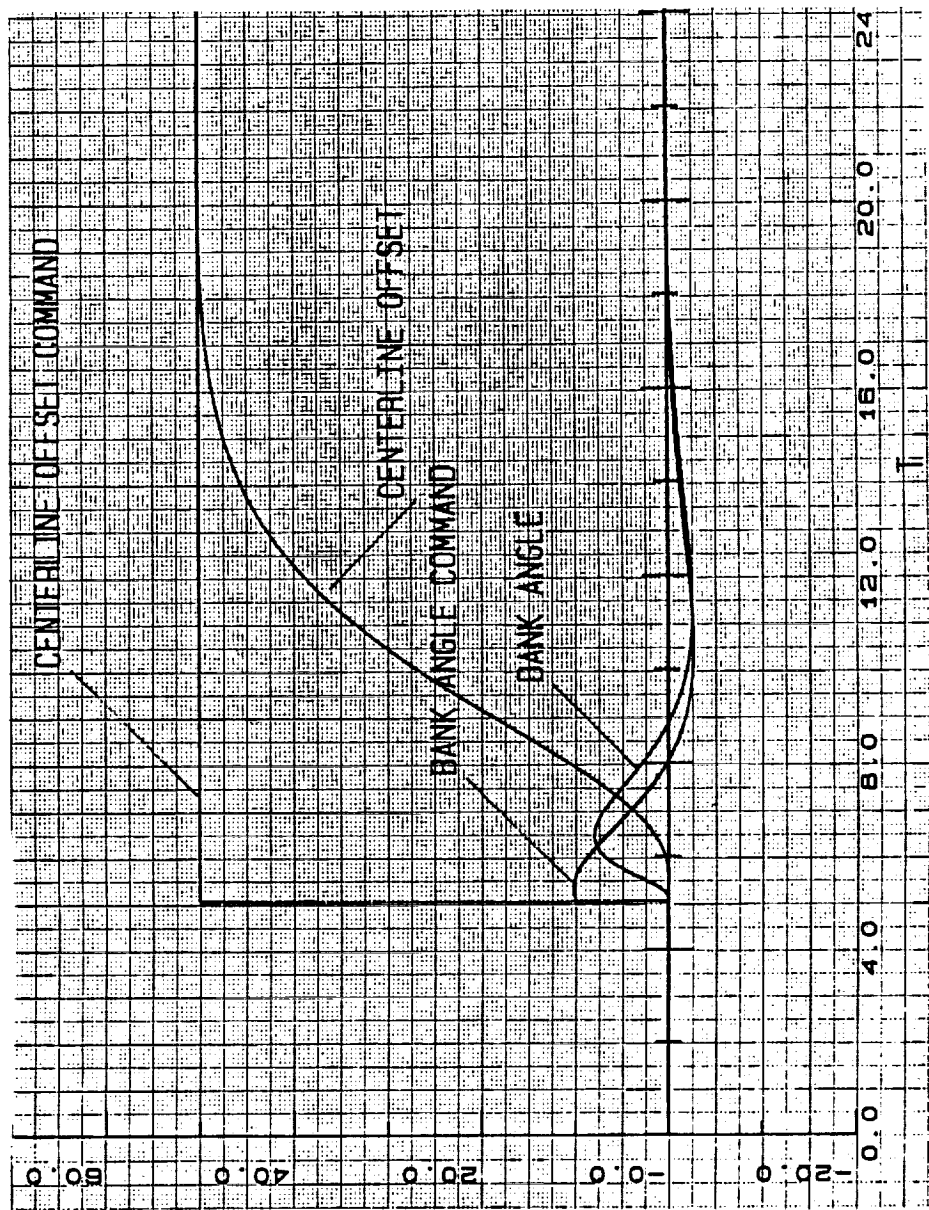
Figure 5-31 Centerline Offset Step Response (Qpres=300psf)

81

5.4 Speed Control

The CERV uses a speed control method similar to the Space Shuttle's. The speed controller is active during the steep constant angle glide phase. The CERV follows a predetermined nominal speed profile which requires a nominal 7.5° deflection of the body flaps speedbrake. The speed controller is to deliver the CERV at the proper inertial speed before the flare maneuver, depending on the wind conditions. The nominal speed at flare is 465 ft/sec. The speedbrake retracts just before flare at about 1200 ft altitude, to the 5° deflection minimum drag configuration. This provides the CERV a clean configuration for the flare maneuver where speed depletion rate is high due to the high angle-of-attack sustained. Furthermore, the speed brake are retracted to leave the body flap ailerons full operating range during the decrab maneuver. The Space Shuttle speadbrake retracts at either 4000, 2500 or 1000 ft, depending on the energy condition to provide the low energy condition energy margin, and the high energy condition ground speed limits.

The structure of the speed controller is shown in figure 5-32. The gains Ksi and Ks are 0.5 and -0.5 respectively. The velocity error integrator is programmed to stop integrating when the speedbrake position is limited. It prevents the integrator from accumulate to large value, which causes large overshoot and long settling time. The speedbrake is biased to 7.5 degrees as the nominal position.

A good portion of this study is devoted in the flare phase. Therefore, in most cases, simulation runs are started at an altitude of 4000 ft, and the speed controller is turned off. It was assumed that the speed controller is able to deliver the CERV at the desired speed at flare. Section 6.6 describes the speed controller performance during the constant glide path angle descent phase.

The speedbrake capability is investigated to determine the speed envelope at the entry of the descent phase. This envelope is determined by setting a fixed speedbrake deflection, and flying the CERV to the nominal flare speed of 465 ft/sec. Figure 5-33 shows the resulting speed profile for a fixed speedbrake deflection of 10° and the minimum speedbrake deflection of 5°. The figure shows a ΔV capability of 200 ft/sec for a speedbrake variation of 5 degrees. This 200 ft/sec speed envelope can serve as a requirement to the guidance as entry speed accuracy limit. Higher speedbrake deflection yields larger speed envelope limits, however, it is desirable to leave ample margins for the body flap aileron for roll control. For this study, a nominal speed profile which requires a 7.5 degrees speedbrake deflection is selected, yielding a +100 ft/sec speed adjustment capability. The nominal entry speed is 850 ft/sec (M=0.8).
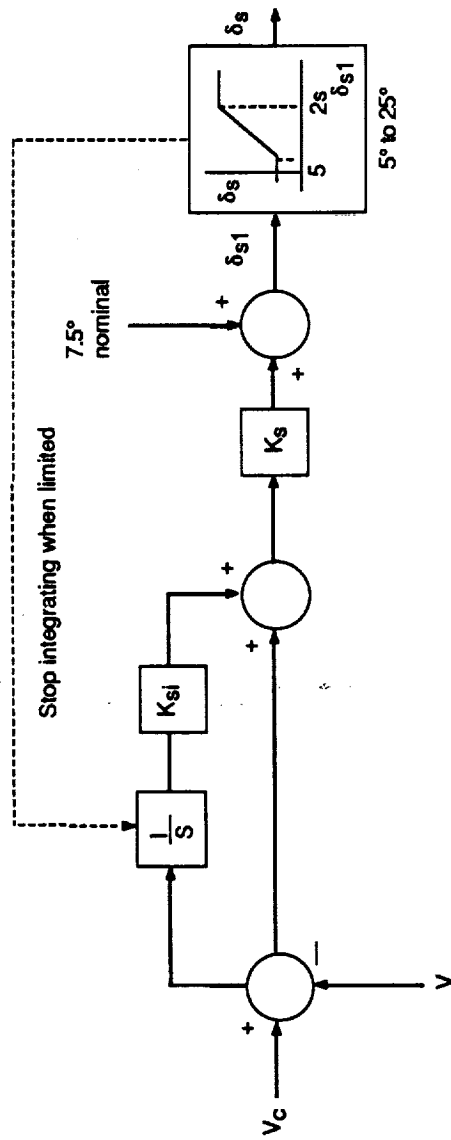
Figure 5-32 Speedbrake Controller
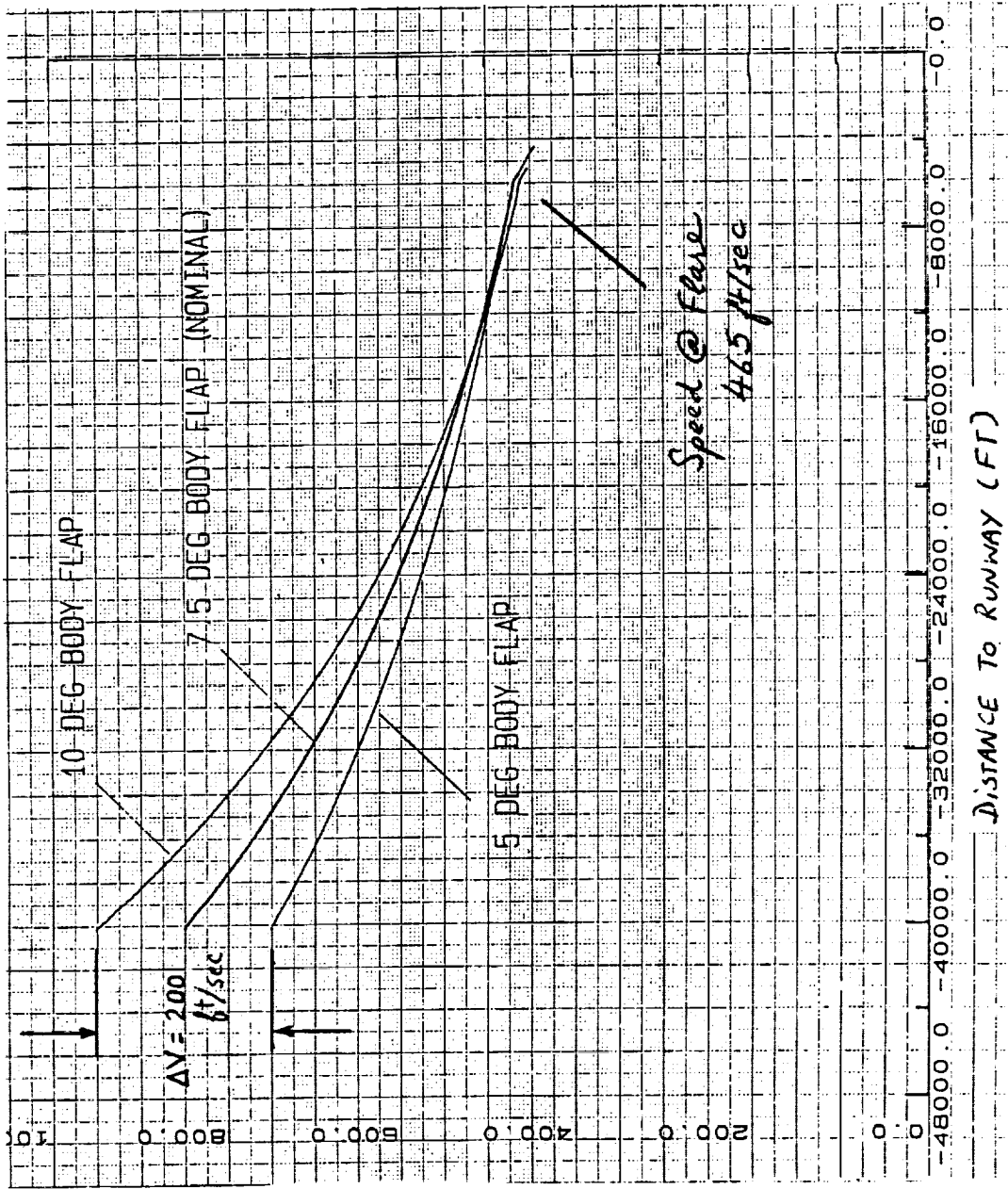
Figure 5-33 Entry Speed Accuracy Limits

Wind conditions will alter the speedbrake performance; however it is assumed that the guidance will compensate for the wind effect by adjusting the glide slope angle. The uncertainty in the knowledge of wind will be corrected by the speed control. An uncompensated tail wind forces the vehicle to reduce the entry speed. On the other hand, an uncompensated head wind forces the vehicle to increase the entry speed. 10 ft/sec was selected as an accuracy requirement for the wind. Figure 5-34 shows an uncertainty of 10 ft/sec (20% of the max wind case) in head and tail wind reduces the speed envelope to 100 ft/sec, yielding a +50 ft/sec entry speed adjustment capability. These figures give a first cut allotment of requirement for guidance accuracy at the state of autoland and wind information.
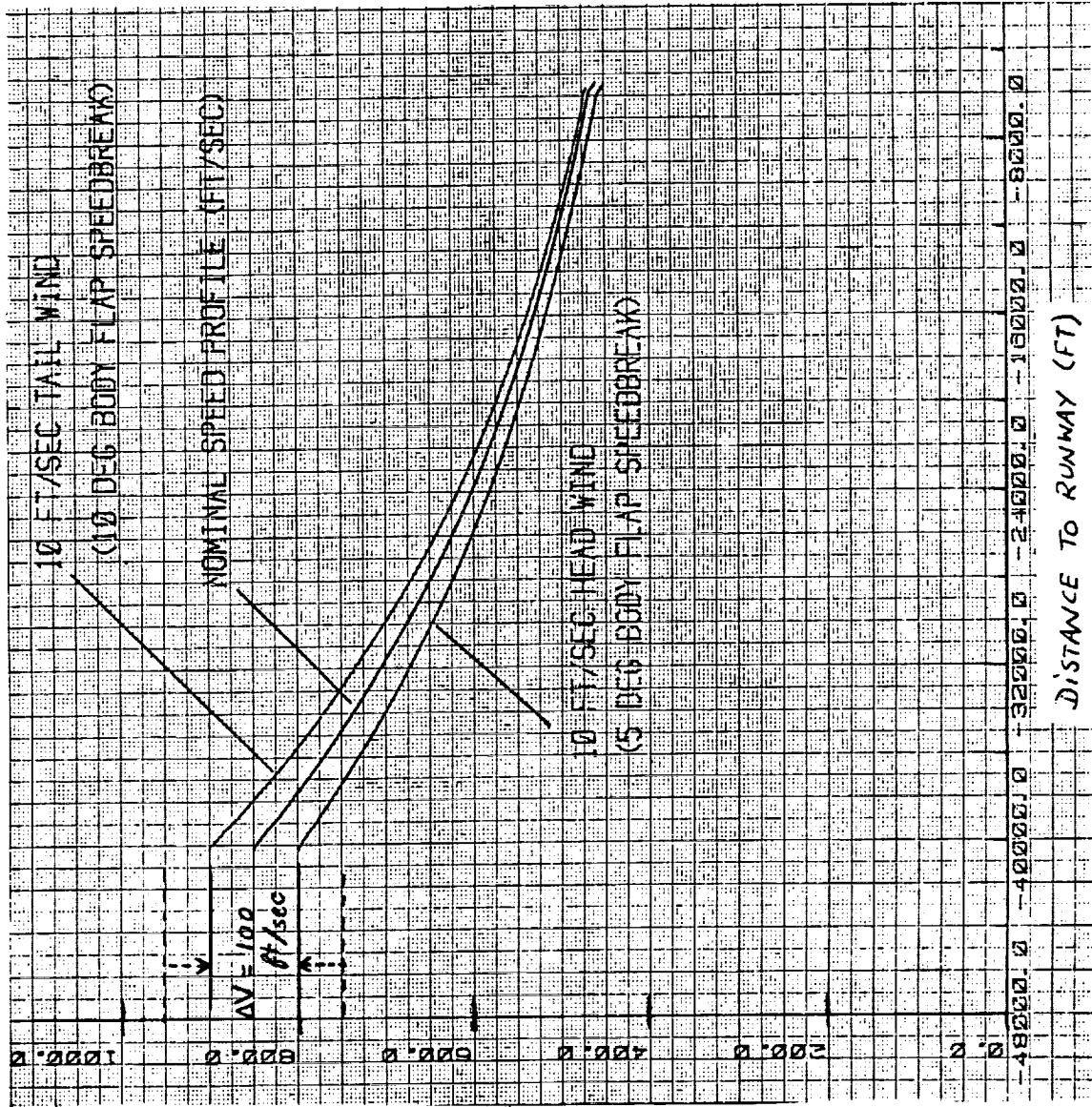
Figure 5-34 Wind Uncertainties Effect on Entry Speed Accuracy Limits

6.0 6DOF Simulation Analysis

The designs described in section 5 are implemented on the 6DOF simulator. The design performance is evaluated in the presence of wind. Sections 6.1 and 6.2 present the performance of the flare and decrab maneuvers respectively. CERV performance in discrete wind gust and wind turbulence are presented 6.3 and 6.4 respectively. Also included in section 6.4 are the actuator rate requirements due to wind. Section 6.5 investigates the rate limit effect on the performance. And section 6.6 shows the results of the speed controller performance.

6.1 Flare Maneuver

Time histories of a nominal flare trajectory are shown in figures 6-1 and 6-2. Shown in these figures are the altitude profile, total speed, sink rate, angle-of-attack, flight path angle, and elevator deflections, dynamic pressure, pitch rate, normal and axial load. Table 6-1 (following figure 6-7) summarizes the nominal values at impact. The parabolic flare maneuver is triggered at approximately 1200 ft. It is readily identifiable by the angle-of-attack command step in figure 6-1. The step is the result of the feedforward normal acceleration being engaged at the start of the flare. After the step, the angle-of-attack continues to increase gradually as the dynamic pressure decreases. At approximately t=30.5 sec, which correspond to an altitude of 10 ft, the parabolic flare is terminated, and the flight path fades into a shallow glide slope of 0.2 degrees. This maneuver is marked by a drop off in angle-of-attack to reduce the pitching rotation and to stabilize the sink rate to the desired value. The angle-of-attack is limited to 16 degrees at landing to avoid tail scrape. The peak normal force experienced during the flare is 1.6 g's.

6.1-1 Flare Maneuver In Constant Head Wind

The flare maneuver is conducted in the presence of a constant 30 knots (51 ft/sec) head wind. The head wind is gradually increased from 4000 ft altitude to the full magnitude at 1375 ft before the flare. The wind profile and time history responses are shown in figures 6-3 to 6-5. The inertial speed at the start of flare is 425 ft/sec. Because of the head wind, the CERV was able to land at a much lower ground speed, but with enough airspeed to maintain the angle-of-attack within the limits.

6.1-2 Flare Maneuver In Head Wind with Wind Shear

A wind shear of magnitude 8 knots/100 ft altitude is added to the constant wind profile discussed in the previous paragraph 6.1-1, the resulting wind profile is shown figure 6-3b. In this

87

case, the CERV must land without the help from the head wind, a slightly higher speed at flare (467 ft/sec) is required. The time histories of the landing are shown in figures 6-6 and 6-7.
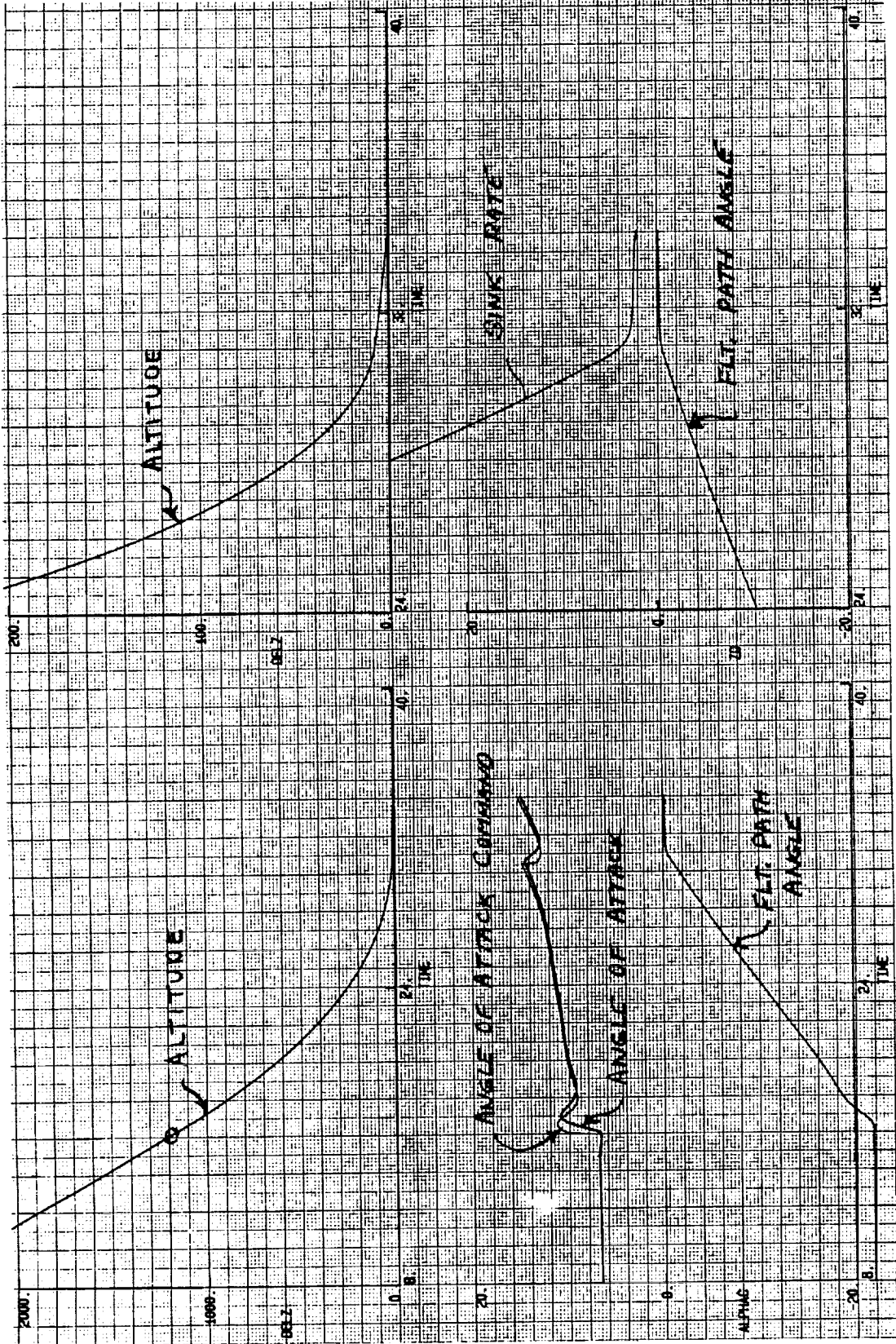
Figure 6-1 Nominal Flare Trajectory Time Histories

C-2
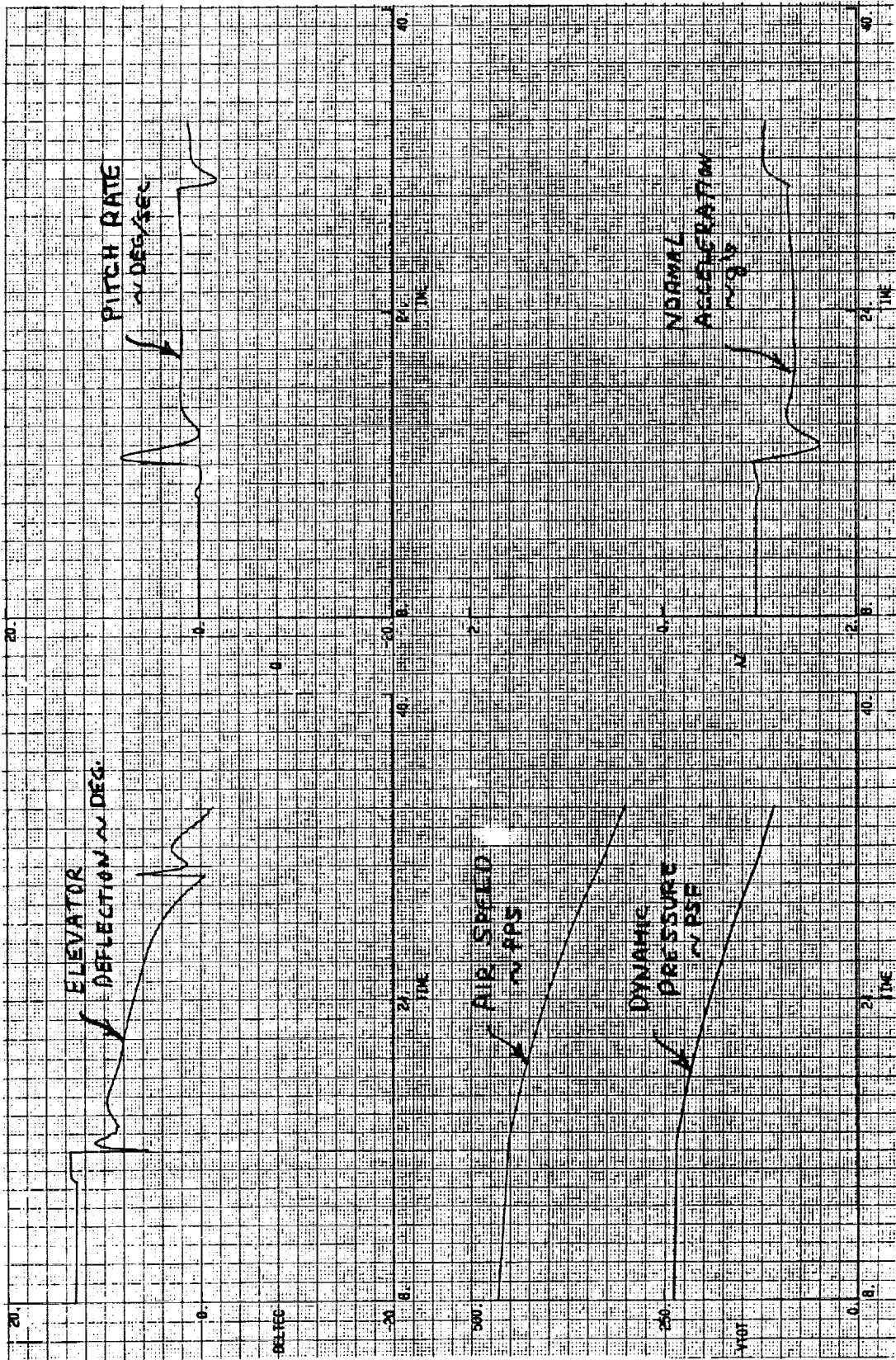
Figure 6-2 Nominal Flare Trajectory Time Histories (Continued)

90
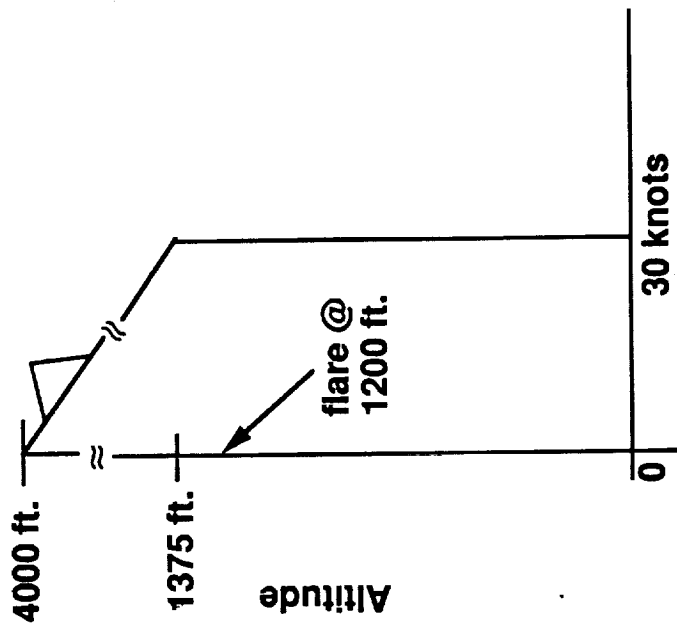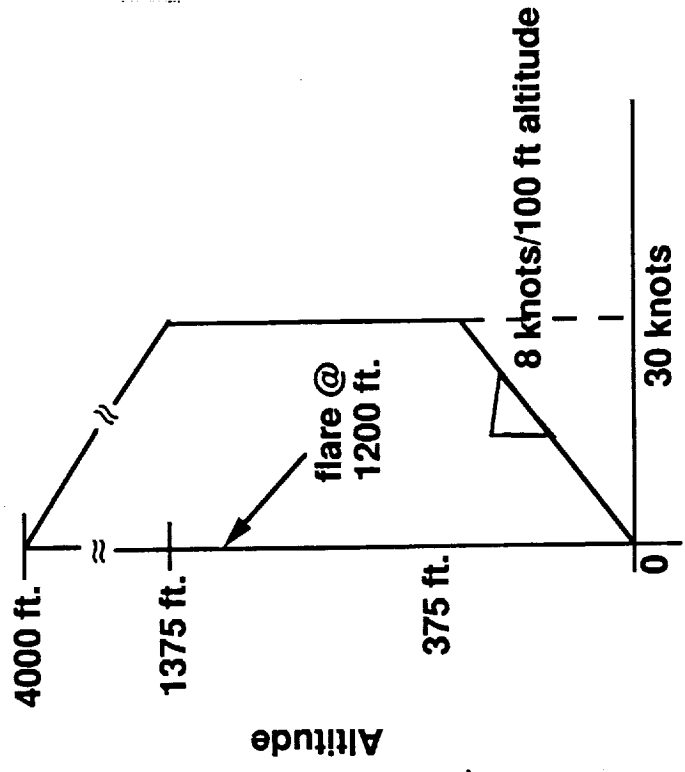
Figure 6-3b Head Wind With Final Shear

Figure 6-3a Head Wind Wind Profile

91
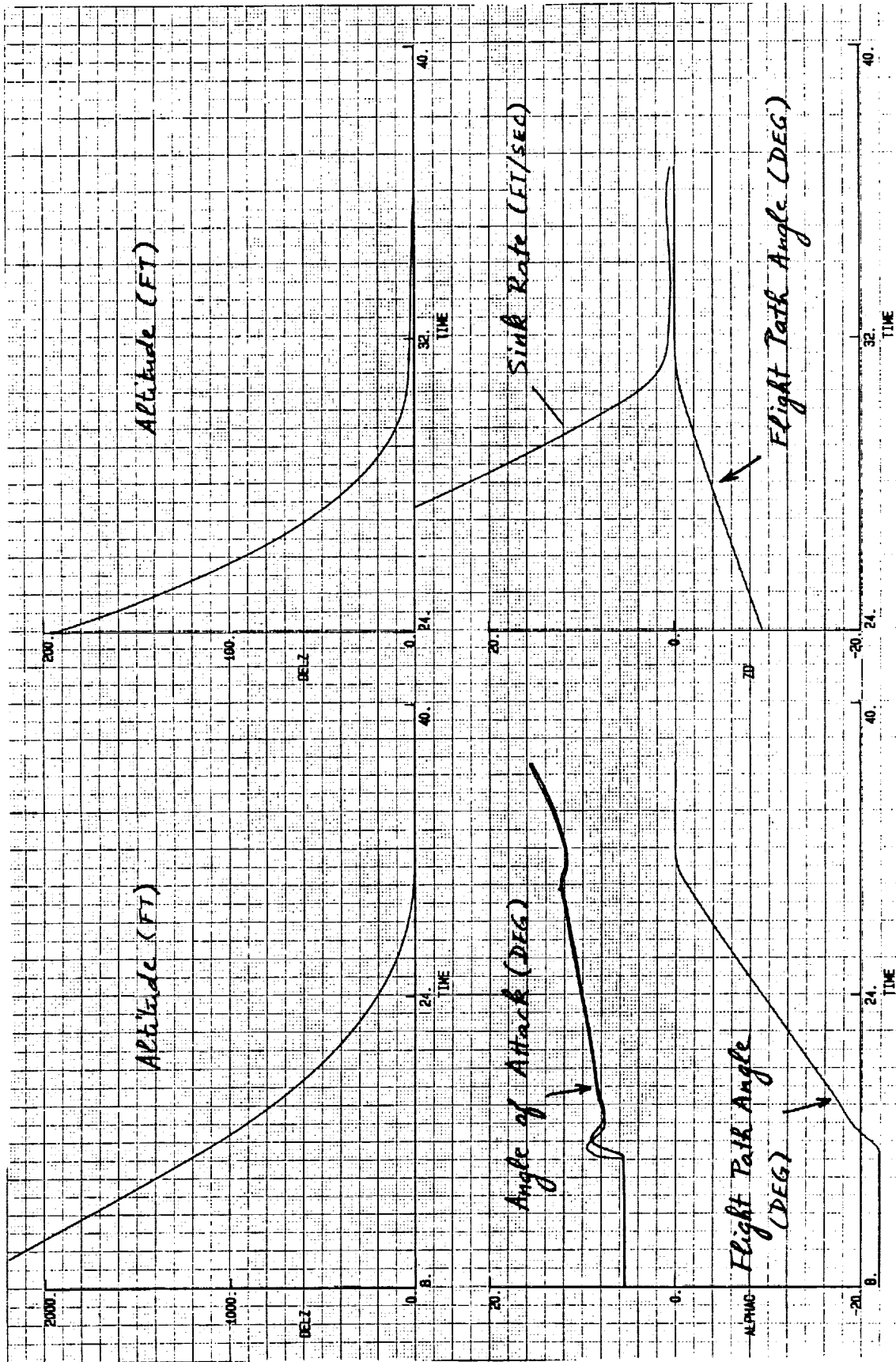
Figure 6-4 Landing Trajectory With Constant Head Wind Time Histories

92
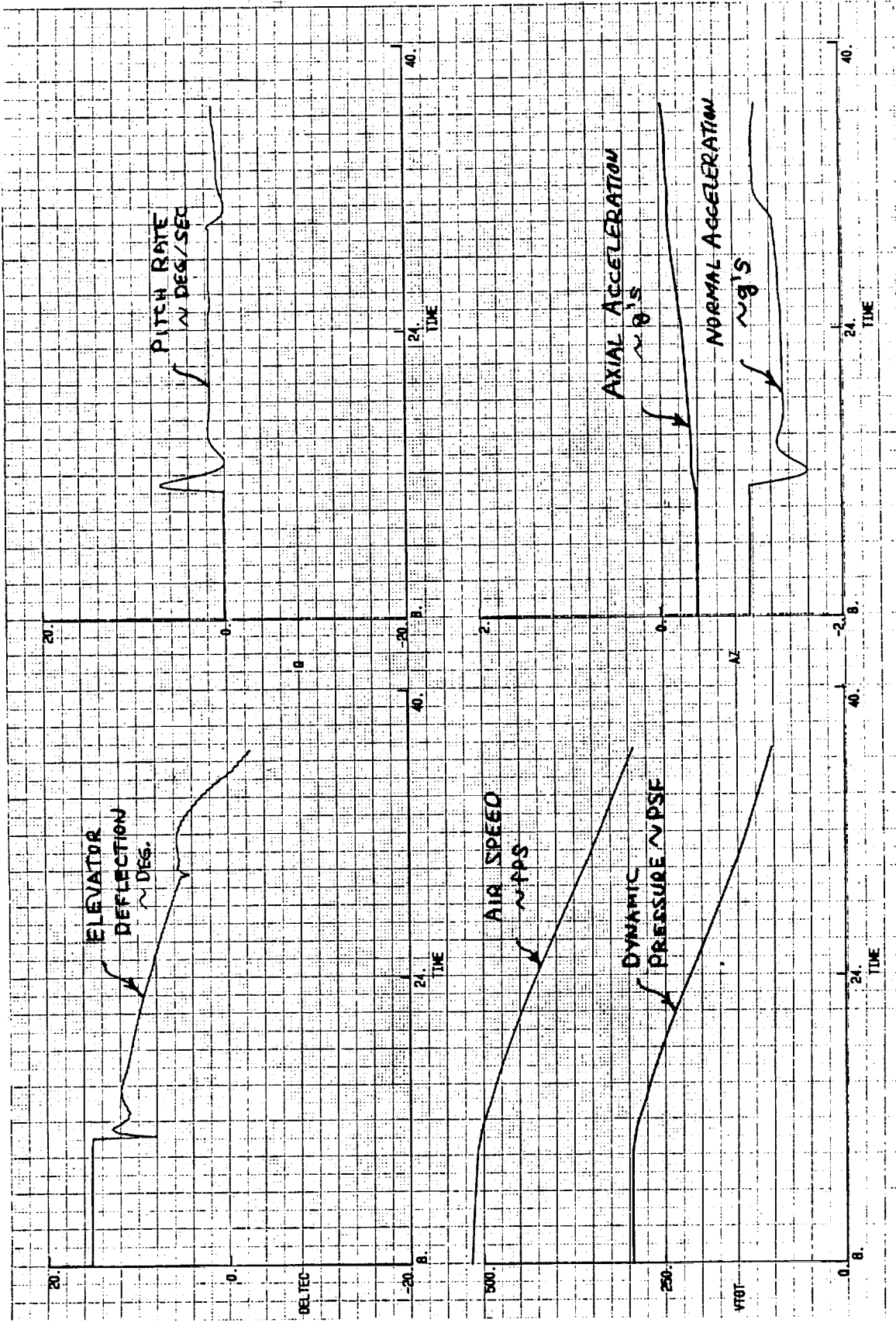
Figure 6-5 Landing Trajectory With Constant Head Wind Time Histories (Continued)

93
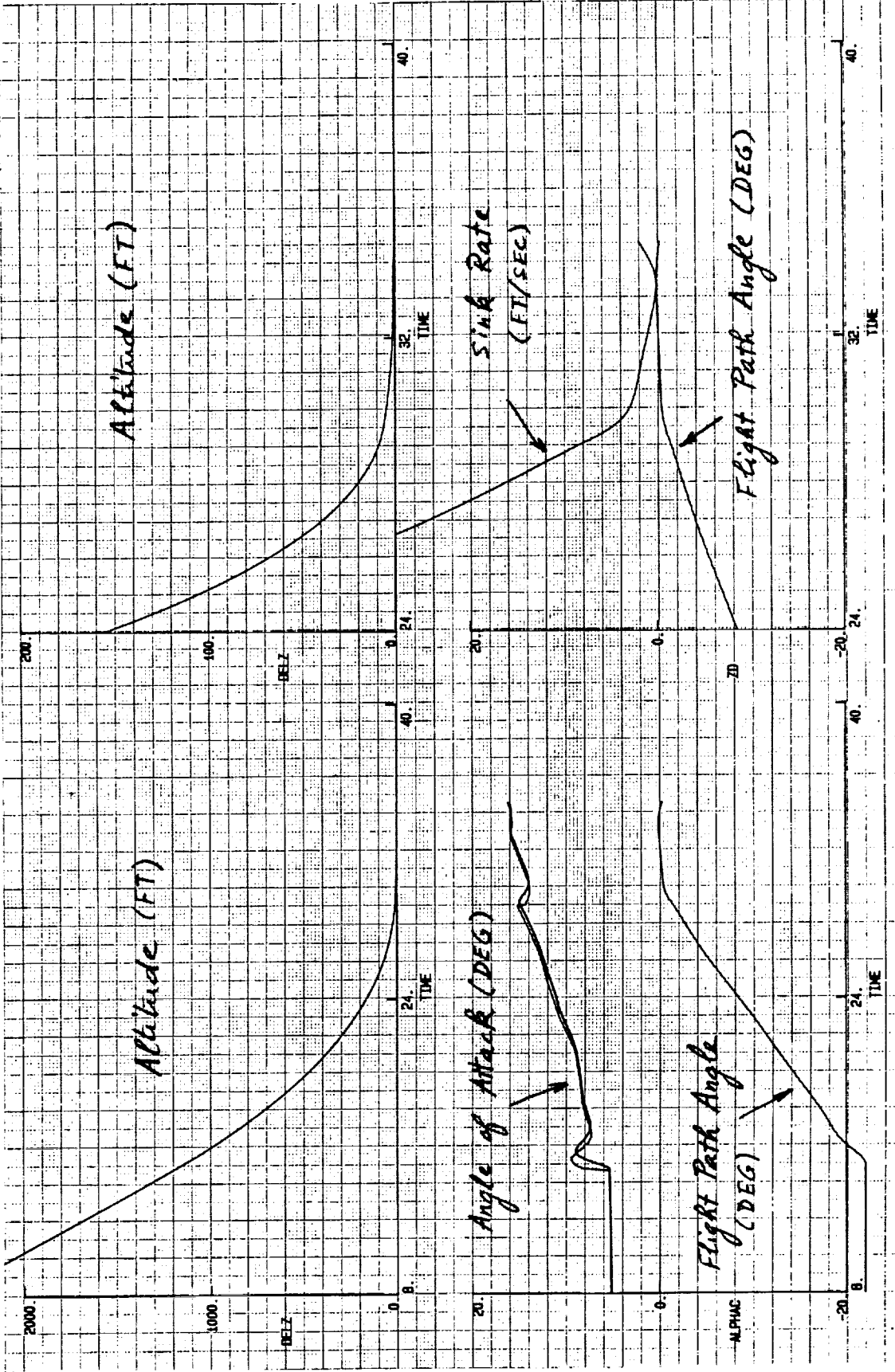
Figure 6-6 Landing Trajectory in Head Wind With 8 knots/100 ft altitude
Wind Shear Time Histories

94
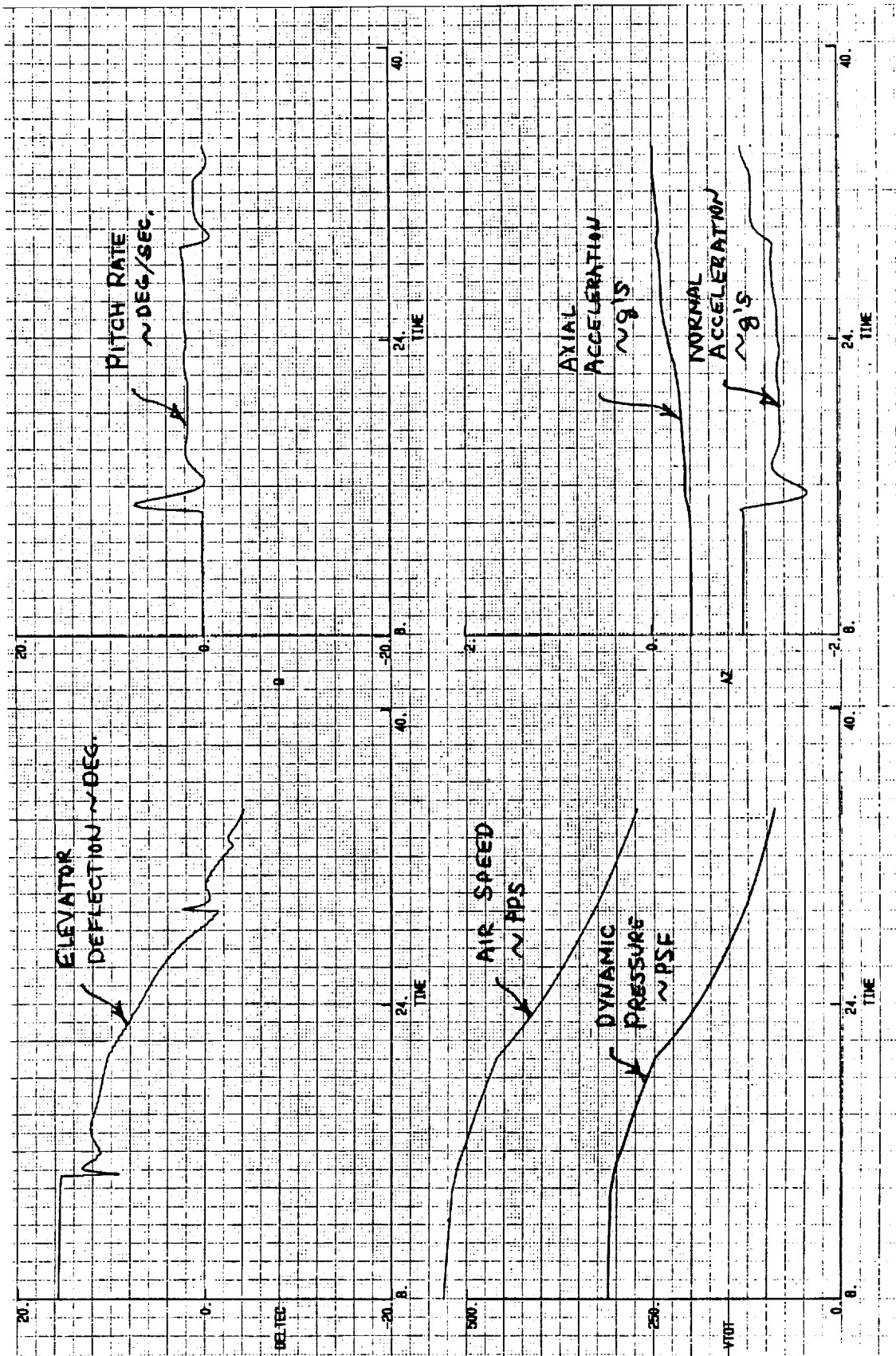
Figure 6-7 Landing Trajectory In Head Wind With 8 knots/100 ft altitude
Wind Shear Time Histories (Continued)

Case	Sink Rate	Ground Speed	Angle-of-Attack	Dynamic Pressure	Speed @ Flare
No wind	1.9 ft/sec	300 ft/sec (176 knots)	15°	110 psf	451 ft/sec
Head wind	0.33	240 ft/sec (141 knots)	15.4°	100 psf	456 ft/sec
Head wind with shear	2.1 ft/sec	269 ft/sec (158 knots)	16°	86 psf	467 ft/sec

Table 6-1 Flare Maneuver Performance Summary for Head Wind Conditions

6.2 Decrab Maneuver

CERV landing in a constant 22 knots cross wind is conducted on the 6DOF simulator to evaluate the decrab autopilot performance. During the descent, the CERV is steering into the wind, and flies at zero aerodynamic sideslip angle. As described in section 5.2, the decrab autopilot is to align the CERV from the crabbed condition at the on set of the maneuver to within 3 degrees of centerline. For a 22 knot sidewind, the pre-determined decrab steady state conditions are: $\phi_{ss}=11^o$, $\delta_{rss}=10^o$, $\delta_{ass}=28^o$ (see section 5.1.2 for more detail). Figures 6-8 shows the time histories of the crab and bank angles, inertial sideslip angle, rudder and aileron deflections, and lateral displacement. The decrab maneuver is initiated at an altitude of 30 ft. As shown in figure 6-8, the crab angle (psi) was reduced from 6° to 1.5^o. The side displacemt remains small (13 ft). The bank angle, rudder and aileron deflections are respectively 10°, 9°, 28°, at touchdown, in good agreement with the pre-determined state. However, because the wing flaps are also used as pitch control, the left wing flap was temporarily saturated when the final flare maneuver kicks in. The wing flap was off the saturation when the elevator trim decreases as the dynamic pressure drops.

During the decrab maneuver, the drag level is high due to the non-zero aerodynamic sideslip angle and the large aileron deflections. The speed at flare was at 472 ft/sec in order to maintain enough dynamic pressure at landing. Inadequate airspeed will cause the aileron to saturate, and the sink rate will increase.

A decrab maneuver in a 8 knots/100 ft altitude cross wind wind shear was also conducted. Figure 6-9 shows the two wind shear profiles used: a decreasing wind speed shear and a increasing wind speed shear. Figure 6-10 and 6-11 show the vehicle responses in both cases. The vehicle has no problem in tracking the shear by steering the heading into the wind. The sideslip angle was kept near zero during the shear. And the decrab maneuver was performed properly.
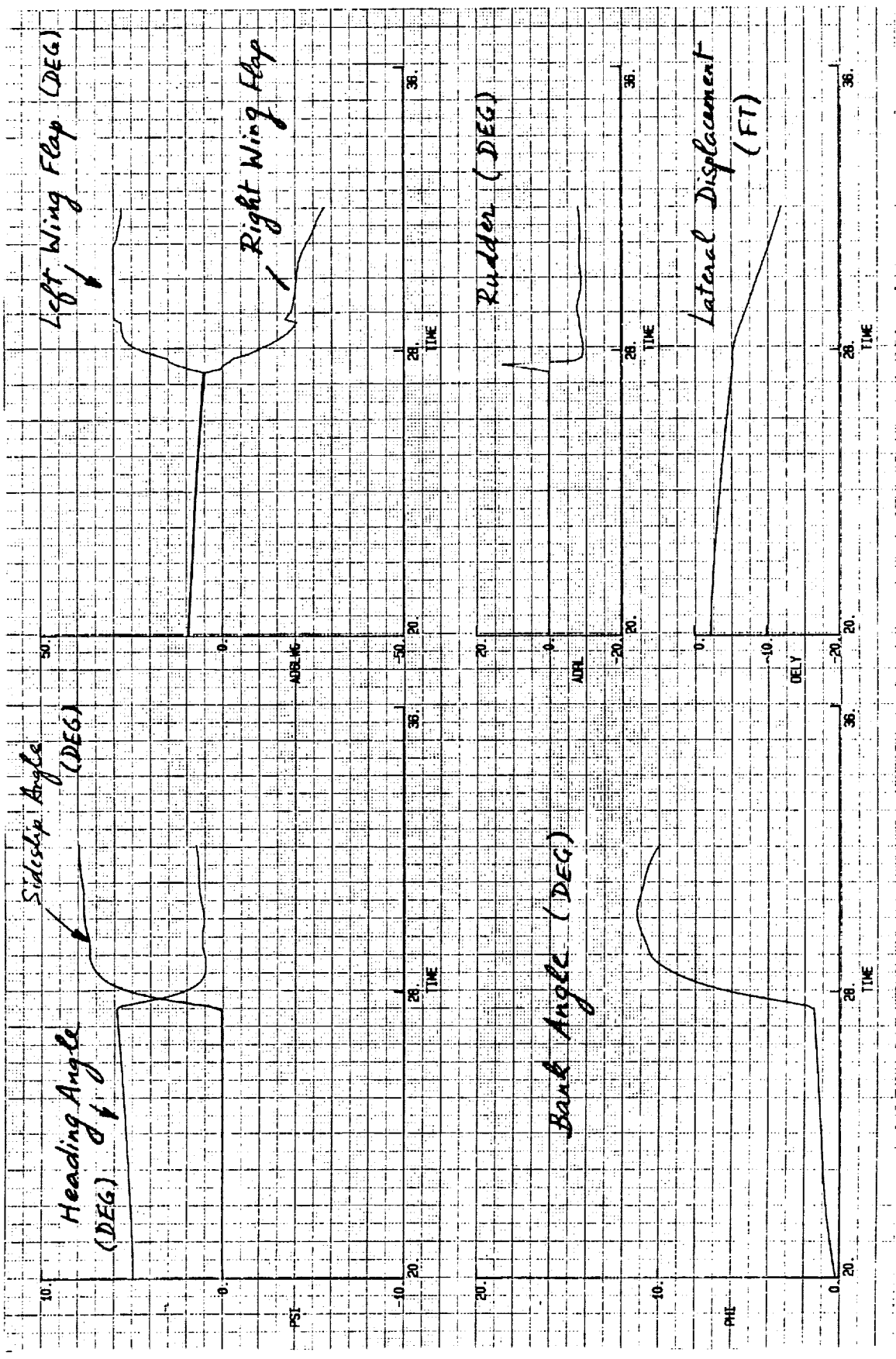
Figure 6-8 Decrab Maneuver for Constant 22 knots side Wind Time Histories

98
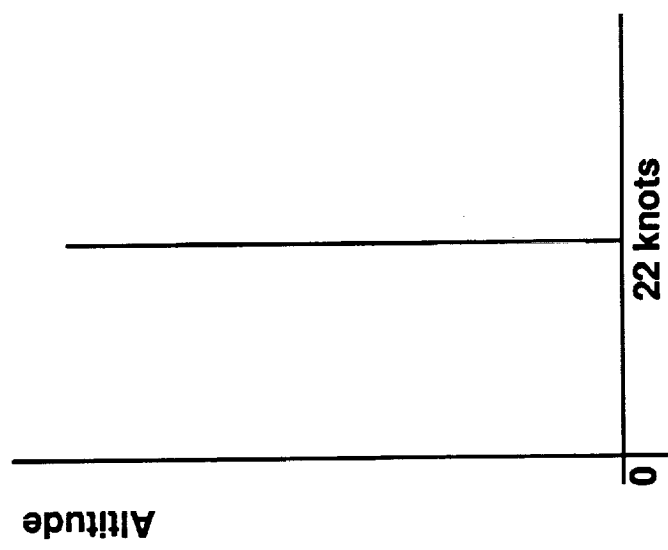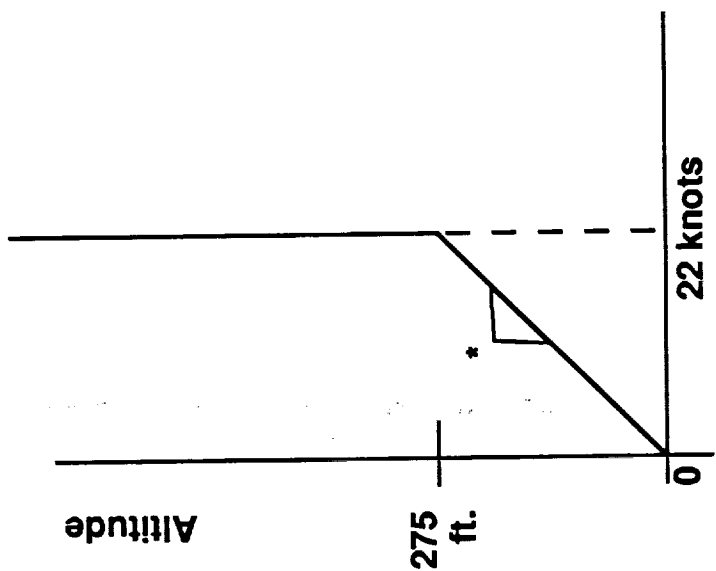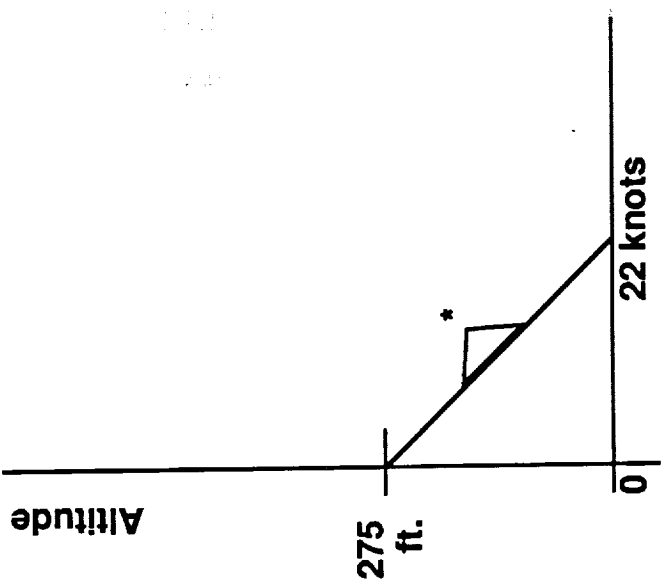
Figure 6-9 Side Wind Profiles

* .8 knots/100 ft. altitude
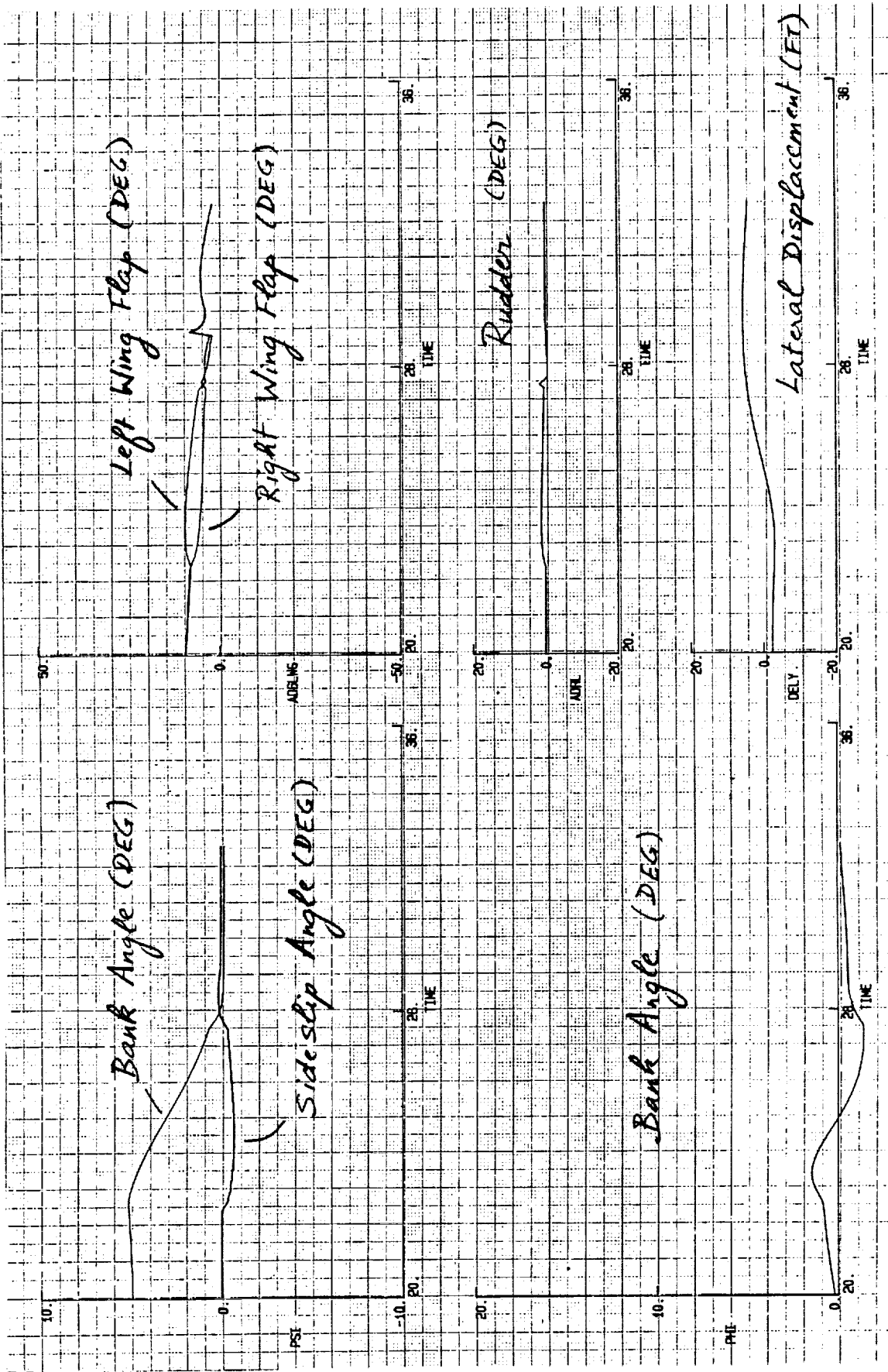
Figure 6-10 Decrab Maneuver in 8 knots/100 ft altitude
Wind Shear Time Histories (Decreasing Wind Speed Shear)

100
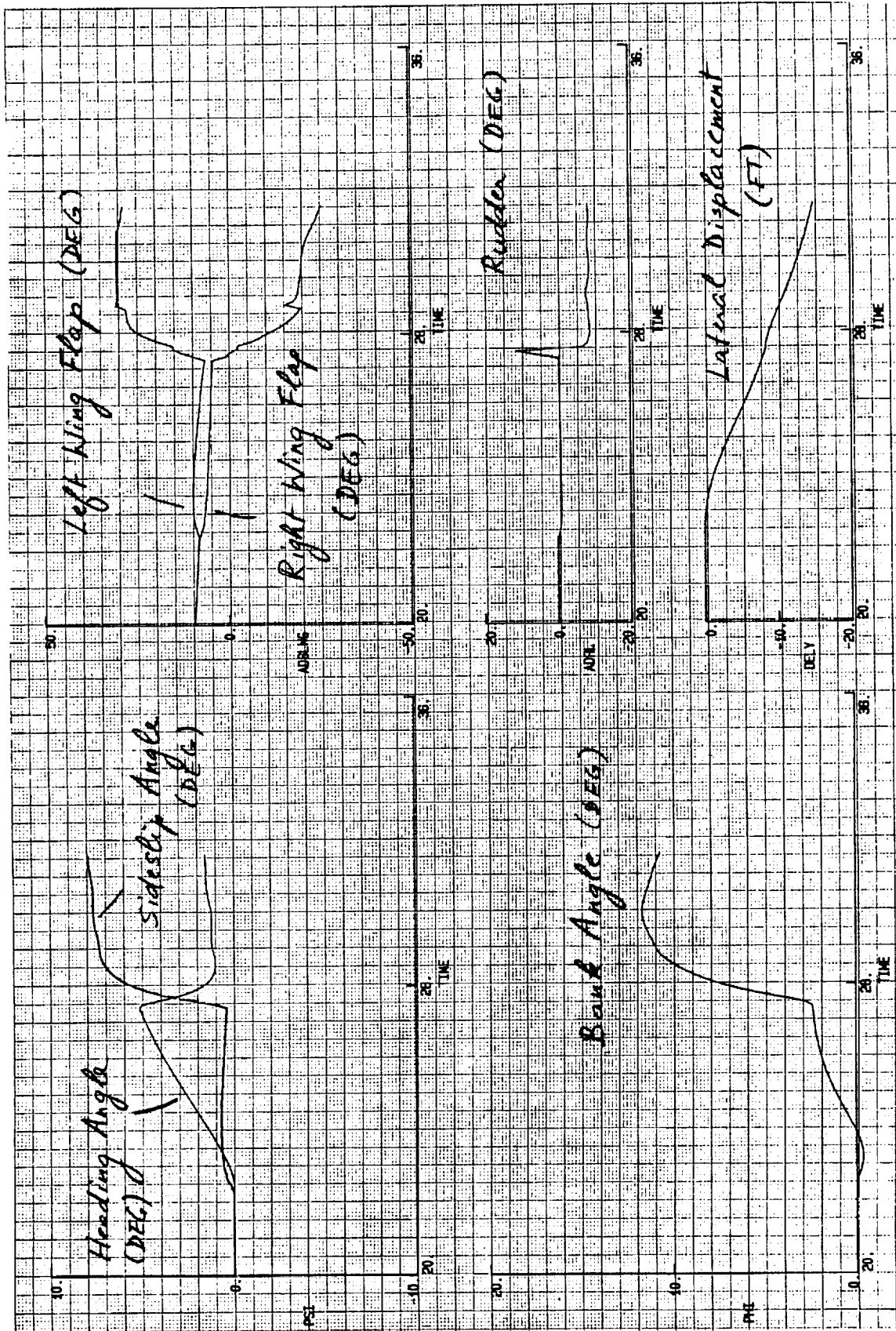
Figure 6-11   Decrab Maneuver in 8 knots/100 ft altitude
Wind Shear Time Histories (Increasing Wind Speed Shear)

101

6.3 Vehicle Performance in Discrete Gust

The discrete wind gust model has a profile of:

$$1/2 * A * (1 - COS (wt)) , 0 < t < 2 pi/w$$

where A is the peak amplitude of the gust and w controls the time length of the gust. The discrete wind gusts are applied at an altitude of 3200 ft prior to flare with the body flap open at 10 degrees for speedbrake, and at an altitude of 700 ft where the dynamic pressure is relatively low (223 psf). All gust applied are side winds and have peak amplitude of 35 ft/sec (21 knots). The gust durations are 1, 2, and 5secs.

- Discrete wind gust at 3200 ft:

At this altitude, the wing flap elevators are deflected at an angle of 13° for trim. In this case, the body flap speedbrake were also opened to 10 degrees to determine if aileron saturation would occur. The dynamic pressure at time of gust is 255 psf. Figure 6-12 shows the vehicle responses to the discrete wind gust of various durations. No fin saturations were observed and the max fin rate, 55 deg/sec, occurs during the 1 sec gust condition.

- Discrete wind gust at 700 ft:

In this case, the wind gust occurs after the flare. The dynamic pressure at time of gust is 223 psf. Figure 6-13 shows the vehicle responses. Again no fin saturations were observed and the max fin rate was 70 deg/sec.

102
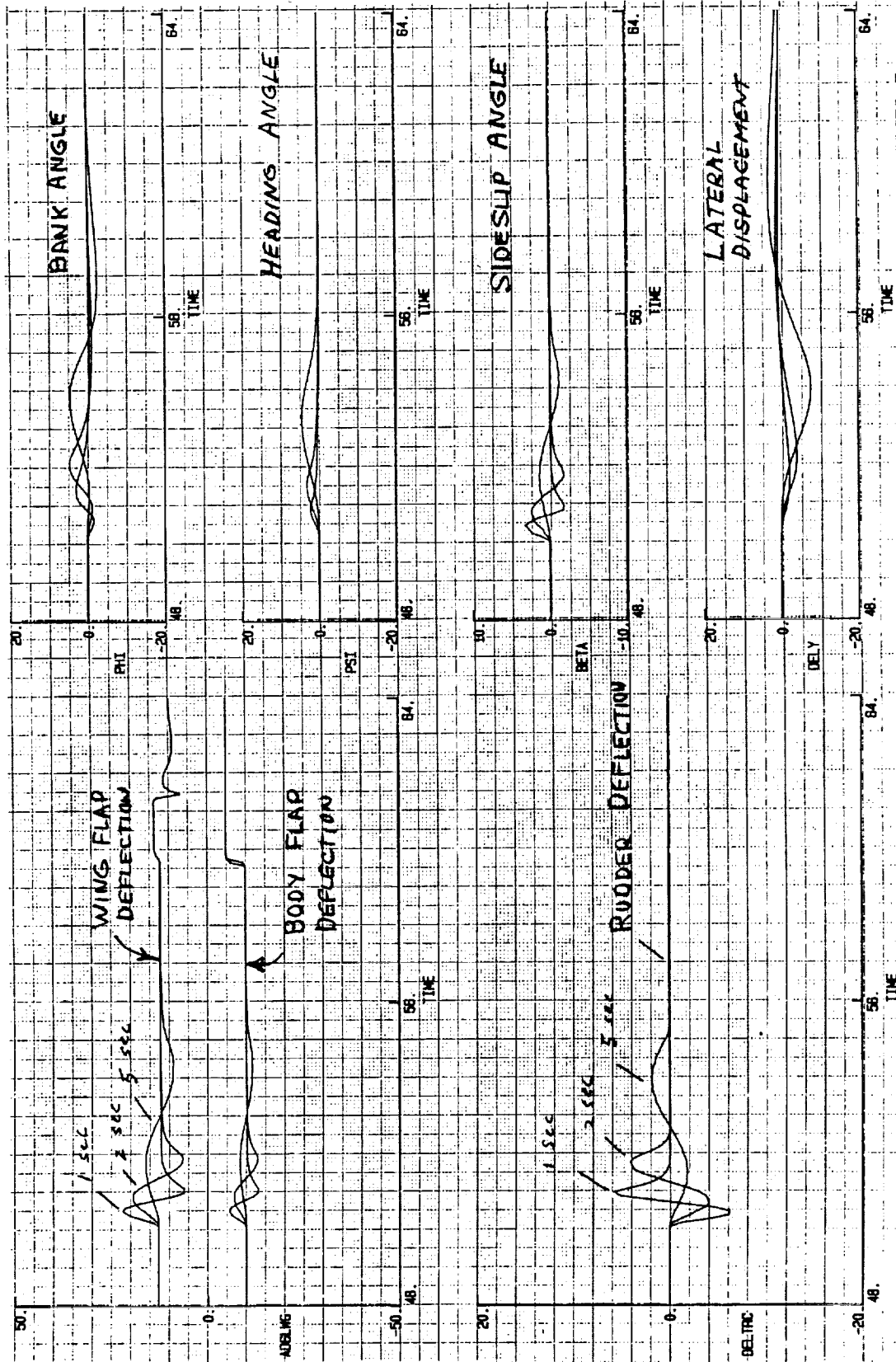
Figure 6-12 Discrete Wind Gust Response at 3200 ft Altitude

103
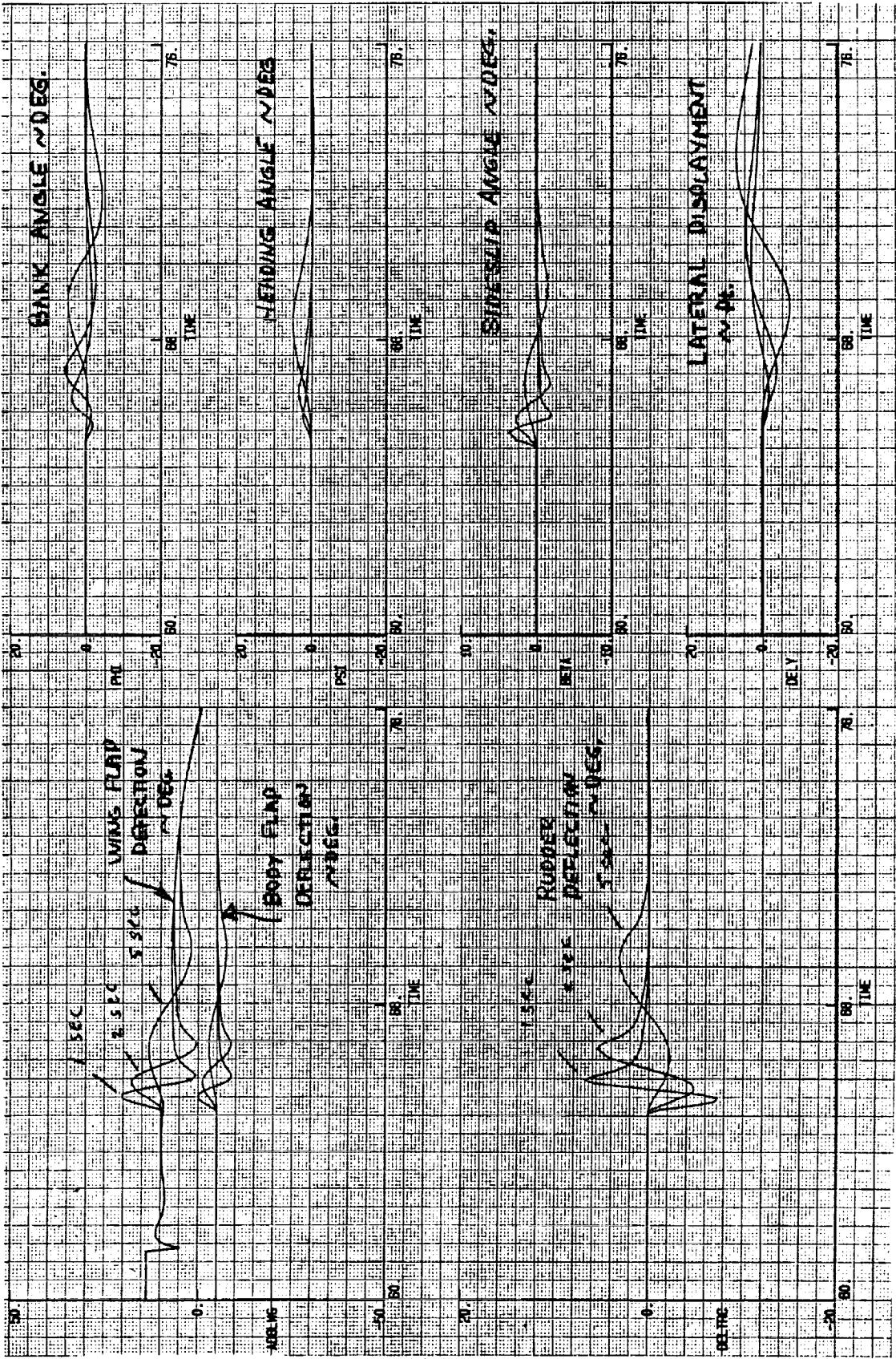
Figure 6-13 Discrete Wind Gust Response at 700 ft Altitude

6.4 Vehicle Performance in Turbulence and Actuator Rate Requirements

The wind turbulence model is extracted from the work of Holley and Bryson, in article "Wind Modeling and Lateral Aircraft Control for Automatic Landing", January 1975, Standford University Department of Aeronautics and Astronautics Report (SUDDAR) No. 489. The model approximates the major characteristics of the Dryden and Van Karman wind models. A detail description of the wind model is included in Appendix C. The CERV nominal flight trajectory was flown through a wind profile augmented with the wind turbulence model. The resulting wind profile is shown in figure 6-14. The wind turbulence has a gaussian distribution of 1σ equal to 5 knots (8.5 ft/sec) for the x and y axes, and 3.5 knots (6 ft/sec) for the z axis. Simulation results show good performance reponses. Figure 6-15 through 6-18 are the typical control surfaces rate and position responses to wind disturbances. The actuator rates are in the order of 100 degrees/sec RMS for the wing flaps, and 80 deg/sec RMS for the rudder. In this study, perfect angle-of-attack (α) and sideslip angle (β) are used as feedback signals. Therefore wind turbulence noise is fed directly to the autopilots, and subsequently to the actuators. The actuators rates can be reduced by using prefilter on body rates and body accelerations information. The body acceleration information is used in the angle-of-attack, and sideslip angle estimators. Figure 1-7 in section 1 summarizes the actuator rate requirements for the mission. Figures 6-19 to 6-21 show typical vehicle roll, pitch and yaw rates in the presence of wind disturbances.
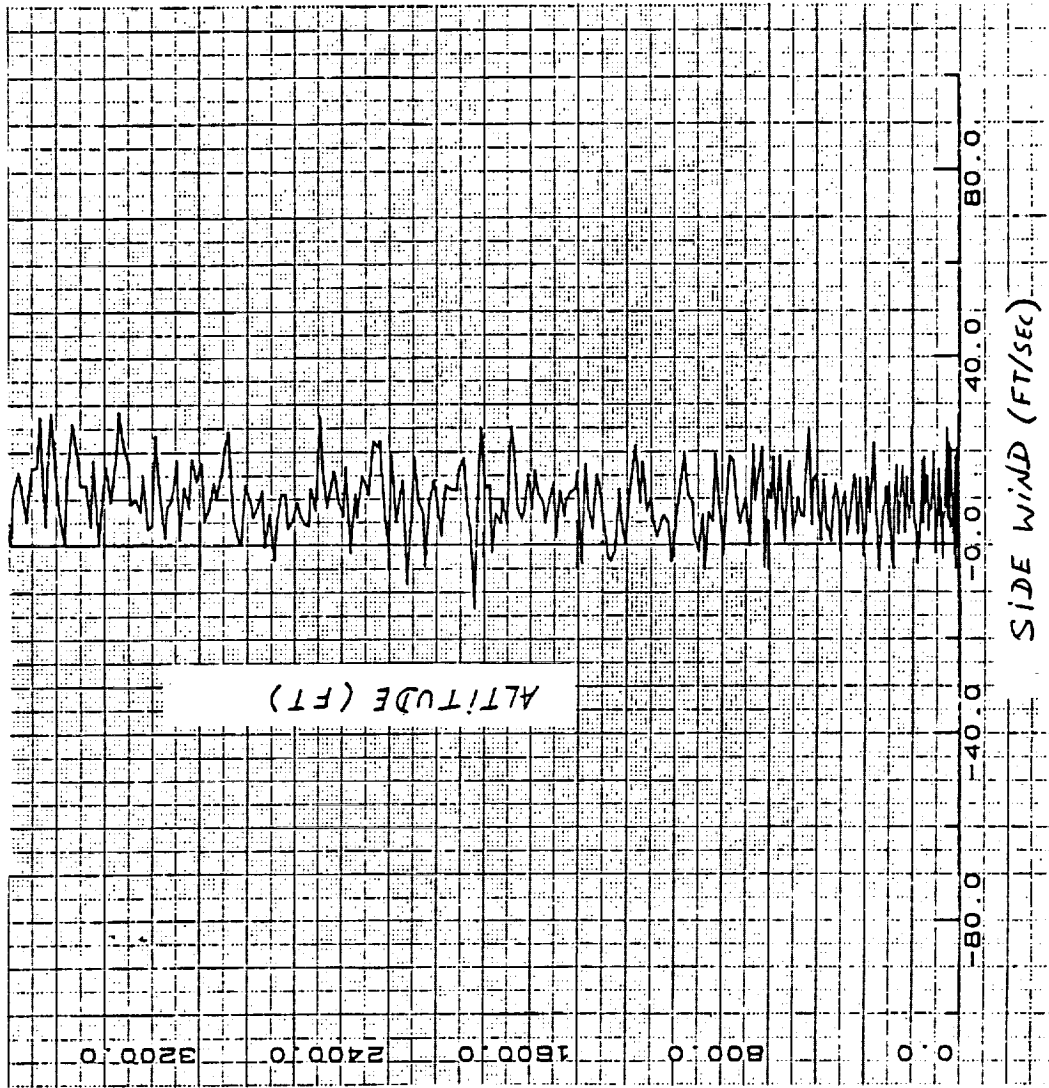
Figure 6-14 Cross Wind Turbulence Profile

106
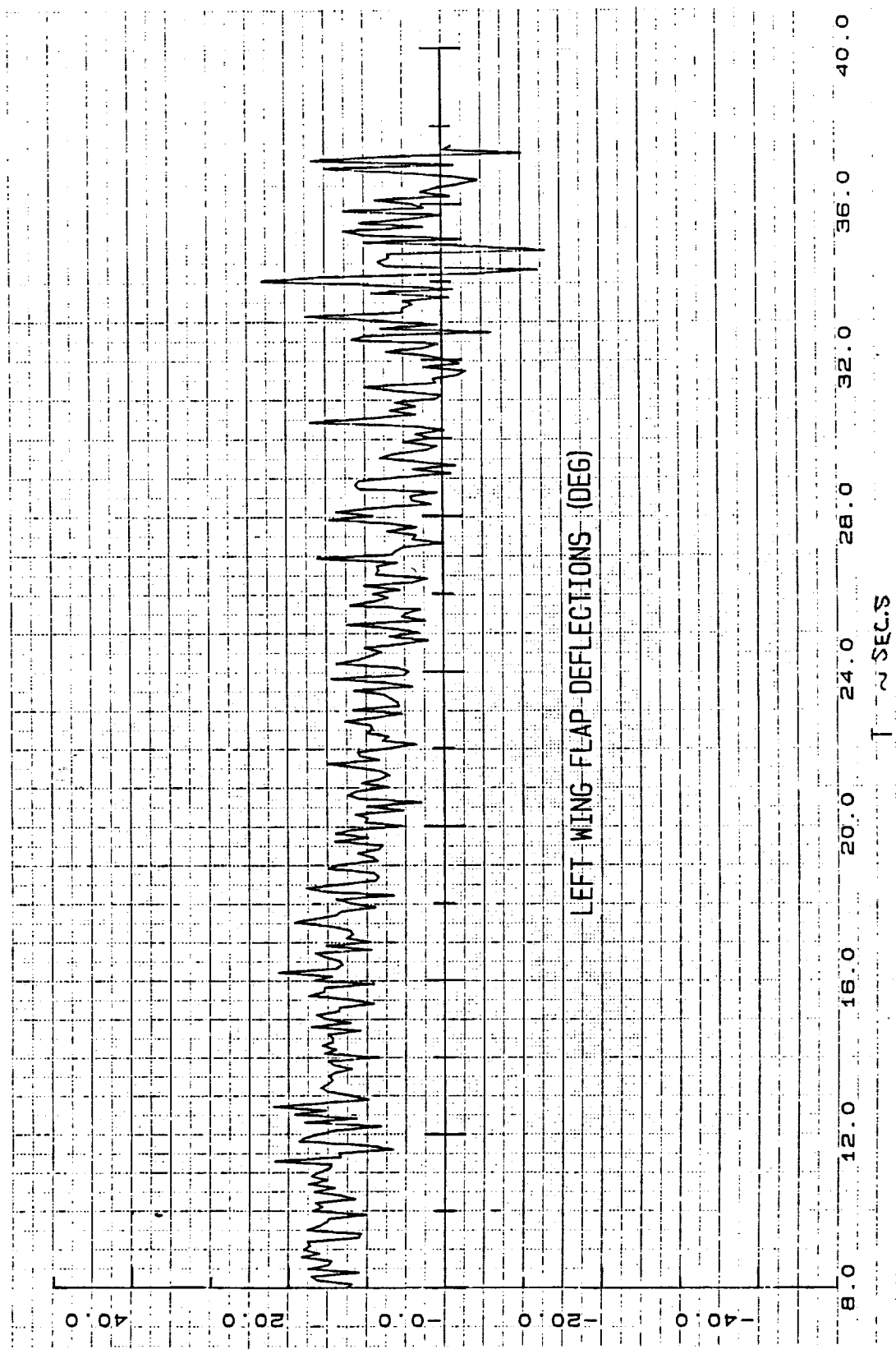
Figure 6-15 Wing Flap Response in Cross Wind Turbulence
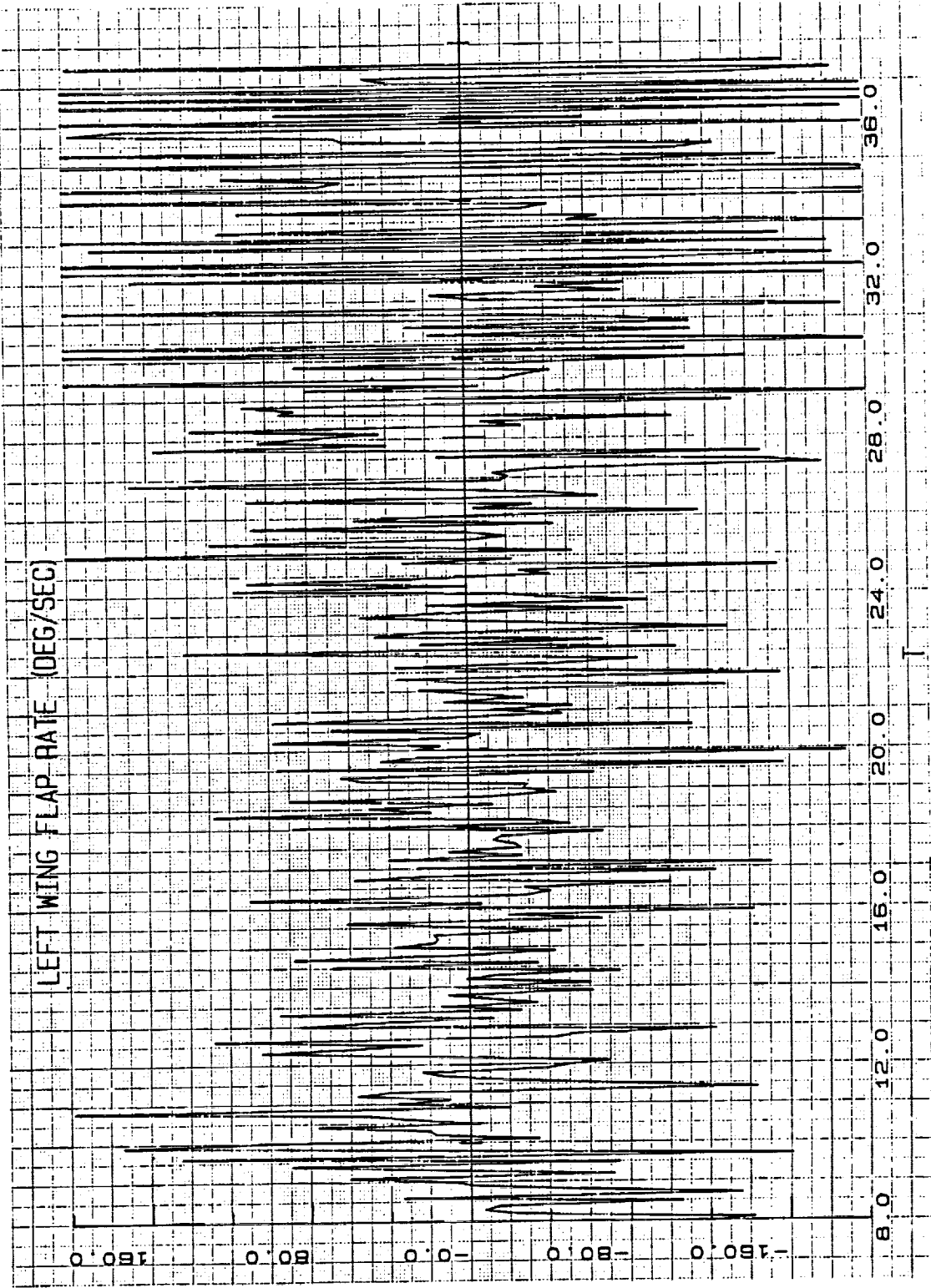
Figure 6-16 Wing Flap Rate in Cross Wind Turbulence
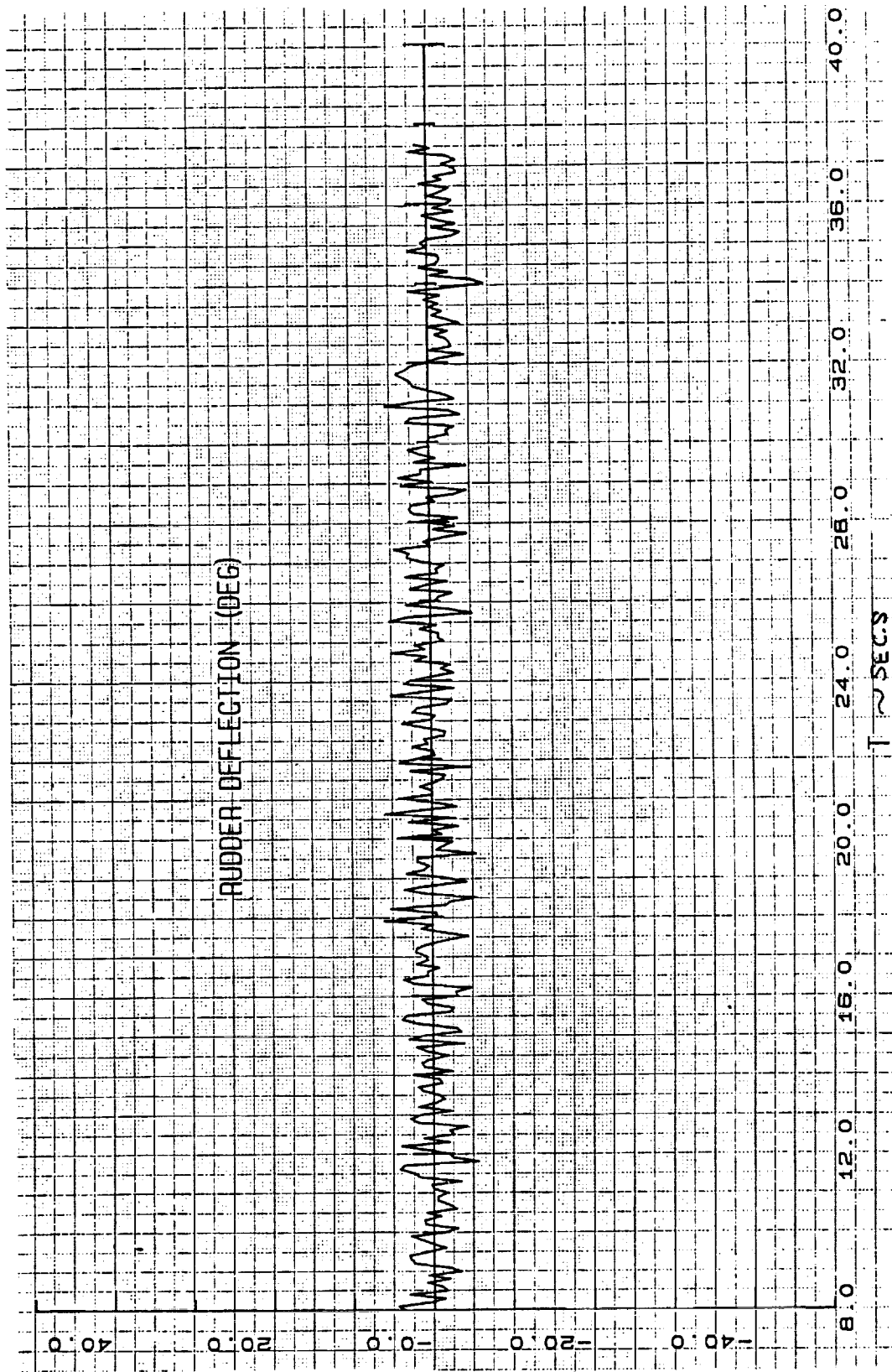
Figure 6-17 Rudder Response in Cross Wind Turbulence

109
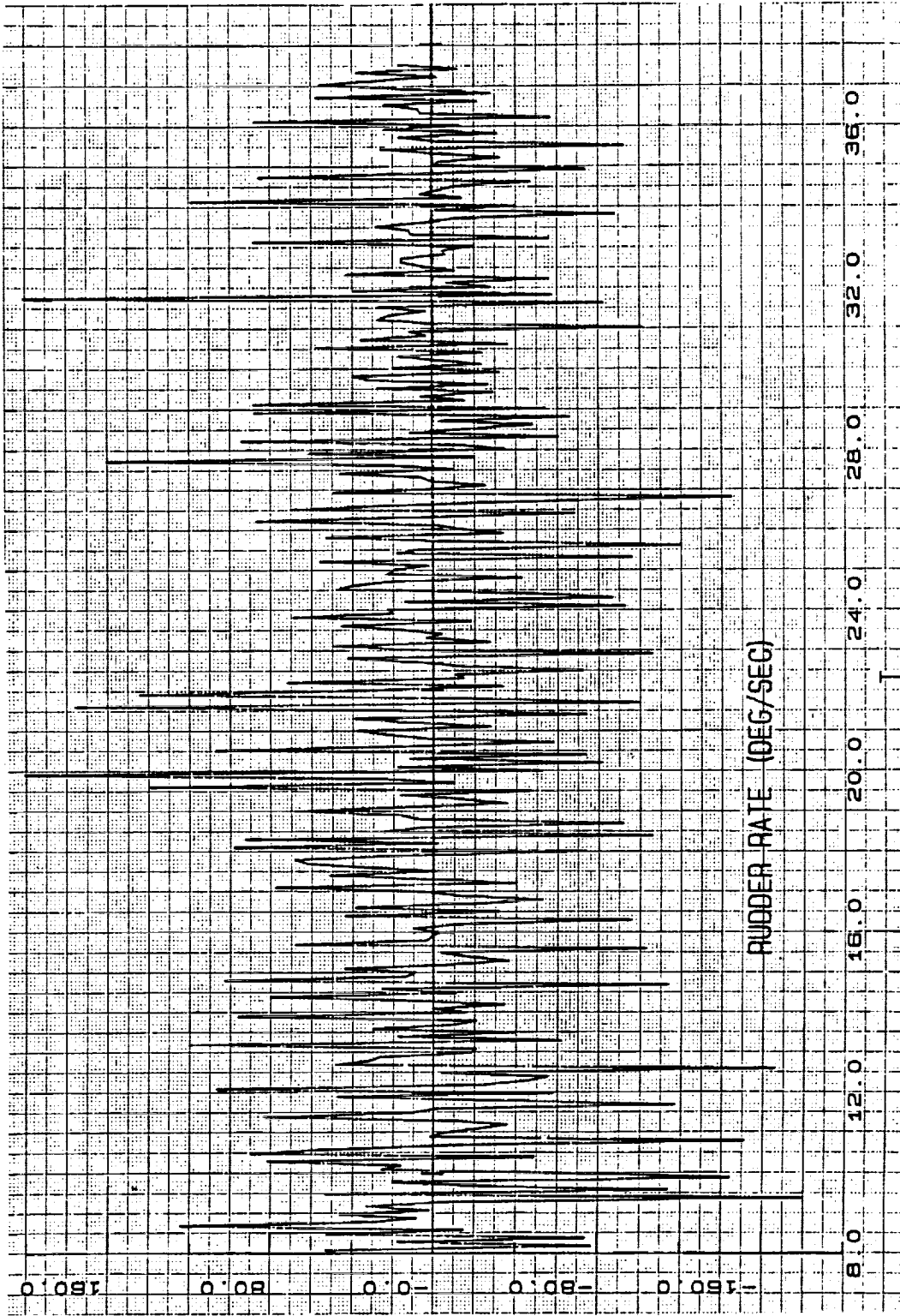
Figure 6-18 Rudder Rate in Cross Wind Turbulence

110
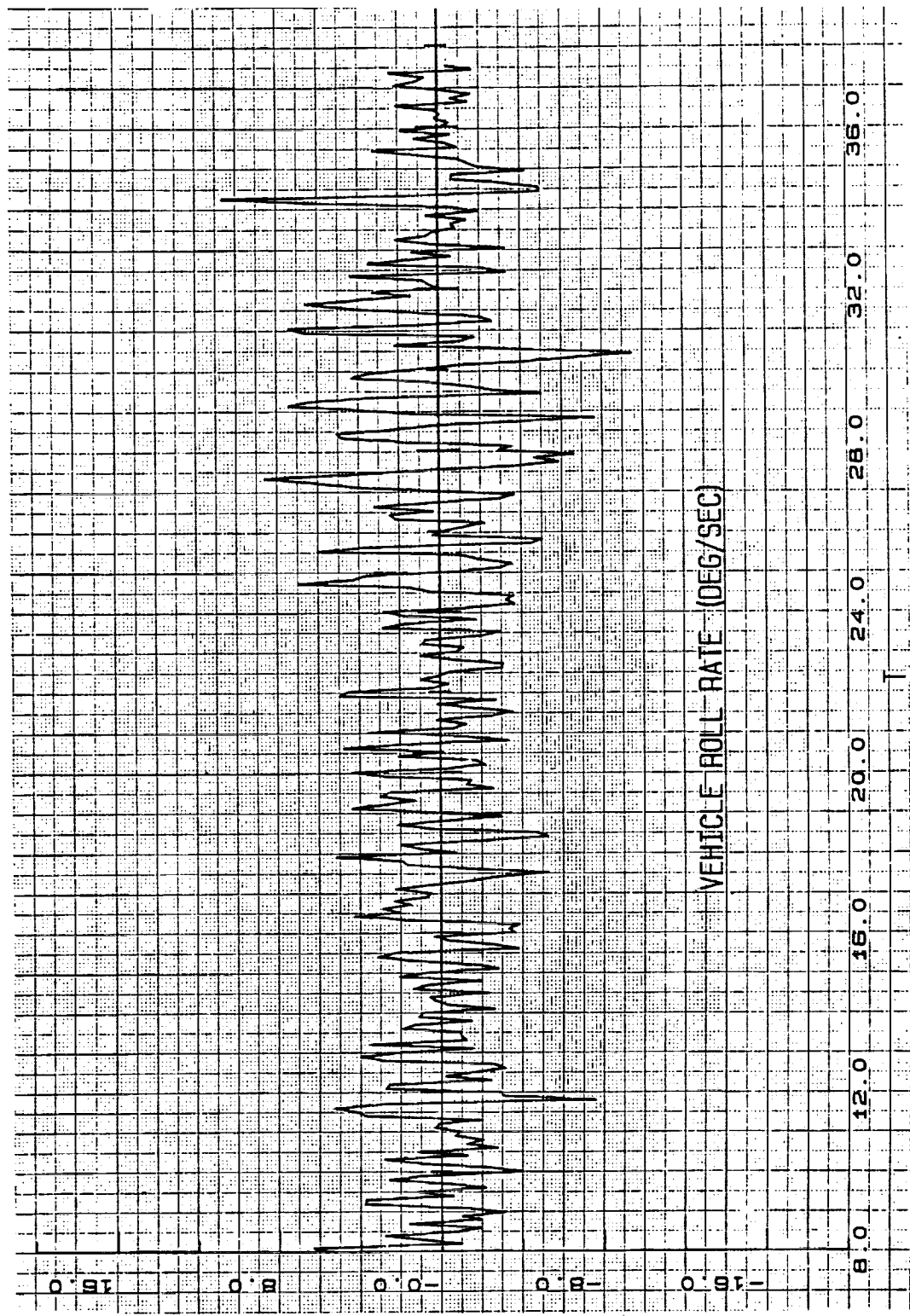
Figure 6-19 Vehicle Roll Rate in Cross Wind Turbulence

111
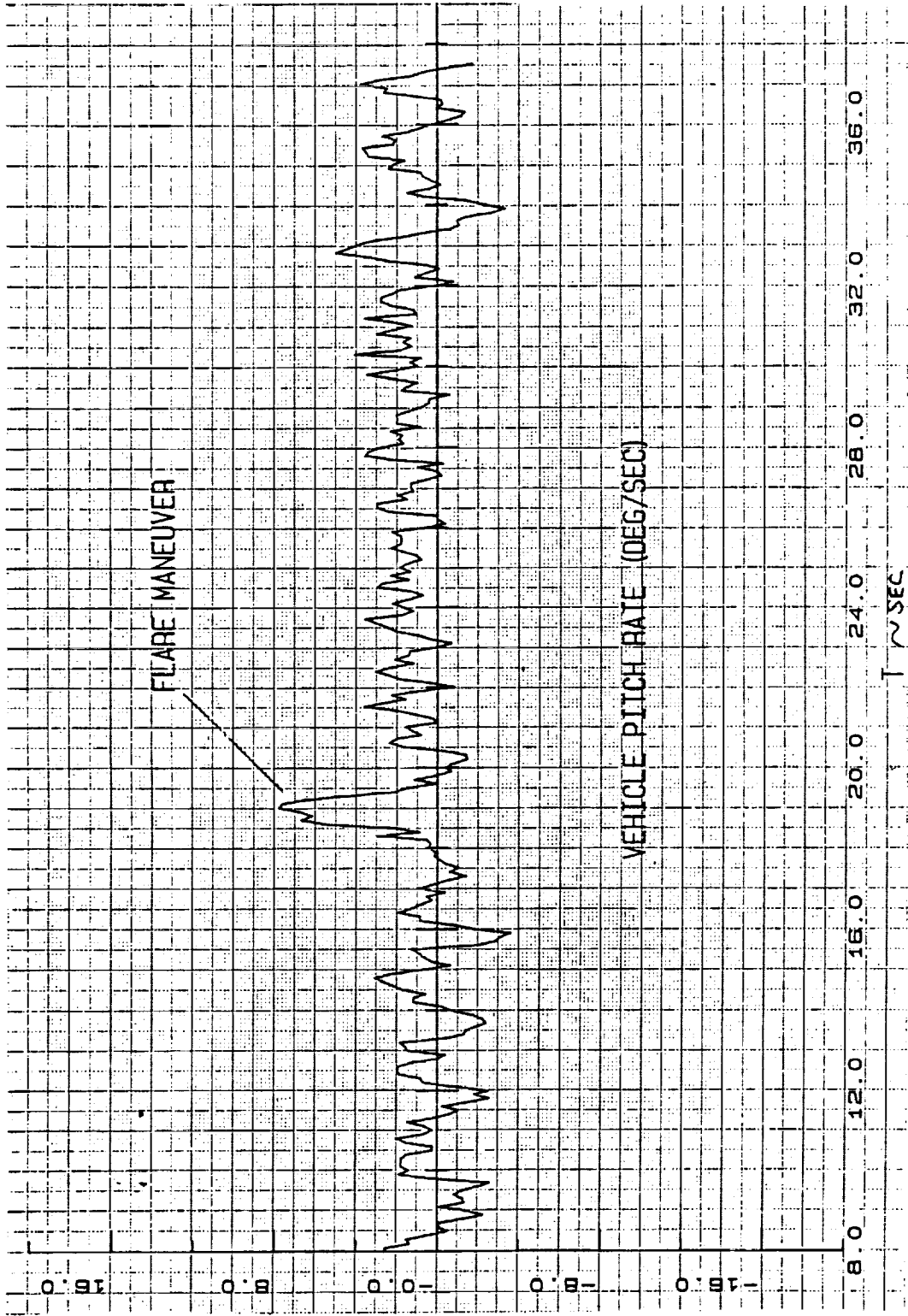
Figure 6-20 Vehicle Pitch Rate in Cross Wind Turbulence

112
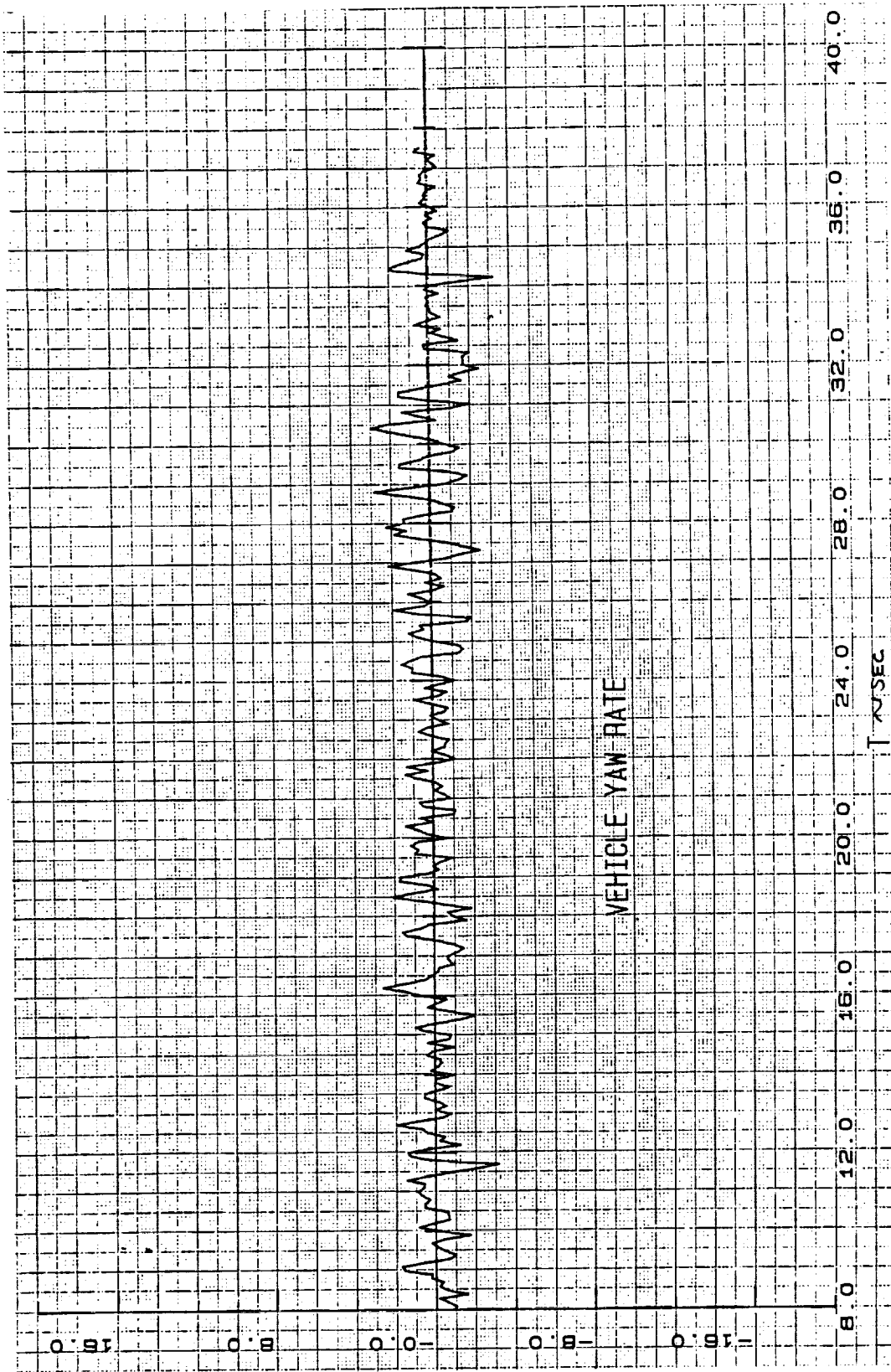
Figure 6-21 Vehicle Yaw Rate in Cross Wind Turbulence

113

6.5 Speed Control Performance

The following section describes the speed controller performance during the constant glide path angle descent phase. Simulation runs with fast and slow initial entry speed were conducted on the simulator. Figure 6-22 and 6-23 show the resulting vehicle speed response and the body flap speedbrake response. For the slow entry speed case, the speedbrake is fully close until the vehicle speed catches up with the nominal speed profile; then the speedbrake starts to open up to the 7.5 degree nominal value.

The vehicle speed responses in tail and head wind gusts are also examined. Figure 6-24 shows the wind profile used as a function of altitude. Figures 6-25 and 6-26 are the speed and speedbrake response results for the tail wind case, and figures 6-27 and 6-28 for the head wind case.
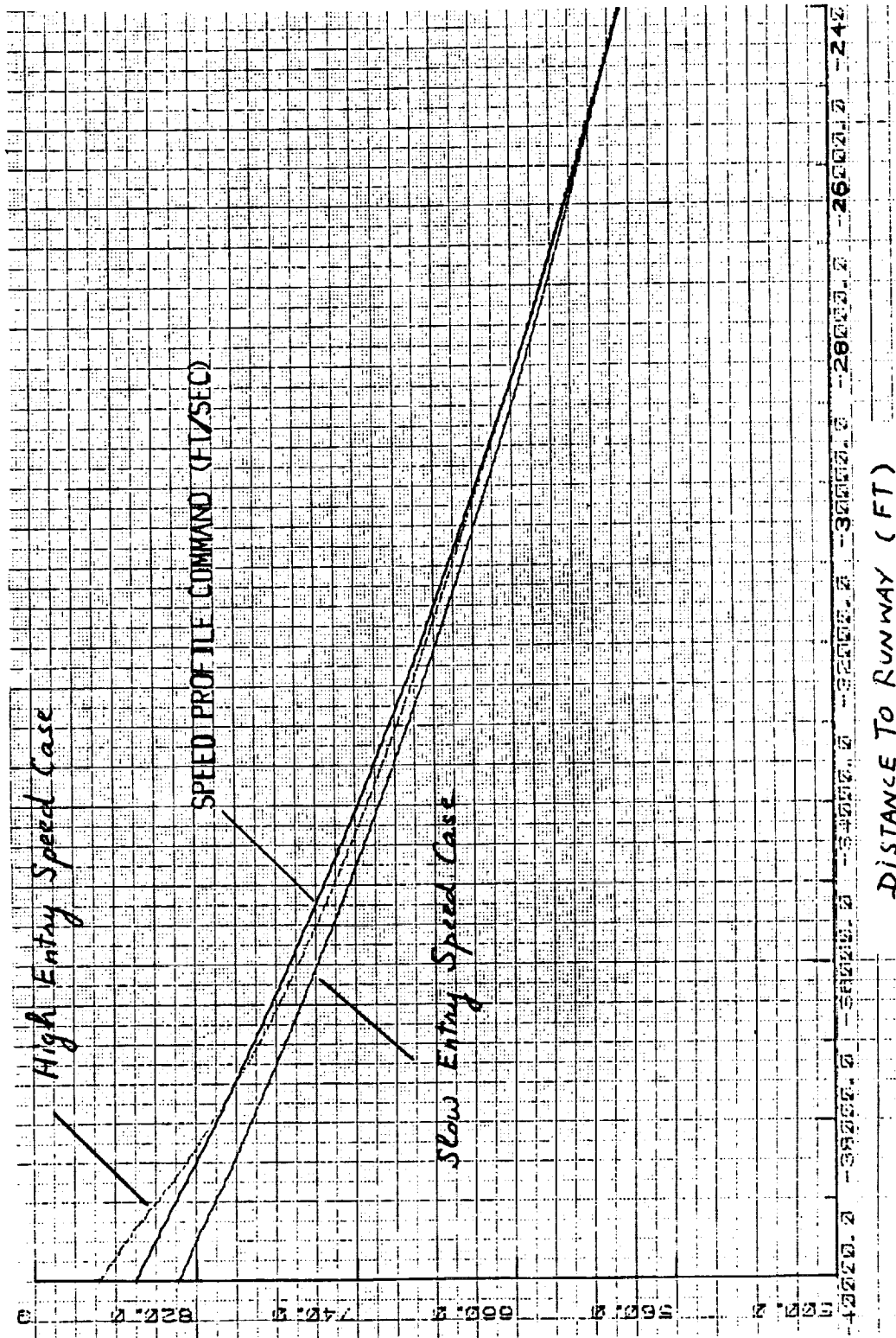
Figure 6-22 Fast and Slow Initial Entry Speed Response

115
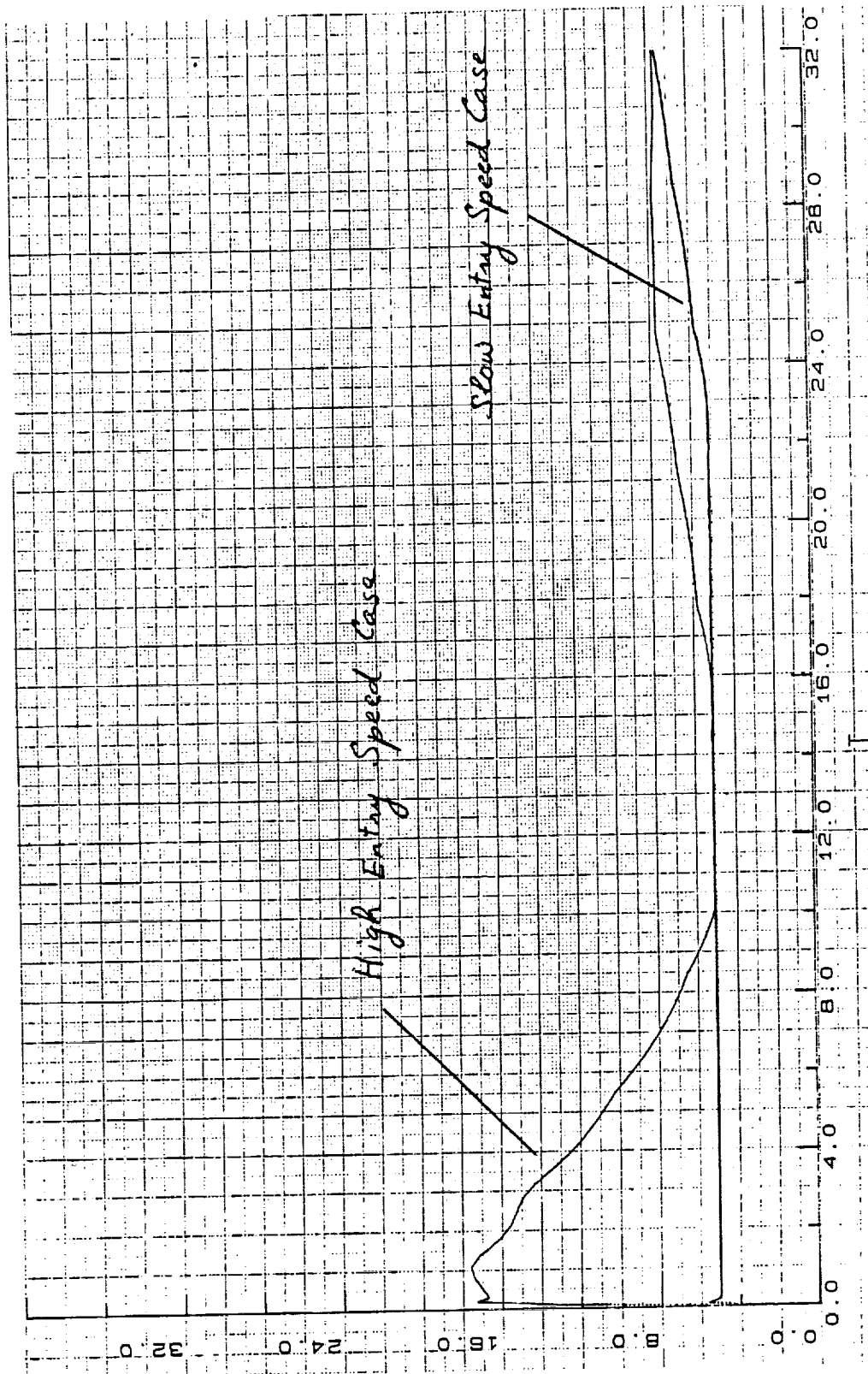
Figure 6-23 Body Flap Speedbrake Response Due to Fast and Slow Entry Speed

116
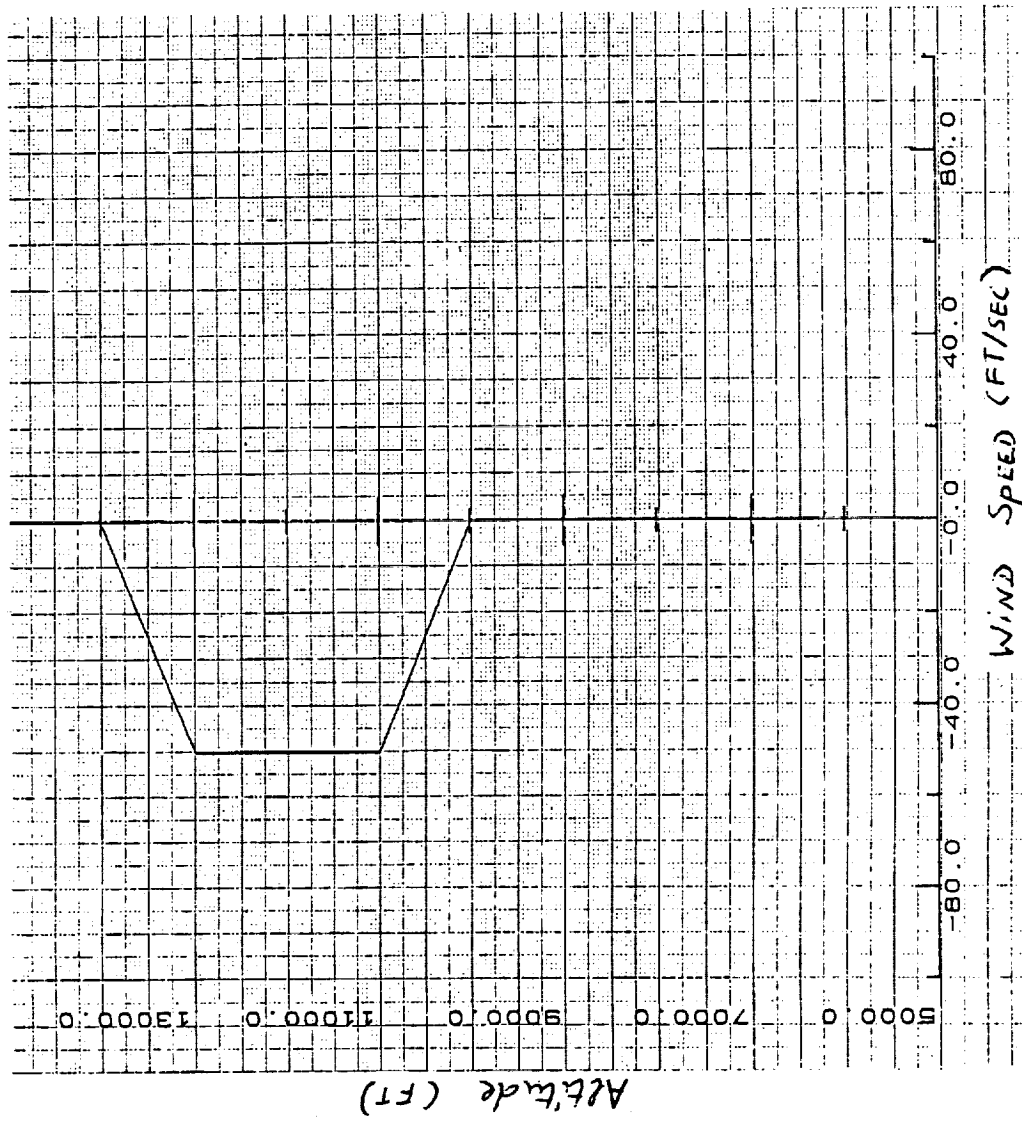
Figure 6-24 Wind Profile Used in Speed Control Test

117
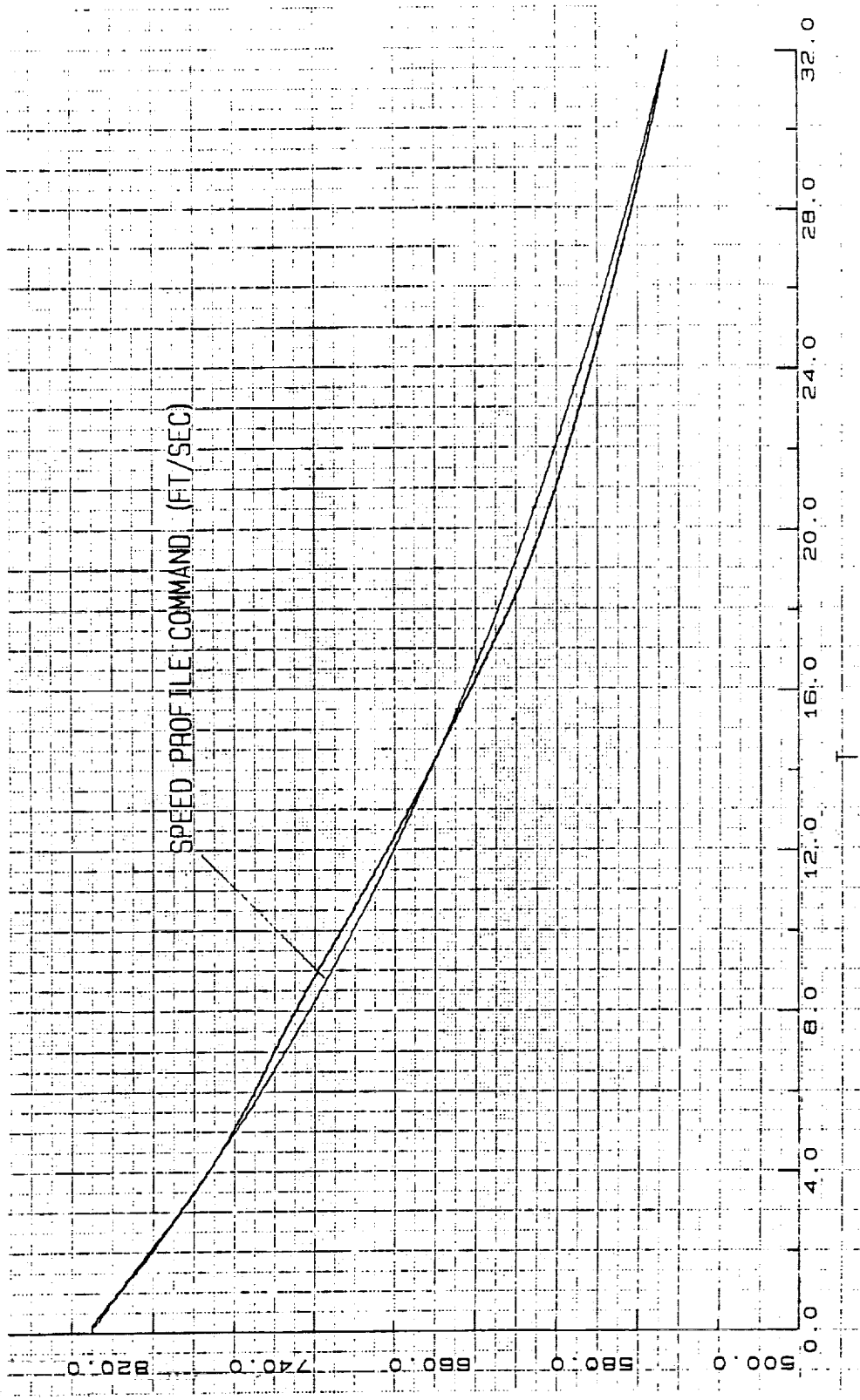
Figure 6-25 Speed Response Due to Tail Wind Gust

118
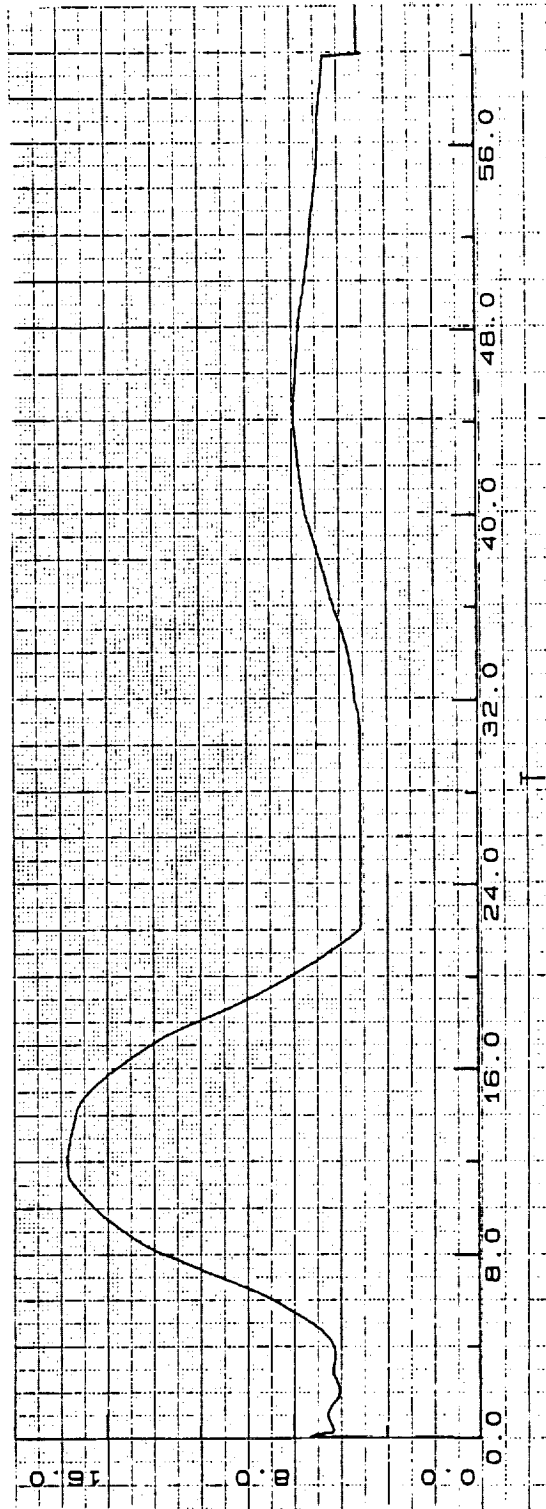
Figure 6-26 Body Flap Speedbrake Response Due to Tail Wind Gust

119
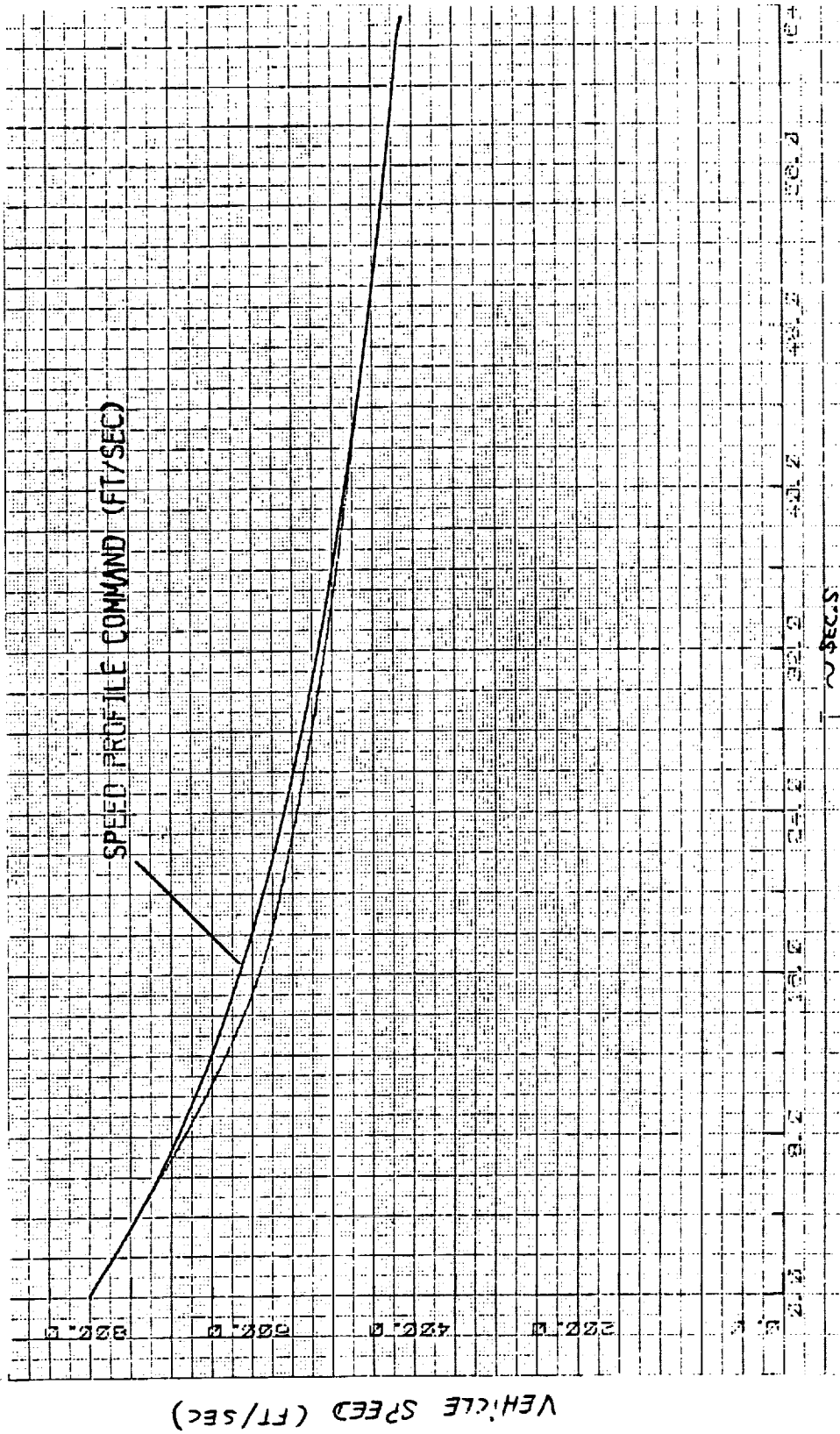
Figure 6-27 Speed Response Due to Head Wind Gust

120

Body Flap Deflections (DEG)
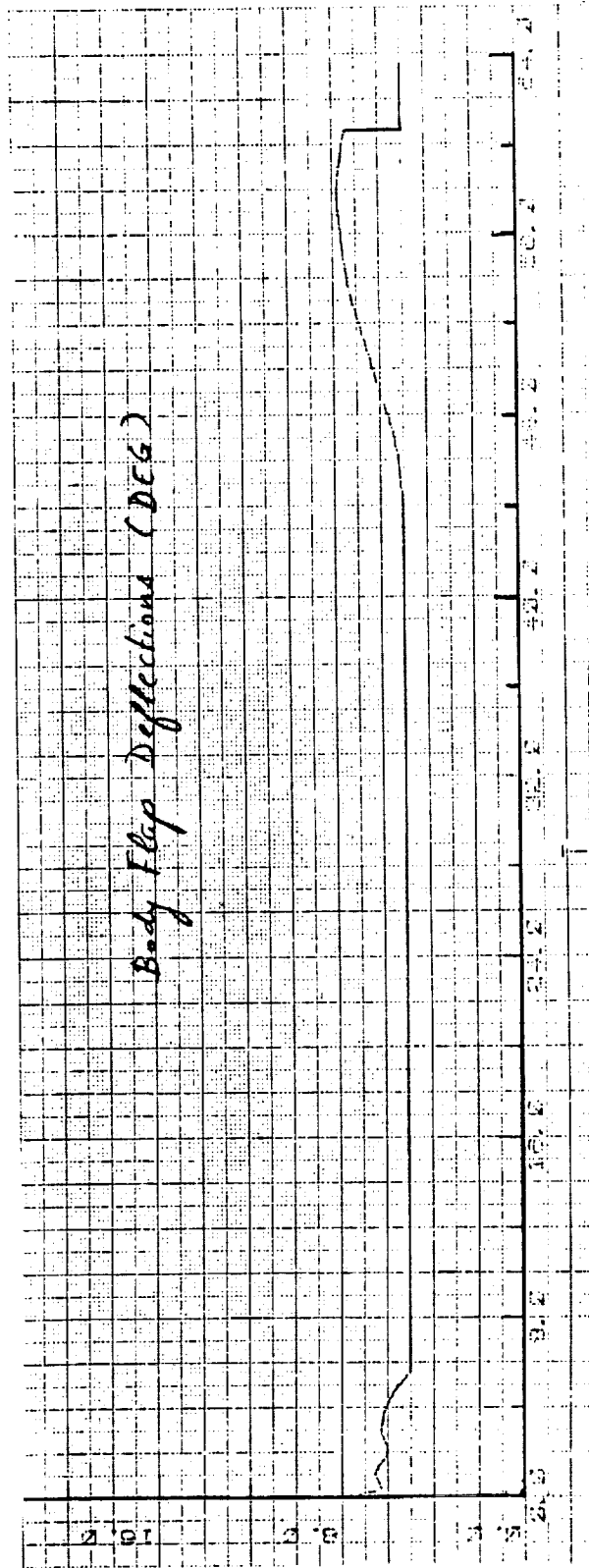
Figure 6-28 Body Flap Speedbrake Response Due to Head Wind Gust

121

7.0 Conclusion

The NASA Langley CERV configuration is a very flyable configuration for performing an autoland mission. Through further control design refinements and slight configuration tailering, the design could achieve nearly all-weather landing capability.

The control surface effectiveness is adequate with the exception of the baseline rudder (configuration No.1, see p.33) which needs to be somewhat larger for the decrab maneuver in a maximum sidewind condition. We selected for study the 60% larger all-moveable rudder (configuration No.2, see p.33) for which wind tunnel testing had been conducted. Further studies are needed to refine the actual rudder size.

Adequate landing performance has been demonstrated using a non-linear 6DOF simulation. The touchdown accuracy on sink rate, speed, and decrab heading were within the requirements. Adequate stability and control was demonstrated for wind turbulence and wind shear, for both headwind and sidewind conditions.

The required control surface actuator position and rate limits are within present state-of-the-art actuator technology. Hinge moment data needs to be developed through windtunnel testing so that the actuator load/rate requirements can be fully developed. Other portions of the flight, such as re-entry and middle course where larger hinge moment could occur, should be considered in selecting the actuator load/rate requirements and actual hardware concepts.

122

8.0 Recommendation

A feasibility study (preliminary design) has been conducted for CERV autoland and results are positive. To increase confidence in the approach, a number of configuration iterations and tailoring, along with control refinements, could be pursued.

Our recommendations include additional aerodynamic analysis and tunnel tests, including:

1) develop control surface hinge moments for use in actuator sizing

2) Conduct parametric tests for the center vertical rudder to refine the design

3) Develop landing gear and door effects on the decrab maneuver trim

4) Develop accurate pitch control effectiveness for the wing elevon. This data was estimated in the feasibility study.

Using results of these aerodynamic analyses and tests, another iteration of the control analysis and simulation studies could be conducted. The simulation would be updated with additional aerodynamic data including the hinge moments. A number of control refinements would be added and the complete autoland performance would be developed. Monte Carlo studies could then be conducted to define statistical touchdown performance.

Appendix A

AERODYNAMIC MODEL

An aerodynamic model for the CERV has been generated from the wind tunnel data provided. Force and moment equations of the model as functions of α, β and the control surfaces are described in figure A-1. The range for these variables are also listed in the figure. The nomenclature for the control surfaces are as followed: (see figure 2-2)

δ_{EU} : Upper body flaps (negative up)

δ_{EL} : Lower body flaps (positive down)

δ_{WF} : Wing flaps as ailerons (positive left trailing edge)

δ_R : Rudder (positive left trailing edge)

δ_{BFA} : Body flaps as ailerons (positive as lower right body flap down and upper left body flap up)

δ_{WFE} : Wing flaps as elevators (positive trailing edge down)

The force and moment equations are obtained by summing the forces due to the body and the incremental contributions from various control surfaces. Figure A-2 to A-8 show how these aerodynamic tables are assembled from the wind tunnel run cases. The wind tunnel data were measured at the CG, therefore, no CG transfer calculation was necessary. However, the data was converted from velocity coordinates to body axis coordinates. The resulting aerodynamic tables are shown in tables 1 thru 38.

A trim program and derivative program have also been developed. The derivatives are calculated around the trim condition. Sample derivatives at trim condition $\alpha=5^\circ$, 11° are shown in figure A-9. For these particular cases, CERV is trimmed using the wing flaps. The derivatives data are used to form the linear model for the autopilot point design analysis. Mass properties and reference area and lengths are as followed:

Weight = 11193 lbs

I_x = 6345 slug-ft^2

I_y = 13994 slug-ft^2

I_z = 17123 slug-ft^2

Reference area = 215.61 ft^2

Reference lengths: b = 12.132 ft , $\bar{c}$ = 24.583 ft

C.G is 13.275 ft from the nose or at 54% of body length

CERV AERODYNAMIC MODEL

$$CX = CX_0(\alpha,\beta) + \Delta CX_{EU}(\alpha,\delta_{EU}) + \Delta CX_{EL}(\alpha,\delta_{EL}) + \Delta CX_{WF}(\alpha,\delta_{WF}) +$$

$$\Delta CX_R(\alpha,\delta_R) + \Delta CX_{BFA}(\alpha,\delta_{BFA}) + \Delta CX_{WFE}(\alpha,\delta_{WFE})$$

$$CY = CY_0(\alpha,\beta) + \Delta CY_{EU}(\alpha,\delta_{EU}) + \Delta CY_{EL}(\alpha,\delta_{EL}) + \Delta CY_{WF}(\alpha,\delta_{WF}) +$$

$$\Delta CY_R(\alpha,\delta_R) + \Delta CY_{BFA}(\alpha,\delta_{BFA}) + 0$$

$$CZ = CZ_0(\alpha,\beta) + \Delta CZ_{EU}(\alpha,\delta_{EU}) + \Delta CZ_{EL}(\alpha,\delta_{EL}) + \Delta CZ_{WF}(\alpha,\delta_{WF}) +$$

$$\Delta CZ_R(\alpha,\delta_R) + \Delta CZ_{BFA}(\alpha,\delta_{BFA}) + \Delta CZ_{WFE}(\alpha,\delta_{WFE})$$

$$Cl = Cl_0(\alpha,\beta) + \Delta Cl_{EU}(\alpha,\delta_{EU}) + \Delta Cl_{EL}(\alpha,\delta_{EL}) + \Delta Cl_{WF}(\alpha,\delta_{WF}) +$$

$$\Delta Cl_R(\alpha,\delta_R) + \Delta Cl_{BFA}(\alpha,\delta_{BFA}) + 0$$

$$Cm = Cm_0(\alpha,\beta) + \Delta Cm_{EU}(\alpha,\delta_{EU}) + \Delta Cm_{EL}(\alpha,\delta_{EL}) + \Delta Cm_{WF}(\alpha,\delta_{WF}) +$$

$$\Delta Cm_R(\alpha,\delta_R) + \Delta Cm_{BFA}(\alpha,\delta_{BFA}) + \Delta Cm_{WFE}(\alpha,\delta_{WFE})$$

$$Cn = Cn_0(\alpha,\beta) + \Delta Cn_{EU}(\alpha,\delta_{EU}) + \Delta Cn_{EL}(\alpha,\delta_{EL}) + \Delta Cn_{WF}(\alpha,\delta_{WF}) +$$

$$\Delta Cn_R(\alpha,\delta_R) + \Delta Cn_{BFA}(\alpha,\delta_{BFA}) + 0$$

α = -10, 0, 5, 10, 12, 14, 16, 18, 20, 25, 30, 35, 40, 45, 50, 55, 60

β = -10, -5, -2, 0, 2, 5, 10

δ_{EU} = 0, -5, -10, -30

δ_{EL} = 0, 5, 10, 30

δ_{WF} = -30, -15, 0, 15, 30

δ_R = -30, -15, 0, 15, 30

δ_{BFA}= -30, 0, 30

δ_{WFE}= -30, -15, 0, 15, 30

Figure A-1 CERV Aerodynamic Model

$$CX_o(\alpha,\beta) \quad , \quad CZ_o(\alpha,\beta) \quad , \quad Cm_o(\alpha,\beta)$$

Case to use

β \ α	-10	0	5	10	12	14	16	18	20	25	30
-10											
-5	45	45	45	45	45	45	45	45	45	45	45
-2						Extrapolate					
0	46	46	46	46	46	46	46	46	46	46	46
2						Interpolate					
5	47	47	47	47	47	47	47	47	47	47	47
10						Extrapolate					

Figure A-2 CXo, CZo, Cmo Table Formation

126

$CY_o(\alpha,\beta)$, $C_{\ell o}(\alpha,\beta)$, $C_{no}(\alpha,\beta)$

Zero Data

β \ α	-10	0	5	10	12	14	16	18	20	25	30
-10											
-5	45-46	45-46	45-46	45-46	45-46	45-46	45-46	45-46	45-46	45-46	45-46
-2					Extrapolate						
0	0	0	0	0	Interpolate 0	0	0	0	0	0	0
2					Interpolate						
5	47-46	47-46	47-46	47-46	47-46	47-46	47-46	47-46	47-46	47-46	47-46
10					Extrapolate						

Figure A-3 CYo, Clo, Cno Table Formation

$$\Delta C_{XEU}, \Delta C_{YEU}, \Delta C_{ZEU}, \Delta C_{\ell EU}, \Delta C_{mEU}, \Delta C_{nEU}$$

α / δEU	-10	0	5	10	12	14	16	18	20	25	30
-30	#35-1	35-1	35-1	35-1	35-1	35-1	35-1	35-1	35-1	35-1	35-1
-10	#13-1	13-1	13-1	13-1	13-1	13-1	13-1	13-1	13-1	13-1	13-1
-5	12-1	12-1	12-1	12-1	12-1	12-1	12-1	12-1	12-1	12-1	12-1
0	0.0	0	0	0	0	0	0	0	0	0	0

← ZERO DATA

$$\Delta C_{XEL}, \Delta C_{YEL}, \Delta C_{ZEL}, \Delta C_{\ell EL}, \Delta C_{mEL}, \Delta C_{nEL}$$

α / δEL	-10	0	5	10	12	14	16	18	20	25	30
0	0.0	0	0	0	0	0	0	0	0	0	0
5	14-1	14-1	14-1	14-1	14-1	14-1	14-1	14-1	14-1	14-1	14-1
10	15-1	15-1	15-1	15-1	15-1	15-1	15-1	15-1	15-1	15-1	15-1
30	34-1	34-1	34-1	34-1	34-1	34-1	34-1	34-1	34-1	34-1	34-1

Figure A-4 ΔCXEU, ΔCYEU, ΔCZEU, ΔClEU, ΔCmEU, ΔCnEU &
CXEL, ΔCYEL, ΔCZEL, ΔClEL, ΔCmEL, ΔCnEL Table Formation

128

$$\Delta C_{X_{WF}}, \quad \Delta C_{Y_{WF}}, \quad \Delta C_{Z_{WF}}, \quad \Delta C_{l_{WF}}, \quad \Delta C_{m_{WF}}, \quad \Delta C_{n_{WF}}$$

ZERO DATA

α_{WF} / δ_{WF}	-10	0	5	10	12	14	16	18	20	25	30
-30	19-1										^
-15	18-1	---									^
0	0,0	O	O	O	O	O	O	O	O	O	O
15	16-1	---									^
30	17-1	---									^

Figure A-5 ΔCXWF, ΔCYWF, ΔCZWF, ΔClWF, ΔCmWF, ΔCnWF Table Formation

$\frac{\alpha}{\delta_R}$	-10	0	5	10	12	14	16	18	20	25	30
-30	X[51-46]										
-15	X[50-46]										
0	0	0	0								
15	50-46										
30	51-46										

ZERO DATA

where

$X = 1$ FOR ΔC_{X_R}, ΔC_{Z_R}, ΔC_{m_R}

$X = -1$ FOR ΔC_{Y_R}, ΔC_{ℓ_R}, ΔC_{n_R}

Figure A-6 ΔCXR, ΔCYR, ΔCZR, ΔClR, ΔCmR, ΔCnR Table Formation

130

BODY FLAPS for ROLL CONTROL

α / δBFA	-10	0	5	10	12	14	16	18	20	25	30
-30	X(24-i)										∨
-15											
0		O	O	O	O	O	O	O	O	O	∪
15											
30	(24-i)										∧

$X = 1$ for $\Delta C_{z_{\delta FA}}(\alpha, \delta_{BFA})$ $\Delta C_{x_{BFA}}(\alpha, \delta_{BFA})$ $\Delta C_{m_{BFA}}(\alpha, \delta_{BFA})$

$X = -1$ for $\Delta C_{Y_{BFA}}(\alpha, \delta_{BFA})$ $\Delta C_{\ell_{BFA}}(\alpha, \delta_{BFA})$ $\Delta C_{n_{BFA}}(\alpha, \delta_{BFA})$

Figure A-7 ΔCXBFA, ΔCYBFA, ΔCZBFA, ΔClBFA, ΔCmBFA, ΔCnBFA Table Formation

131

WING FLAPS FOR PITCH CONTROL

$$\Delta C_{m_{WFE}} = \frac{b}{\bar{c}} \frac{1}{\tan\Gamma} \, \Delta C_{n_{WF}}$$

$$\Delta C_{z_{WFE}} = \frac{-1}{\tan\Gamma} \, \Delta C_{Y_{WF}}$$

$$\Delta C_{x_{WFE}} = \Delta C_{x_{WF}}$$

$$\Delta C_{n_{WFE}} = 0$$

$$\Delta C_{\ell_{WFE}} = 0$$

$$\Delta C_{Y_{WFE}} = 0$$

where $\Gamma = 52°$

Figure A-8 ΔCXWFE, ΔCYWFE, ΔCZWFE, ΔClWFE, ΔCmWFE, ΔCnWFE
Table Formation

TABLE 1   CX0 (α, β)

```
B -0.083774, -0.079265, -0.077010, -0.061378, -0.053661, -0.042878,
B -0.040105, -0.025730, -0.013992,  0.024980,  0.055291,  0.040362,
B  0.070808,  0.099219,  0.104150,  0.320802,
B -0.090221, -0.081218, -0.076717, -0.060131, -0.049641, -0.042010,
B -0.030353, -0.017242, -0.004883,  0.029350,  0.057490,  0.049927,
B  0.075266,  0.107247,  0.139854,  0.160401,
B -0.094090, -0.082391, -0.076541, -0.059382, -0.047229, -0.041489,
B -0.024502, -0.012149,  0.000583,  0.031972,  0.058810,  0.055666,
B  0.077941,  0.112063,  0.161277,  0.064160,
B -0.096669, -0.083172, -0.076423, -0.058883, -0.045621, -0.041142,
B -0.020601, -0.008753,  0.004227,  0.033720,  0.059690,  0.059493,
B  0.079725,  0.115274,  0.175559,  0.000000,
B -0.087601, -0.079426, -0.075338, -0.057576, -0.046205, -0.040400,
B -0.022178, -0.009640,  0.002511,  0.032395,  0.051415,  0.057356,
B  0.078039,  0.116066,  0.162301,  0.061250,
B -0.073998, -0.073806, -0.073710, -0.055616, -0.047082, -0.039288,
B -0.024543, -0.010969, -0.000062,  0.030408,  0.039002,  0.054152,
B  0.075510,  0.117253,  0.142414,  0.153125,
B -0.051326, -0.064439, -0.070996, -0.052348, -0.048542, -0.037433,
B -0.028485, -0.013185, -0.004352,  0.027097,  0.018314,  0.048812,
B  0.071296,  0.119233,  0.109269,  0.306249,
```

TABLE 2 ΔCXEU (α, δ_{EU})

```
U  0.000000,  0.000000,  0.000000,  0.000000,  0.000000,  0.000000,
U  0.000000,  0.000000,  0.000000,  0.000000,  0.000000,  0.000000,
U  0.000000,  0.000000,  0.000000,  0.000000,  0.000000,
U  0.009949,  0.007537,  0.006331, -0.000478,  0.004189,  0.003565,
U  0.004047,  0.003407, -0.004075, -0.001848,  0.004240, -0.007211,
U -0.003752, -0.011033, -0.005735,  0.005570,  0.015208,
U  0.012337,  0.004982,  0.001305, -0.002110,  0.001757,  0.001833,
U  0.001535, -0.000536, -0.002718, -0.003685, -0.003712, -0.007130,
U -0.010321, -0.015906, -0.003778, -0.013710,  0.007385,
U -0.012583, -0.018058, -0.020796, -0.028995, -0.024731, -0.026834,
U -0.023378, -0.026607, -0.033058, -0.035004, -0.030566, -0.031741,
U -0.036410, -0.041112, -0.052216, -0.038154, -0.140867/
```

TABLE 3 ΔCXEL (α, δ_{EL})

```
L  0.000000,  0.000000,  0.000000,  0.000000,  0.000000,  0.000000,
L  0.000000,  0.000000,  0.000000,  0.000000,  0.000000,  0.000000,
L  0.000000,  0.000000,  0.000000,  0.000000,  0.000000,
L  0.016374,  0.009535,  0.006115,  0.001265,  0.005936,  0.001228,
L  0.002111,  0.004937, -0.000500, -0.002172,  0.002840, -0.005243,
L  0.000135, -0.007628, -0.009824, -0.187355, -0.140867,
L  0.015708,  0.008180,  0.004415, -0.002402,  0.000704, -0.003140,
L  0.000707,  0.000775,  0.000887, -0.002979, -0.001142, -0.008309,
L -0.006250, -0.010541, -0.011967, -0.010865,  0.001759,
L  0.006294, -0.014282, -0.024570, -0.029439, -0.025401, -0.024728,
L -0.026929, -0.025816, -0.022833, -0.023932, -0.020450, -0.021857,
L -0.031321, -0.031486, -0.034848, -0.025121, -0.140867/
```

133

TABLE 4 $\Delta\text{CXWF}(\alpha, \delta_{WF})$

```
F -0.018412,  -0.027308,  -0.031756,  -0.021001,  -0.017080,  -0.011739,
F -0.010949,  -0.012952,  -0.015334,  -0.020076,  -0.017362,  -0.012852,
F -0.012439,  -0.008153,  -0.001678,   0.007802,   0.017593,
F -0.011369,  -0.007937,  -0.006222,  -0.010240,  -0.006644,  -0.002695,
F -0.001659,  -0.004221,  -0.005353,  -0.006951,  -0.006968,  -0.012466,
F -0.004212,  -0.003347,  -0.001454,   0.005222,   0.008719,
F  0.000000,   0.000000,   0.000000,   0.000000,   0.000000,   0.000000,
F  0.000000,   0.000000,   0.000000,   0.000000,   0.000000,   0.000000,
F  0.000000,   0.000000,   0.000000,   0.000000,   0.000000,
F -0.009680,  -0.007520,  -0.006439,  -0.005387,  -0.003082,  -0.003799,
F  0.000990,  -0.005413,  -0.006682,  -0.007704,  -0.002760,  -0.005221,
F -0.002762,  -0.004692,   0.000417,   0.003460,   0.011877,
F -0.024351,  -0.025775,  -0.026487,  -0.017158,  -0.016313,  -0.016970,
F -0.009853,  -0.013087,  -0.014540,  -0.016793,  -0.015565,  -0.013463,
F -0.005388,  -0.002639,  -0.003048,  -0.007018,   0.007603/
```

TABLE 5 $\Delta\text{CXR}(\alpha, \delta_R)$

```
B -0.033682,  -0.031600,  -0.030559,  -0.033942,  -0.036193,  -0.029848,
B -0.034992,  -0.028637,  -0.031074,  -0.028227,  -0.022218,  -0.023128,
B -0.010194,  -0.008103,  -0.038535,   0.157261,   0.000000,
B -0.011806,  -0.007566,  -0.005446,  -0.013785,  -0.016809,  -0.006486,
B -0.010805,  -0.008232,  -0.003779,   0.002980,  -0.005443,  -0.003555,
B  0.009351,   0.013878,  -0.011627,   0.182762,   0.000000,
B  0.000000,   0.000000,   0.000000,   0.000000,   0.000000,   0.000000,
B  0.000000,   0.000000,   0.000000,   0.000000,   0.000000,   0.000000,
B  0.000000,   0.000000,   0.000000,   0.000000,   0.000000,
B -0.011806,  -0.007566,  -0.005446,  -0.013785,  -0.016809,  -0.006486,
B -0.010805,  -0.008232,  -0.003779,   0.002980,  -0.005443,  -0.003555,
B  0.009351,   0.013878,  -0.011627,   0.182762,   0.000000,
B -0.033682,  -0.031600,  -0.030559,  -0.033942,  -0.036193,  -0.029848,
B -0.034992,  -0.028637,  -0.031074,  -0.028227,  -0.022218,  -0.023128,
B -0.010194,  -0.008103,  -0.038535,   0.157261,   0.000000/
```

TABLE 6 $\Delta\text{CXBFA}(\alpha, \delta_{BFA})$

```
W -0.007646,  -0.019007,  -0.024687,  -0.031015,  -0.026714,  -0.020801,
W -0.022432,  -0.022473,  -0.027535,  -0.024786,  -0.022941,  -0.022512,
W -0.030824,  -0.035858,  -0.042342,  -0.032674,  -0.140867,
W  0.000000,   0.000000,   0.000000,   0.000000,   0.000000,   0.000000,
W  0.000000,   0.000000,   0.000000,   0.000000,   0.000000,   0.000000,
W  0.000000,   0.000000,   0.000000,   0.000000,   0.000000,
W -0.007646,  -0.019007,  -0.024687,  -0.031015,  -0.026714,  -0.020801,
W -0.022432,  -0.022473,  -0.027535,  -0.024786,  -0.022941,  -0.022512,
W -0.030824,  -0.035858,  -0.042342,  -0.032674,  -0.140867/
```

134

```
                           TABLE 7    CY0  (α, β)

B   0.145697,   0.150744,   0.153268,   0.165486,   0.158406,   0.136291,
B   0.164645,   0.193978,   0.157081,   0.152387,   0.144044,   0.183712,
B   0.167333,   0.206619,   0.240914,   0.202180,
B   0.072848,   0.075372,   0.076634,   0.082743,   0.079203,   0.068145,
B   0.082323,   0.096989,   0.078541,   0.076194,   0.072022,   0.091856,
B   0.083666,   0.103310,   0.120457,   0.101090,
B   0.029139,   0.030149,   0.030654,   0.033097,   0.031681,   0.027258,
B   0.032929,   0.038796,   0.031416,   0.030477,   0.028809,   0.036742,
B   0.033467,   0.041324,   0.048183,   0.040436,
B   0.000000,   0.000000,   0.000000,   0.000000,   0.000000,   0.000000,
B   0.000000,   0.000000,   0.000000,   0.000000,   0.000000,   0.000000,
B   0.000000,   0.000000,   0.000000,   0.000000,
B  -0.017565,  -0.026916,  -0.031591,  -0.026402,  -0.029141,  -0.030363,
B  -0.027623,  -0.025732,  -0.028925,  -0.030449,  -0.027337,  -0.028512,
B  -0.036763,  -0.046850,  -0.050665,  -0.044956,
B  -0.043913,  -0.067289,  -0.078977,  -0.066006,  -0.072853,  -0.075907,
B  -0.069056,  -0.064330,  -0.072311,  -0.076121,  -0.068343,  -0.071279,
B  -0.091909,  -0.117124,  -0.126663,  -0.112390,
B  -0.087825,  -0.134578,  -0.157954,  -0.132012,  -0.145706,  -0.151813,
B  -0.138113,  -0.128660,  -0.144623,  -0.152243,  -0.136686,  -0.142558,
B  -0.183817,  -0.234249,  -0.253326,  -0.224780,


                          TABLE 8   ΔCYEU (α, δEU)

U   0.000000,   0.000000,   0.000000,   0.000000,   0.000000,   0.000000,
U   0.000000,   0.000000,   0.000000,   0.000000,   0.000000,   0.000000,
U   0.000000,   0.000000,   0.000000,   0.000000,   0.000000,
U   0.042400,   0.015229,   0.001643,   0.000672,  -0.005585,  -0.003169,
U   0.002307,  -0.007911,  -0.002550,  -0.006880,  -0.002818,  -0.006047,
U  -0.003548,   0.013959,   0.006761,  -0.006292,   0.013689,
U   0.023675,   0.002451,  -0.008161,   0.001747,  -0.005727,  -0.001569,
U  -0.003329,  -0.005899,   0.003344,  -0.010304,  -0.004682,   0.008789,
U   0.004942,   0.001897,   0.013917,   0.002860,   0.021143,
U  -0.002251,   0.006055,   0.010208,   0.015119,   0.012823,   0.004671,
U   0.010311,   0.003415,   0.014418,   0.007677,   0.019767,   0.011259,
U   0.009975,   0.006245,   0.026186,   0.008073,   0.025604/


                          TABLE 9   ΔCYEL (α, δEL)

L   0.000000,   0.000000,   0.000000,   0.000000,   0.000000,   0.000000,
L   0.000000,   0.000000,   0.000000,   0.000000,   0.000000,   0.000000,
L   0.000000,   0.000000,   0.000000,   0.000000,   0.000000,
L   0.060367,   0.018232,  -0.002836,   0.001639,   0.001064,  -0.000190,
L   0.004227,  -0.003156,  -0.006818,  -0.002216,   0.000501,  -0.000740,
L   0.004444,  -0.002310,   0.002437,   0.020781,   0.025604,
L   0.030944,   0.008214,  -0.003151,   0.000518,  -0.000503,  -0.006426,
L  -0.003905,   0.005644,  -0.004448,  -0.006473,  -0.001797,  -0.004026,
L   0.001159,   0.011515,   0.012265,   0.006925,   0.011029,
L   0.064309,   0.023164,   0.002591,   0.012051,   0.015421,   0.017094,
L   0.021700,   0.011595,   0.021886,   0.017717,   0.022423,   0.023217,
L   0.013899,   0.018141,   0.012654,   0.001474,   0.025604/
```

135

TABLE 10 $\Delta CYWF$ (α, δ_{WF})

```
F -0.067789,  -0.079307,  -0.085066,  -0.078007,  -0.082157,  -0.076796,
F -0.067564,  -0.062286,  -0.050954,  -0.050637,  -0.029813,  -0.034951,
F -0.029961,  -0.015860,  -0.015993,  -0.008794,  -0.010513,
F -0.022054,  -0.042012,  -0.051991,  -0.042248,  -0.047775,  -0.044390,
F -0.041909,  -0.039295,  -0.030347,  -0.033351,  -0.013353,  -0.016815,
F -0.016156,  -0.011591,   0.012868,  -0.000541,  -0.019483,
F  0.000000,   0.000000,   0.000000,   0.000000,   0.000000,   0.000000,
F  0.000000,   0.000000,   0.000000,   0.000000,   0.000000,   0.000000,
F  0.000000,   0.000000,   0.000000,   0.000000,   0.000000,
F  0.114416,   0.070248,   0.048164,   0.049915,   0.043208,   0.036830,
F  0.037473,   0.032787,   0.036676,   0.022219,   0.020903,   0.016061,
F  0.010609,   0.030406,   0.011574,   0.013733,   0.009350,
F  0.119160,   0.101112,   0.092088,   0.084641,   0.081127,   0.076927,
F  0.065848,   0.064982,   0.057705,   0.041834,   0.035012,   0.036698,
F  0.015962,   0.037293,   0.009727,   0.019654,   0.006929/
```

TABLE 11 ΔCYR (α, δ_R)

```
B -0.121557,  -0.095711,  -0.082788,  -0.100121,  -0.095788,  -0.089544,
B -0.101648,  -0.104201,  -0.099463,  -0.104079,  -0.112143,  -0.088769,
B -0.073021,  -0.064250,  -0.081907,  -0.063673,   0.000000,
B -0.127253,  -0.070287,  -0.041804,  -0.054126,  -0.061332,  -0.053610,
B -0.066297,  -0.065672,  -0.062263,  -0.062864,  -0.074104,  -0.060339,
B -0.044557,  -0.006780,  -0.032827,  -0.005582,   0.000000,
B  0.000000,   0.000000,   0.000000,   0.000000,   0.000000,   0.000000,
B  0.000000,   0.000000,   0.000000,   0.000000,   0.000000,   0.000000,
B  0.000000,   0.000000,   0.000000,   0.000000,   0.000000,
B  0.127253,   0.070287,   0.041804,   0.054126,   0.061332,   0.053610,
B  0.066297,   0.065672,   0.062263,   0.062864,   0.074104,   0.060339,
B  0.044557,   0.006780,   0.032827,   0.005582,   0.000000,
B  0.121557,   0.095711,   0.082788,   0.100121,   0.095788,   0.089544,
B  0.101648,   0.104201,   0.099463,   0.104079,   0.112143,   0.088769,
B  0.073021,   0.064250,   0.081907,   0.063673,   0.000000/
```

TABLE 12 $\Delta CYBFA$ (α, δ_{BFA})

```
W -0.018569,  -0.009371,  -0.004772,  -0.005753,  -0.003013,  -0.005892,
W -0.020539,  -0.003103,  -0.017208,  -0.016168,  -0.020750,  -0.026383,
W -0.019994,  -0.039044,  -0.034995,  -0.022963,  -0.025604,
W  0.000000,   0.000000,   0.000000,   0.000000,   0.000000,   0.000000,
W  0.000000,   0.000000,   0.000000,   0.000000,   0.000000,   0.000000,
W  0.000000,   0.000000,   0.000000,   0.000000,   0.000000,
W  0.018569,   0.009371,   0.004772,   0.005753,   0.003013,   0.005892,
W  0.020539,   0.003103,   0.017208,   0.016168,   0.020750,   0.026383,
W  0.019994,   0.039044,   0.034995,   0.022963,   0.025604/
```

TABLE 13   CZO (α, β)

```
B   0.360005,   0.011818,  -0.162275,  -0.340066,  -0.433226,  -0.483405,
B  -0.550172,  -0.637260,  -0.712926,  -0.818836,  -0.938191,  -0.957664,
B  -1.049807,  -1.235959,  -1.304726,  -2.947199,
B   0.427070,   0.043777,  -0.147870,  -0.342627,  -0.423949,  -0.482075,
B  -0.559188,  -0.638931,  -0.716791,  -0.864254,  -0.975542,  -1.015258,
B  -1.113738,  -1.256478,  -1.403957,  -1.473599,
B   0.467309,   0.062951,  -0.139227,  -0.344164,  -0.418383,  -0.481277,
B  -0.564598,  -0.639934,  -0.719110,  -0.891504,  -0.997953,  -1.049815,
B  -1.152096,  -1.268790,  -1.463495,  -0.589440,
B   0.494135,   0.075735,  -0.133466,  -0.345188,  -0.414673,  -0.480744,
B  -0.568205,  -0.640603,  -0.720656,  -0.909671,  -1.012893,  -1.072852,
B  -1.177668,  -1.276998,  -1.503187,   0.000000,
B   0.471962,   0.069569,  -0.131628,  -0.340932,  -0.415384,  -0.485087,
B  -0.571171,  -0.647807,  -0.719224,  -0.895921,  -0.991084,  -1.059049,
B  -1.169723,  -1.276415,  -1.462823,  -0.597934,
B   0.438703,   0.060320,  -0.128872,  -0.334547,  -0.416450,  -0.491600,
B  -0.575620,  -0.658614,  -0.717076,  -0.875295,  -0.958372,  -1.038343,
B  -1.157805,  -1.275541,  -1.402275,  -1.494835,
B   0.383271,   0.044905,  -0.124278,  -0.323906,  -0.418227,  -0.502455,
B  -0.583034,  -0.676625,  -0.713497,  -0.840918,  -0.903851,  -1.003833,
B  -1.137943,  -1.274084,  -1.301363,  -2.989671,
```

TABLE 14 ΔCZEU (α, δ_{EU})

```
U   0.000000,   0.000000,   0.000000,   0.000000,   0.000000,   0.000000,
U   0.000000,   0.000000,   0.000000,   0.000000,   0.000000,   0.000000,
U   0.000000,   0.000000,   0.000000,   0.000000,   0.000000,
U   0.147860,   0.056957,   0.011505,   0.026549,   0.020336,   0.013269,
U   0.006228,   0.007365,   0.023647,   0.018988,   0.000915,   0.025363,
U   0.031079,   0.031458,   0.025479,   0.010853,  -0.001338,
U   0.083740,   0.055400,   0.041229,   0.039475,   0.039811,   0.015109,
U   0.017690,   0.016983,   0.025469,   0.036798,   0.032334,   0.025545,
U   0.033461,   0.040287,   0.020410,   0.012671,   0.005906,
U   0.188132,   0.120953,   0.087364,   0.091922,   0.110593,   0.093460,
U   0.083671,   0.091596,   0.108894,   0.108895,   0.086727,   0.066644,
U   0.086153,   0.073330,   0.086448,   0.048651,   1.456891/
```

TABLE 15   ΔCZEL (α, δ_{EL})

```
L   0.000000,   0.000000,   0.000000,   0.000000,   0.000000,   0.000000,
L   0.000000,   0.000000,   0.000000,   0.000000,   0.000000,   0.000000,
L   0.000000,   0.000000,   0.000000,   0.000000,   0.000000,
L   0.184903,   0.051152,  -0.015723,   0.003390,  -0.015292,  -0.020006,
L  -0.022216,  -0.031683,  -0.021658,  -0.007864,  -0.024498,  -0.004463,
L  -0.006142,   0.004043,   0.017715,   1.510521,   1.456891,
L   0.060991,  -0.000132,  -0.030694,  -0.024978,  -0.018917,  -0.015370,
L  -0.032379,  -0.045550,  -0.041368,  -0.021260,  -0.024370,  -0.005474,
L  -0.006838,  -0.003596,  -0.001556,   0.006624,   0.008185,
L  -0.008047,  -0.079809,  -0.115689,  -0.110863,  -0.104557,  -0.119981,
L  -0.117580,  -0.115454,  -0.110738,  -0.113227,  -0.108999,  -0.094685,
L  -0.054911,  -0.043554,  -0.020011,  -0.005203,   1.456891/
```

TABLE 16 $\Delta CZWF$ (α, δ_{WF})

```
F   0.142733,   0.057875,   0.015446,   0.014171,   0.024535,  -0.001967,
F   0.003678,  -0.001655,   0.013463,   0.035906,   0.020681,   0.018087,
F   0.013440,  -0.005766,  -0.000203,  -0.002162,   0.015294,
F   0.097409,   0.030917,  -0.002329,   0.010634,   0.011756,  -0.002479,
F  -0.005078,  -0.010871,   0.002295,   0.007379,   0.002016,   0.004292,
F   0.006590,   0.006708,   0.001678,  -0.003597,   0.025219,
F   0.000000,   0.000000,   0.000000,   0.000000,   0.000000,   0.000000,
F   0.000000,   0.000000,   0.000000,   0.000000,   0.000000,   0.000000,
F   0.000000,   0.000000,   0.000000,   0.000000,   0.000000,
F   0.106498,   0.043286,   0.011681,   0.032405,   0.019998,   0.014260,
F  -0.007548,   0.006327,   0.017258,   0.025003,   0.000816,   0.014152,
F   0.008893,  -0.002191,   0.006541,   0.011938,   0.018313,
F   0.041903,   0.014028,   0.000091,   0.012352,   0.007650,   0.008122,
F  -0.008201,  -0.008938,   0.006441,   0.020190,   0.017744,   0.018138,
F   0.007330,  -0.004644,   0.017519,  -0.002095,  -0.025129/
```

TABLE 17 ΔCZR (α, δ_R)

```
B  -0.051026,  -0.016378,   0.000946,   0.028821,   0.020485,   0.011084,
B   0.016490,   0.002720,   0.021635,   0.033873,  -0.001065,   0.018360,
B   0.029104,   0.039394,   0.125096,  -1.465608,
B   0.011572,  -0.001860,  -0.008576,   0.022165,   0.025182,   0.001094,
B   0.005604,   0.001188,   0.006646,   0.007389,   0.004627,   0.014885,
B   0.002842,   0.024662,   0.111710,  -1.495457,
B   0.000000,   0.000000,   0.000000,   0.000000,   0.000000,   0.000000,
B   0.000000,   0.000000,   0.000000,   0.000000,   0.000000,   0.000000,
B   0.000000,   0.000000,   0.000000,   0.000000,
B   0.011572,  -0.001860,  -0.008576,   0.022165,   0.025182,   0.001094,
B   0.005604,   0.001188,   0.006646,   0.007389,   0.004627,   0.014885,
B   0.002842,   0.024662,   0.111710,  -1.495457,
B  -0.051026,  -0.016378,   0.000946,   0.028821,   0.020485,   0.011084,
B   0.016490,   0.002720,   0.021635,   0.033873,  -0.001065,   0.018360,
B   0.029104,   0.039394,   0.125096,  -1.465608,
```

TABLE 18 $\Delta CZBFA$ (α, δ_{BFA})

```
W   0.053417,   0.013124,  -0.007023,  -0.017671,  -0.019754,  -0.035394,
W  -0.013441,  -0.021985,  -0.001870,   0.003286,  -0.017325,  -0.019555,
W   0.020679,   0.024901,   0.043877,   0.028226,   1.456891,
W   0.000000,   0.000000,   0.000000,   0.000000,   0.000000,   0.000000,
W   0.000000,   0.000000,   0.000000,   0.000000,   0.000000,   0.000000,
W   0.000000,   0.000000,   0.000000,   0.000000,   0.000000,
W   0.053417,   0.013124,  -0.007023,  -0.017671,  -0.019754,  -0.035394,
W  -0.013441,  -0.021985,  -0.001870,   0.003286,  -0.017325,  -0.019555,
W   0.020679,   0.024901,   0.043877,   0.028226,   1.456891/
```

TABLE 19 ΔCZWFE (α, δ_{WFE})

```
U   0.052962,   0.061961,   0.066460,   0.060945,   0.064188,   0.059999,
U   0.052786,   0.048663,   0.039809,   0.039562,   0.023292,   0.027307,
U   0.023408,   0.012391,   0.012495,   0.006871,   0.008214,
U   0.017230,   0.032823,   0.040620,   0.033008,   0.037326,   0.034681,
U   0.032743,   0.030701,   0.023710,   0.026056,   0.010432,   0.013137,
U   0.012622,   0.009056,  -0.010054,   0.000423,   0.015222,
U   0.000000,   0.000000,   0.000000,   0.000000,   0.000000,   0.000000,
U   0.000000,   0.000000,   0.000000,   0.000000,   0.000000,   0.000000,
U   0.000000,   0.000000,   0.000000,   0.000000,   0.000000,
U  -0.089391,  -0.054883,  -0.037630,  -0.038998,  -0.033758,  -0.028775,
U  -0.029277,  -0.025616,  -0.028654,  -0.017359,  -0.016331,  -0.012548,
U  -0.008288,  -0.023756,  -0.009043,  -0.010729,  -0.007305,
U  -0.093097,  -0.078997,  -0.071947,  -0.066128,  -0.063383,  -0.060102,
U  -0.051446,  -0.050769,  -0.045084,  -0.032684,  -0.027354,  -0.028671,
U  -0.012471,  -0.029136,  -0.007600,  -0.015355,  -0.005413/
```

TABLE 20   CL0 (α, β)

```
B   0.024198,   0.060467,   0.078602,   0.097711,   0.096352,   0.086037,
B   0.094903,   0.126337,   0.112495,   0.076174,   0.103795,   0.035775,
B   0.061357,   0.056537,   0.068228,   0.072046,
B   0.012099,   0.030234,   0.039301,   0.048856,   0.048176,   0.043019,
B   0.047451,   0.063169,   0.056248,   0.038087,   0.051897,   0.017887,
B   0.030678,   0.028268,   0.034114,   0.036023,
B   0.004840,   0.012093,   0.015720,   0.019542,   0.019270,   0.017207,
B   0.018981,   0.025267,   0.022499,   0.015235,   0.020759,   0.007155,
B   0.012271,   0.011307,   0.013646,   0.014409,
B   0.000000,   0.000000,   0.000000,   0.000000,   0.000000,   0.000000,
B   0.000000,   0.000000,   0.000000,   0.000000,   0.000000,   0.000000,
B   0.000000,   0.000000,   0.000000,   0.000000,
B  -0.000606,  -0.010143,  -0.014911,  -0.015477,  -0.018680,  -0.018395,
B  -0.020245,  -0.018217,  -0.016655,  -0.023058,  -0.014782,  -0.009052,
B  -0.009605,  -0.013727,  -0.009883,  -0.017997,
B  -0.001516,  -0.025357,  -0.037278,  -0.038692,  -0.046700,  -0.045989,
B  -0.050614,  -0.045543,  -0.041638,  -0.057644,  -0.036956,  -0.022631,
B  -0.024013,  -0.034317,  -0.024708,  -0.044993,
B  -0.003032,  -0.050715,  -0.074556,  -0.077385,  -0.093400,  -0.091977,
B  -0.101227,  -0.091087,  -0.083277,  -0.115288,  -0.073911,  -0.045261,
B  -0.048025,  -0.068633,  -0.049416,  -0.089986,
```

TABLE 21 ΔCLEU (α, δ_{EU})

```
U   0.000000,   0.000000,   0.000000,   0.000000,   0.000000,   0.000000,
U   0.000000,   0.000000,   0.000000,   0.000000,   0.000000,   0.000000,
U   0.000000,   0.000000,   0.000000,   0.000000,   0.000000,
U   0.011852,   0.004756,   0.001208,  -0.003100,  -0.004266,  -0.002587,
U   0.000671,  -0.006074,  -0.006608,  -0.004492,  -0.002989,   0.002553,
U  -0.000629,  -0.003406,   0.000040,   0.001680,  -0.000547,
U   0.009745,  -0.000148,  -0.005094,  -0.002726,  -0.005377,   0.000590,
U   0.001913,  -0.004338,   0.000387,  -0.008565,  -0.002592,  -0.002473,
U  -0.000342,  -0.002657,  -0.003285,   0.002729,  -0.004927,
U  -0.001886,   0.001835,   0.003695,   0.003034,   0.006160,   0.002791,
U   0.005367,  -0.002801,  -0.001075,  -0.003354,   0.009442,   0.002805,
U   0.005345,   0.004888,   0.003171,   0.002551,  -0.001622/
```

TABLE 22 ΔCLEL (α, δ_{EL})

```
L   0.000000,   0.000000,   0.000000,   0.000000,   0.000000,   0.000000,
L   0.000000,   0.000000,   0.000000,   0.000000,   0.000000,   0.000000,
L   0.000000,   0.000000,   0.000000,   0.000000,   0.000000,
L   0.022530,   0.006810,  -0.001050,  -0.003663,   0.000444,   0.000013,
L   0.004076,  -0.007128,  -0.006779,  -0.001141,  -0.003196,   0.000662,
L  -0.001459,  -0.000997,  -0.003195,   0.003795,  -0.001622,
L   0.010850,   0.003367,  -0.000375,  -0.002599,  -0.001170,  -0.003694,
L   0.000717,   0.002463,  -0.001833,  -0.005726,  -0.002203,  -0.001872,
L   0.001799,  -0.000247,   0.003220,   0.003128,  -0.008848,
L   0.022287,   0.008206,   0.001165,   0.003721,   0.007110,   0.007322,
L   0.007424,   0.006337,   0.007106,   0.005499,   0.014519,   0.007430,
L   0.006574,   0.007802,   0.001391,  -0.001713,  -0.001622/
```

TABLE 23 ΔCLWF (α, δ_{WF})

```
F  -0.054628,  -0.062415,  -0.066309,  -0.065461,  -0.066979,  -0.063218,
F  -0.049749,  -0.048834,  -0.043229,  -0.036419,  -0.014244,  -0.007932,
F  -0.000993,   0.001055,   0.004708,   0.007333,  -0.009813,
F  -0.030032,  -0.037717,  -0.041560,  -0.036562,  -0.039599,  -0.035227,
F  -0.032391,  -0.034322,  -0.028527,  -0.026170,  -0.007329,  -0.003904,
F  -0.002707,  -0.001896,  -0.003323,   0.004882,  -0.001583,
F   0.000000,   0.000000,   0.000000,   0.000000,   0.000000,   0.000000,
F   0.000000,   0.000000,   0.000000,   0.000000,   0.000000,   0.000000,
F   0.000000,   0.000000,   0.000000,   0.000000,   0.000000,
F   0.066742,   0.048335,   0.039131,   0.038964,   0.038240,   0.031190,
F   0.033815,   0.025877,   0.028226,   0.013993,   0.012336,   0.002379,
F   0.001364,   0.001584,   0.001544,   0.000856,  -0.010688,
F   0.067941,   0.071748,   0.073651,   0.066040,   0.068073,   0.064106,
F   0.055769,   0.051256,   0.045573,   0.029180,   0.014971,   0.002172,
F   0.000508,  -0.000063,  -0.002633,  -0.001967,  -0.005848/
```

TABLE 24 ΔCLR (α, δ_R)

```
B  -0.019818,  -0.009301,  -0.004042,  -0.008106,  -0.004312,  -0.001501,
B   0.000270,  -0.001999,  -0.006989,  -0.001236,  -0.023202,  -0.034867,
B  -0.035923,  -0.014458,  -0.007822,  -0.005362,
B  -0.037362,  -0.012147,   0.000460,  -0.002286,  -0.006147,  -0.004534,
B  -0.004323,  -0.010038,  -0.007188,  -0.002965,  -0.018537,  -0.028752,
B  -0.032855,  -0.023634,  -0.017802,  -0.006511,
B   0.000000,   0.000000,   0.000000,   0.000000,   0.000000,   0.000000,
B   0.000000,   0.000000,   0.000000,   0.000000,   0.000000,   0.000000,
B   0.000000,   0.000000,   0.000000,   0.000000,
B   0.037362,   0.012147,  -0.000460,   0.002286,   0.006147,   0.004534,
B   0.004323,   0.010038,   0.007188,   0.002965,   0.018537,   0.028752,
B   0.032855,   0.023634,   0.017802,   0.006511,
B   0.019818,   0.009301,   0.004042,   0.008106,   0.004312,   0.001501,
B  -0.000270,   0.001999,   0.006989,   0.001236,   0.023202,   0.034867,
B   0.035923,   0.014458,   0.007822,   0.005362,
```

TABLE 25 ΔCLBFA (α, δ_{BFA})

```
W   0.017541,   0.016992,   0.016718,   0.020160,   0.018841,   0.019287,
W   0.016558,   0.023380,   0.018022,   0.020491,   0.019296,   0.012483,
W   0.015608,   0.013082,   0.015034,   0.003013,   0.001622,
W   0.000000,   0.000000,   0.000000,   0.000000,   0.000000,   0.000000,
W   0.000000,   0.000000,   0.000000,   0.000000,   0.000000,   0.000000,
W   0.000000,   0.000000,   0.000000,   0.000000,   0.000000,
W  -0.017541,  -0.016992,  -0.016718,  -0.020160,  -0.018841,  -0.019287,
W  -0.016558,  -0.023380,  -0.018022,  -0.020491,  -0.019296,  -0.012483,
W  -0.015608,  -0.013082,  -0.015034,  -0.003013,  -0.001622/
```

TABLE 26   CM0 (α, β)

```
B   0.046378,   0.026062,   0.015904,   0.007432,   0.004341,   0.002487,
B  -0.002278,  -0.006152,  -0.010247,  -0.008652,  -0.009112,  -0.004697,
B  -0.008303,  -0.019344,  -0.027056,  -0.007038,
B   0.045195,   0.026341,   0.016914,   0.007046,   0.003668,   0.001252,
B  -0.003140,  -0.007069,  -0.011389,  -0.014639,  -0.016245,  -0.012736,
B  -0.016671,  -0.020568,  -0.017170,  -0.003519,
B   0.044485,   0.026508,   0.017520,   0.006814,   0.003264,   0.000510,
B  -0.003658,  -0.007619,  -0.012074,  -0.018231,  -0.020525,  -0.017559,
B  -0.021692,  -0.021302,  -0.011238,  -0.001408,
B   0.044012,   0.026620,   0.017924,   0.006660,   0.002994,   0.000016,
B  -0.004003,  -0.007985,  -0.012531,  -0.020626,  -0.023378,  -0.020775,
B  -0.025039,  -0.021792,  -0.007284,   0.000000,
B   0.043195,   0.026196,   0.017696,   0.006544,   0.003013,  -0.000089,
B  -0.004326,  -0.008487,  -0.012337,  -0.019218,  -0.020223,  -0.019294,
B  -0.025725,  -0.023420,  -0.010226,  -0.001417,
B   0.041969,   0.025559,   0.017354,   0.006369,   0.003040,  -0.000247,
B  -0.004811,  -0.009240,  -0.012045,  -0.017106,  -0.015491,  -0.017072,
B  -0.026755,  -0.025861,  -0.014640,  -0.003544,
B   0.039926,   0.024498,   0.016784,   0.006078,   0.003086,  -0.000511,
B  -0.005619,  -0.010495,  -0.011559,  -0.013586,  -0.007604,  -0.013369,
B  -0.028471,  -0.029930,  -0.021996,  -0.007087,
```

TABLE 27 ΔCMEU (α, δ_{EU})

```
U   0.000000,   0.000000,   0.000000,   0.000000,   0.000000,   0.000000,
U   0.000000,   0.000000,   0.000000,   0.000000,   0.000000,   0.000000,
U   0.000000,   0.000000,   0.000000,   0.000000,   0.000000,
U   0.011149,   0.006449,   0.004099,   0.005818,   0.005581,   0.004224,
U   0.004081,   0.003996,   0.005488,   0.005710,   0.002516,   0.008213,
U   0.005749,   0.007077,   0.010758,   0.003887,   0.000325,
U   0.010092,   0.009300,   0.008904,   0.008185,   0.009187,   0.008060,
U   0.008023,   0.007515,   0.008846,   0.010793,   0.010794,   0.008711,
U   0.010611,   0.010014,   0.011550,   0.007360,   0.002145,
U   0.027163,   0.026657,   0.026404,   0.024845,   0.027305,   0.025486,
U   0.025781,   0.024757,   0.028624,   0.030321,   0.030727,   0.026063,
U   0.027205,   0.025017,   0.029498,   0.014064,   0.000198/
```

TABLE 28 ΔCMEL (α, δ_{EL})

```
L   0.000000,   0.000000,   0.000000,   0.000000,   0.000000,   0.000000,
L   0.000000,   0.000000,   0.000000,   0.000000,   0.000000,   0.000000,
L   0.000000,   0.000000,   0.000000,   0.000000,   0.000000,
L   0.004738,  -0.001100,  -0.004019,  -0.003297,  -0.003253,  -0.004088,
L  -0.003716,  -0.004676,  -0.003766,  -0.003182,  -0.005444,  -0.002230,
L  -0.001838,  -0.001851,   0.003202,   0.003673,   0.000198,
L  -0.007478,  -0.008608,  -0.009173,  -0.009336,  -0.008302,  -0.007256,
L  -0.008609,  -0.009834,  -0.009680,  -0.007136,  -0.007996,  -0.005115,
L  -0.005088,  -0.004080,   0.004263,  -0.002127,  -0.002547,
L  -0.029444,  -0.029763,  -0.029923,  -0.028861,  -0.028171,  -0.029727,
L  -0.029641,  -0.029282,  -0.027874,  -0.026922,  -0.026789,  -0.025612,
L  -0.015280,  -0.012172,  -0.007503,  -0.012771,   0.000198/
```

TABLE 29 ΔCMWF (α, δ_{WF})

```
F   0.011696,   0.008862,   0.007445,   0.007353,   0.007727,   0.005724,
F   0.005954,   0.007485,   0.008287,   0.013436,   0.010178,   0.006611,
F   0.004765,   0.000839,   0.006634,   0.000908,   0.000135,
F  -0.003962,  -0.000198,   0.001684,   0.001423,   0.002457,   0.001123,
F   0.000503,   0.001756,   0.002945,   0.007492,   0.004271,   0.003600,
F   0.003199,   0.000564,   0.001494,   0.002037,   0.001135,
F   0.000000,   0.000000,   0.000000,   0.000000,   0.000000,   0.000000,
F   0.000000,   0.000000,   0.000000,   0.000000,   0.000000,   0.000000,
F   0.000000,   0.000000,   0.000000,   0.000000,   0.000000,
F   0.005013,   0.003975,   0.003456,   0.004769,   0.005824,   0.003568,
F   0.002766,   0.002855,   0.004702,   0.006054,   0.001839,   0.003319,
F   0.003407,   0.000612,   0.003850,   0.003100,   0.002285,
F  -0.006320,   0.000768,   0.004312,   0.004285,   0.005047,   0.003990,
F   0.003461,   0.004302,   0.006653,   0.010486,   0.007985,   0.006207,
F   0.004660,   0.001934,   0.006239,   0.002301,  -0.000401/
```

TABLE 30 ΔCMR (α, δ_R)

```
B   0.007232,   0.005732,   0.004982,   0.007927,   0.007788,   0.006520,
B   0.007743,   0.005624,   0.008924,   0.007598,   0.006310,   0.013242,
B   0.014736,   0.015006,   0.001379,   0.009011,
B   0.006881,   0.001657,  -0.000955,   0.000802,   0.000577,   0.000472,
B   0.000356,   0.001472,  -0.000095,  -0.000317,   0.001694,   0.004740,
B   0.002103,   0.000987,  -0.011218,  -0.001394,
B   0.000000,   0.000000,   0.000000,   0.000000,   0.000000,   0.000000,
B   0.000000,   0.000000,   0.000000,   0.000000,   0.000000,   0.000000,
B   0.000000,   0.000000,   0.000000,   0.000000,
B   0.006881,   0.001657,  -0.000955,   0.000802,   0.000577,   0.000472,
B   0.000356,   0.001472,  -0.000095,  -0.000317,   0.001694,   0.004740,
B   0.002103,   0.000987,  -0.011218,  -0.001394,
B   0.007232,   0.005732,   0.004982,   0.007927,   0.007788,   0.006520,
B   0.007743,   0.005624,   0.008924,   0.007598,   0.006310,   0.013242,
B   0.014736,   0.015006,   0.001379,   0.009011,
```

TABLE 31 ΔCMBFA (α, δ_{BFA})

```
W -0.005201, -0.003227, -0.002240, -0.003011, -0.002370, -0.003214,
W -0.001429, -0.001927, -0.000010,  0.004228,  0.002519,  0.001381,
W  0.005392,  0.005594,  0.015781,  0.002345,  0.000198,
W  0.000000,  0.000000,  0.000000,  0.000000,  0.000000,  0.000000,
W  0.000000,  0.000000,  0.000000,  0.000000,  0.000000,  0.000000,
W  0.000000,  0.000000,  0.000000,  0.000000,  0.000000,
W -0.005201, -0.003227, -0.002240, -0.003011, -0.002370, -0.003214,
W -0.001429, -0.001927, -0.000010,  0.004228,  0.002519,  0.001381,
W  0.005392,  0.005594,  0.015781,  0.002345,  0.000198/
```

TABLE 32 ΔCMWFE (α, δ_{WFE})

```
B  0.028695,  0.027940,  0.027563,  0.025704,  0.025451,  0.024534,
B  0.021919,  0.021268,  0.017823,  0.017617,  0.012096,  0.011973,
B  0.010502,  0.007056,  0.007655,  0.002302,  0.000553,
B  0.015394,  0.016256,  0.016687,  0.015904,  0.016285,  0.014921,
B  0.013859,  0.012676,  0.010291,  0.009126,  0.005758,  0.007155,
B  0.004807,  0.004445,  0.003892,  0.002490,  0.002631,
B  0.000000,  0.000000,  0.000000,  0.000000,  0.000000,  0.000000,
B  0.000000,  0.000000,  0.000000,  0.000000,  0.000000,  0.000000,
B  0.000000,  0.000000,  0.000000,  0.000000,  0.000000,
B -0.023021, -0.019099, -0.017139, -0.015869, -0.015315, -0.013159,
B -0.012719, -0.009698, -0.012371, -0.009901, -0.007620, -0.003469,
B -0.005421, -0.005403, -0.001016, -0.005093, -0.004638,
B -0.029975, -0.030430, -0.030658, -0.027058, -0.027189, -0.024436,
B -0.021551, -0.020885, -0.019780, -0.016916, -0.013709, -0.009418,
B -0.009035, -0.009791, -0.003731, -0.008100, -0.000904/
```

TABLE 33 CNO (α, β)

```
B -0.030445, -0.041865, -0.047575, -0.048654, -0.047172, -0.038604,
B -0.044259, -0.046001, -0.044440, -0.025409, -0.021678,  0.006026,
B  0.024944, -0.015041, -0.015411, -0.025452,
B -0.015223, -0.020932, -0.023787, -0.024327, -0.023586, -0.019302,
B -0.022130, -0.023000, -0.022220, -0.012704, -0.010839,  0.003013,
B  0.012472, -0.007520, -0.007706, -0.012726,
B -0.006089, -0.008373, -0.009515, -0.009731, -0.009434, -0.007721,
B -0.008852, -0.009200, -0.008888, -0.005082, -0.004336,  0.001205,
B  0.004989, -0.003008, -0.003082, -0.005090,
B  0.000000,  0.000000,  0.000000,  0.000000,  0.000000,  0.000000,
B  0.000000,  0.000000,  0.000000,  0.000000,  0.000000,  0.000000,
B  0.000000,  0.000000,  0.000000,  0.000000,
B  0.007779,  0.008395,  0.008703,  0.007407,  0.009274,  0.008424,
B  0.008761,  0.008840,  0.007765,  0.007339,  0.004021,  0.002095,
B  0.005725,  0.004467,  0.002126,  0.005012,
B  0.019447,  0.020987,  0.021757,  0.018517,  0.023184,  0.021059,
B  0.021902,  0.022100,  0.019413,  0.018348,  0.010052,  0.005238,
B  0.014312,  0.011168,  0.005316,  0.012531,
B  0.038893,  0.041973,  0.043513,  0.037034,  0.046368,  0.042118,
B  0.043805,  0.044199,  0.038826,  0.036695,  0.020103,  0.010476,
B  0.028625,  0.022337,  0.010631,  0.025062,
```

TABLE 34 ΔCNEU (α, δ_{EU})

```
U  0.000000,  0.000000,  0.000000,  0.000000,  0.000000,  0.000000,
U  0.000000,  0.000000,  0.000000,  0.000000,  0.000000,  0.000000,
U  0.000000,  0.000000,  0.000000,  0.000000,  0.000000,
U -0.011026, -0.005221, -0.002318,  0.002075,  0.002782,  0.001419,
U -0.002758,  0.005574, -0.003961,  0.000034,  0.003505,  0.004681,
U  0.001890, -0.000058,  0.000582, -0.004180, -0.006326,
U -0.004527,  0.000615,  0.003185, -0.001587,  0.002199,  0.000595,
U -0.001578,  0.005600, -0.004437,  0.002454,  0.002135,  0.004100,
U  0.000029, -0.003194,  0.000378,  0.000810,  0.000410,
U -0.000257, -0.003894, -0.005712, -0.003797, -0.003788, -0.001922,
U -0.003895, -0.002000, -0.006623,  0.001177, -0.001792,  0.004124,
U -0.000677, -0.008027,  0.000446, -0.007699, -0.004180/
```

TABLE 35 ΔCNEL (α, δ_{EL})

```
L  0.000000,  0.000000,  0.000000,  0.000000,  0.000000,  0.000000,
L  0.000000,  0.000000,  0.000000,  0.000000,  0.000000,  0.000000,
L  0.000000,  0.000000,  0.000000,  0.000000,  0.000000,
L -0.017525, -0.005123,  0.001078,  0.000178, -0.000534,  0.001293,
L -0.003541,  0.001939, -0.000205,  0.003223, -0.002268,  0.003791,
L  0.000011,  0.002530,  0.001439, -0.004819, -0.004180,
L -0.008328, -0.003248, -0.000708,  0.001414,  0.001205,  0.002711,
L  0.000131,  0.000590, -0.000942,  0.001208, -0.000533,  0.002253,
L  0.000418, -0.001356,  0.001670, -0.003461,  0.006784,
L -0.011825, -0.006394, -0.003679, -0.003205, -0.002744, -0.003102,
L -0.005108, -0.002828, -0.008958, -0.002424, -0.005162,  0.000074,
L -0.000430, -0.005784,  0.001562, -0.000382, -0.004180/
```

TABLE 36 ΔCNWF (α, δ_{WF})

```
F  0.074422,  0.072466,  0.071488,  0.066667,  0.066011,  0.063632,
F  0.056850,  0.055161,  0.046226,  0.045691,  0.031373,  0.031053,
F  0.027237,  0.018302,  0.019854,  0.005971,  0.001433,
F  0.039925,  0.042161,  0.043279,  0.041249,  0.042238,  0.038700,
F  0.035946,  0.032878,  0.026690,  0.023668,  0.014934,  0.018556,
F  0.012467,  0.011529,  0.010094,  0.006458,  0.006823,
F  0.000000,  0.000000,  0.000000,  0.000000,  0.000000,  0.000000,
F  0.000000,  0.000000,  0.000000,  0.000000,  0.000000,  0.000000,
F  0.000000,  0.000000,  0.000000,  0.000000,  0.000000,
F -0.059707, -0.049537, -0.044452, -0.041160, -0.039721, -0.034129,
F -0.032990, -0.025152, -0.032087, -0.025680, -0.019764, -0.008996,
F -0.014059, -0.014013, -0.002634, -0.013210, -0.012028,
F -0.077743, -0.078925, -0.079516, -0.070179, -0.070517, -0.063377,
F -0.055896, -0.054167, -0.051303, -0.043873, -0.035556, -0.024428,
F  -0.023435, -0.025394, -0.009676, -0.021009, -0.002344/
```

TABLE 37 ΔCNR (α, δ_R)

```
B   0.067871,   0.065661,   0.064557,   0.068952,   0.067912,   0.067702,
B   0.068871,   0.068571,   0.072521,   0.073280,   0.078653,   0.076386,
B   0.061588,   0.051056,   0.042780,   0.027523,
B   0.054461,   0.042259,   0.036157,   0.037343,   0.042267,   0.039087,
B   0.043373,   0.041898,   0.044401,   0.043737,   0.050238,   0.051275,
B   0.043764,   0.037586,   0.034818,   0.023518,
B   0.000000,   0.000000,   0.000000,   0.000000,   0.000000,   0.000000,
B   0.000000,   0.000000,   0.000000,   0.000000,   0.000000,   0.000000,
B   0.000000,   0.000000,   0.000000,   0.000000,
B  -0.054461,  -0.042259,  -0.036157,  -0.037343,  -0.042267,  -0.039087,
B  -0.043373,  -0.041898,  -0.044401,  -0.043737,  -0.050238,  -0.051275,
B  -0.043764,  -0.037586,  -0.034818,  -0.023518,
B  -0.067871,  -0.065661,  -0.064557,  -0.068952,  -0.067912,  -0.067702,
B  -0.068871,  -0.068571,  -0.072521,  -0.073280,  -0.078653,  -0.076386,
B  -0.061588,  -0.051056,  -0.042780,  -0.027523,
```

TABLE 38 ΔCNBFA $(\alpha, \delta_{\beta FA})$

```
W  -0.003340,  -0.000054,   0.001589,   0.000668,  -0.000634,   0.002387,
W   0.005257,  -0.001778,   0.005632,  -0.001258,  -0.000561,  -0.004677,
W  -0.001133,   0.007019,  -0.005245,   0.011070,   0.004180,
W   0.000000,   0.000000,   0.000000,   0.000000,   0.000000,   0.000000,
W   0.000000,   0.000000,   0.000000,   0.000000,   0.000000,   0.000000,
W   0.000000,   0.000000,   0.000000,   0.000000,   0.000000,
W   0.003340,   0.000054,  -0.001589,  -0.000668,   0.000634,  -0.002387,
W  -0.005257,   0.001778,  -0.005632,   0.001258,   0.000561,   0.004677,
W   0.001133,  -0.007019,   0.005245,  -0.011070,  -0.004180/
```

C

145

```
1 ALPHA=  5.00       PITCHING MOMENT TRIM
  COEFF   DEL=  5.00      DEU=  -5.00     DWFE=  15.96

DERIVATIVE WITH RESPECT TO  (NON ALPHA)
         BETA       DEU        DEL        WF        RUD        BFA        WFE
CX   0.000301 -0.005833 -0.001449 -0.000007  0.000000  0.000000 -0.001337
CY  -0.015561 -0.002228  0.000287  0.003339  0.002787  0.000159
CZ   0.001900  0.056129 -0.004250  0.000467  0.000000  0.000000 -0.002288
CL  -0.007658 -0.002255  0.000077  0.002690 -0.000031 -0.000557
CM   0.000044  0.014556 -0.001037  0.000059  0.000000  0.000000 -0.001826
CN   0.004554  0.000312 -0.000149 -0.002924 -0.002410 -0.000053


DERIVATIVE WITH RESPECT TO ALPHA
         BOD   +   DEU   +   DEL   +   WF   +   RUD   +   BFA   +   WFE
CX   0.002429 -0.000833 -0.001206  0.000000  0.000000  0.000000  0.000255
CY   0.000000  0.000245 -0.000880  0.000000  0.000000  0.000000
CZ  -0.042092 -0.002016 -0.002685  0.000000  0.000000  0.000000  0.001569
CL   0.000000 -0.000136 -0.000549  0.000000  0.000000  0.000000
CM  -0.001996 -0.000134 -0.000020  0.000000  0.000000  0.000000  0.000656
CN   0.000000 -0.000146  0.000419  0.000000  0.000000  0.000000

--------------------------------------------------------------------------
1 ALPHA=  11.00      PITCHING MOMENT TRIM
  COEFF   DEL=  5.00      DEU=  -5.00     DWFE=   6.98

DERIVATIVE WITH RESPECT TO  (NON ALPHA)
         BETA       DEU        DEL        WF        RUD        BFA        WFE
CX   0.000354  0.000849 -0.000890  0.000140  0.000000  0.000000 -0.000282
CY  -0.015040 -0.002225 -0.000269  0.003052  0.003849  0.000146
CZ   0.000779  0.031464 -0.003199  0.000500  0.000000  0.000000 -0.002425
CL  -0.009121 -0.003865 -0.000055  0.002556  0.000281 -0.000650
CM  -0.000065  0.007178 -0.001109  0.000112  0.000000  0.000000 -0.002106
CN   0.004481  0.001377  0.000298 -0.002739 -0.002654 -0.000001


DERIVATIVE WITH RESPECT TO ALPHA
         BOD   +   DEU   +   DEL   +   WF   +   RUD   +   BFA   +   WFE
CX   0.006631  0.002135  0.001948  0.000000  0.000000  0.000000  0.000536
CY   0.000000 -0.003430 -0.000398  0.000000  0.000000  0.000000
CZ  -0.034743 -0.001485 -0.003215  0.000000  0.000000  0.000000  0.001218
CL   0.000000 -0.000951  0.001390  0.000000  0.000000  0.000000
CM  -0.001833  0.000188  0.000267  0.000000  0.000000 , 0.000000  0.000261
CN   0.000000  0.001116 -0.000231  0.000000  0.000000  0.000000
```

Figure A-9 Sample Derivative Data at Trim Condition $\alpha=5^{\circ}$, 11°

Appendix B

6DOF NON-LINEAR SIMULATION

The computer resources used in the 6DOF simulation are shown in figure B-1. The non-linear equations of motion are hosted on the AD100. The autopilot and other slower processes are hosted on the Harris 1000. The CERV simulation runs three times real time. Figure B-2 shows the CERV simulation functional block diagram. The major blocks consist of the autopilot, guidance, 6DOF equations of motion, actuator models, rate gyro models, and the gain computer. The autopilot operates at a 20 ms cycle, with a 10 ms computational delay. Autopilot gains are updated from the gain computer every 120 ms. Perfect knowledge of α, β and ϕ is assumed and used as feedback signals. Autopilot fin commands are fed to a mixer set equations to obtain the proper command to the actuators. The actual fin positions are then un-mixed before going to the aerodynamic model. A block diagram of the mixer sets is shown in figure B-3. The actuators are modeled as a second order filter with a 10 hz bandwidth and 0.5 damping, and a rate limit of 200 degrees/sec.

The guidance operates at a 60 ms cycle. Perfect knowledge of the spacecraft position and inertial velocities is assumed and used as feedback signals to the guidance. Longitudinal and lateral guidance designs are described in more detail in sections 5.2 and 5.3. Rate gyro sensors are modeled as second order filters with a bandwidth of 60 hz and 0.4 damping. The turbulence wind model is described in more detail in Appendix C.
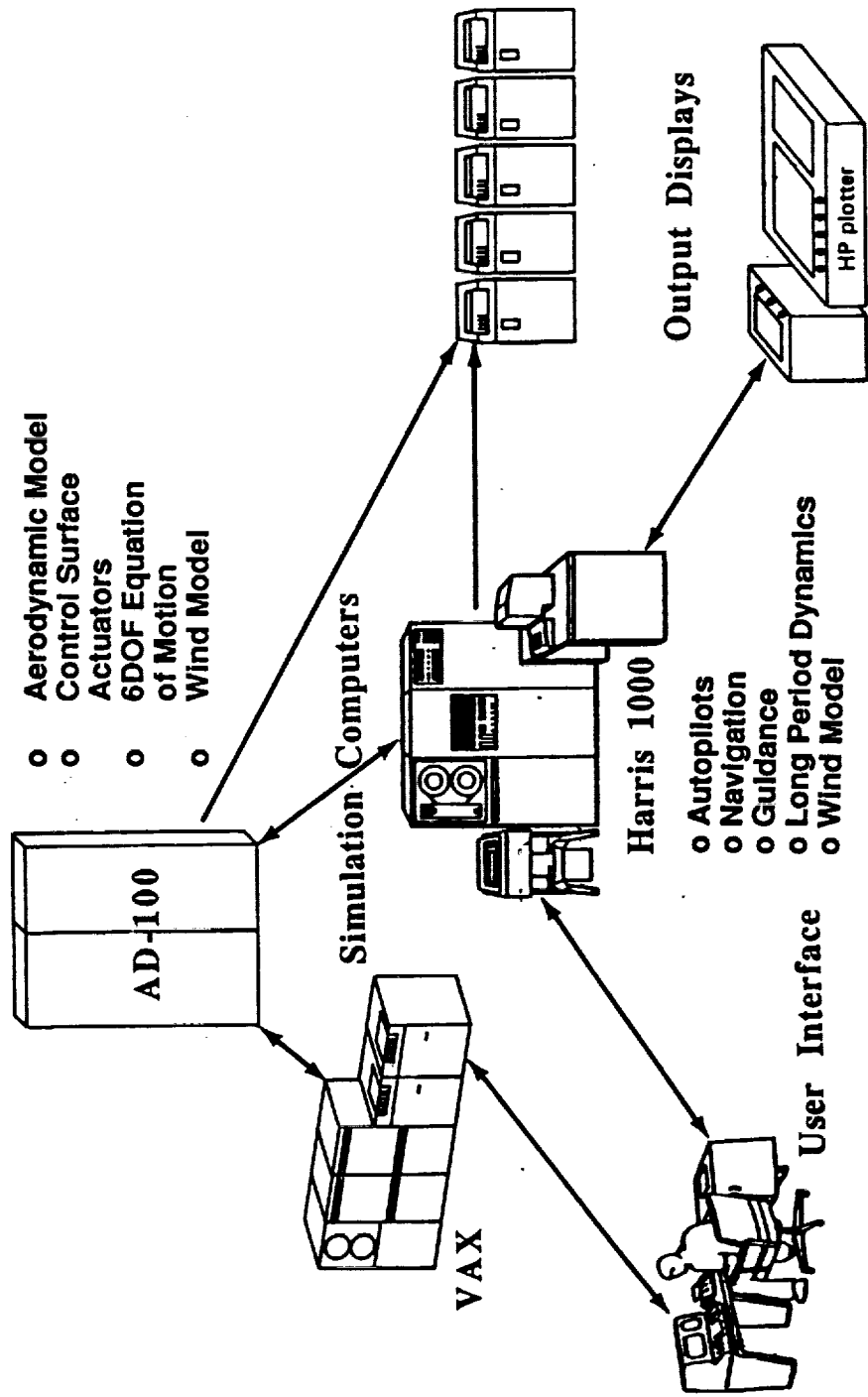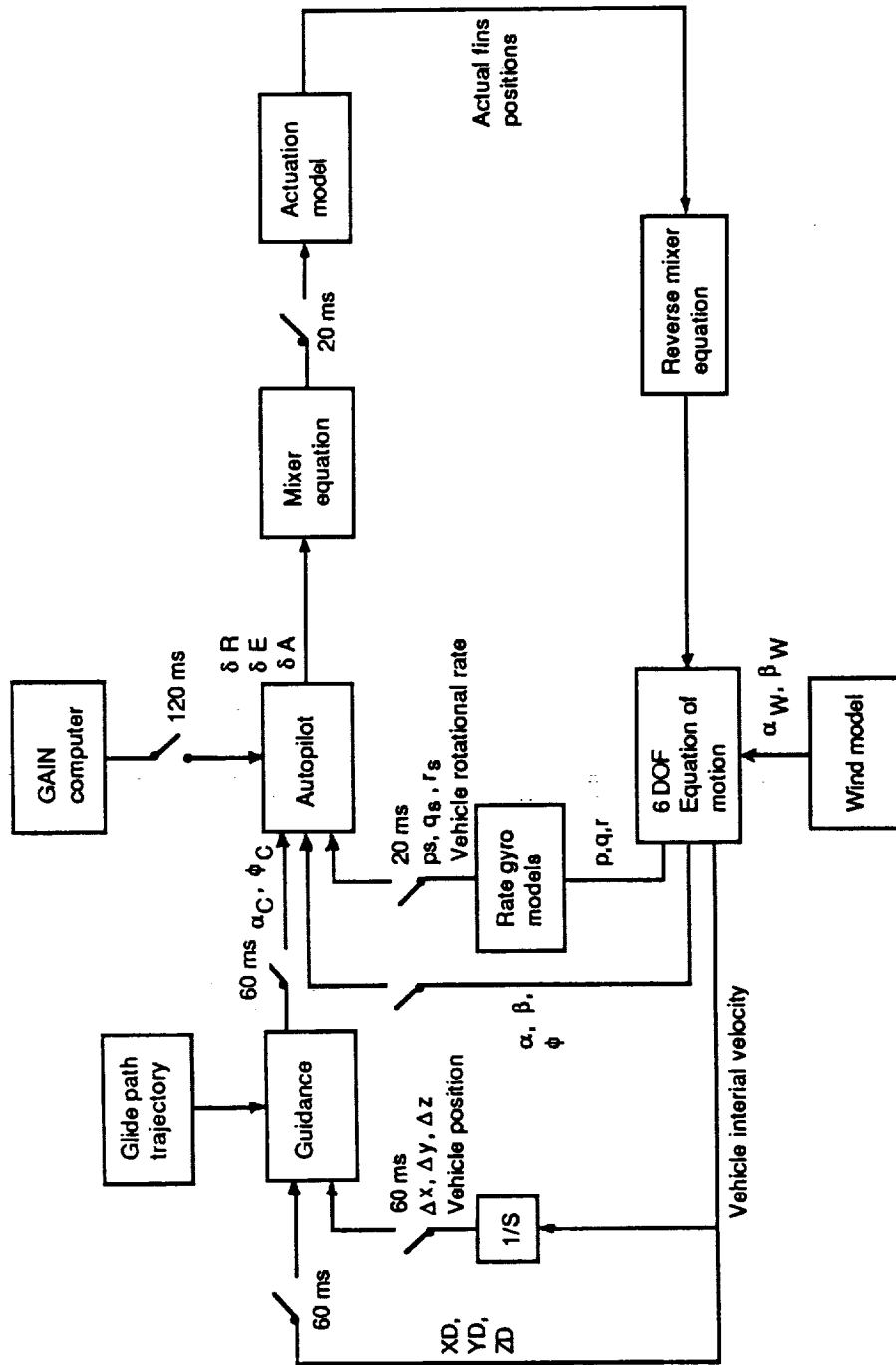
147

Figure B-1 Computer Resources Used in 6DOF Simulation

Simulation Computers

AD-100
o Aerodynamic Model
o Control Surface
  Actuators
o 6DOF Equation
  of Motion
o Wind Model

Harris 1000
o Autopilots
o Navigation
o Guidance
o Long Period Dynamics
o Wind Model

Output Displays

HP plotter

User Interface
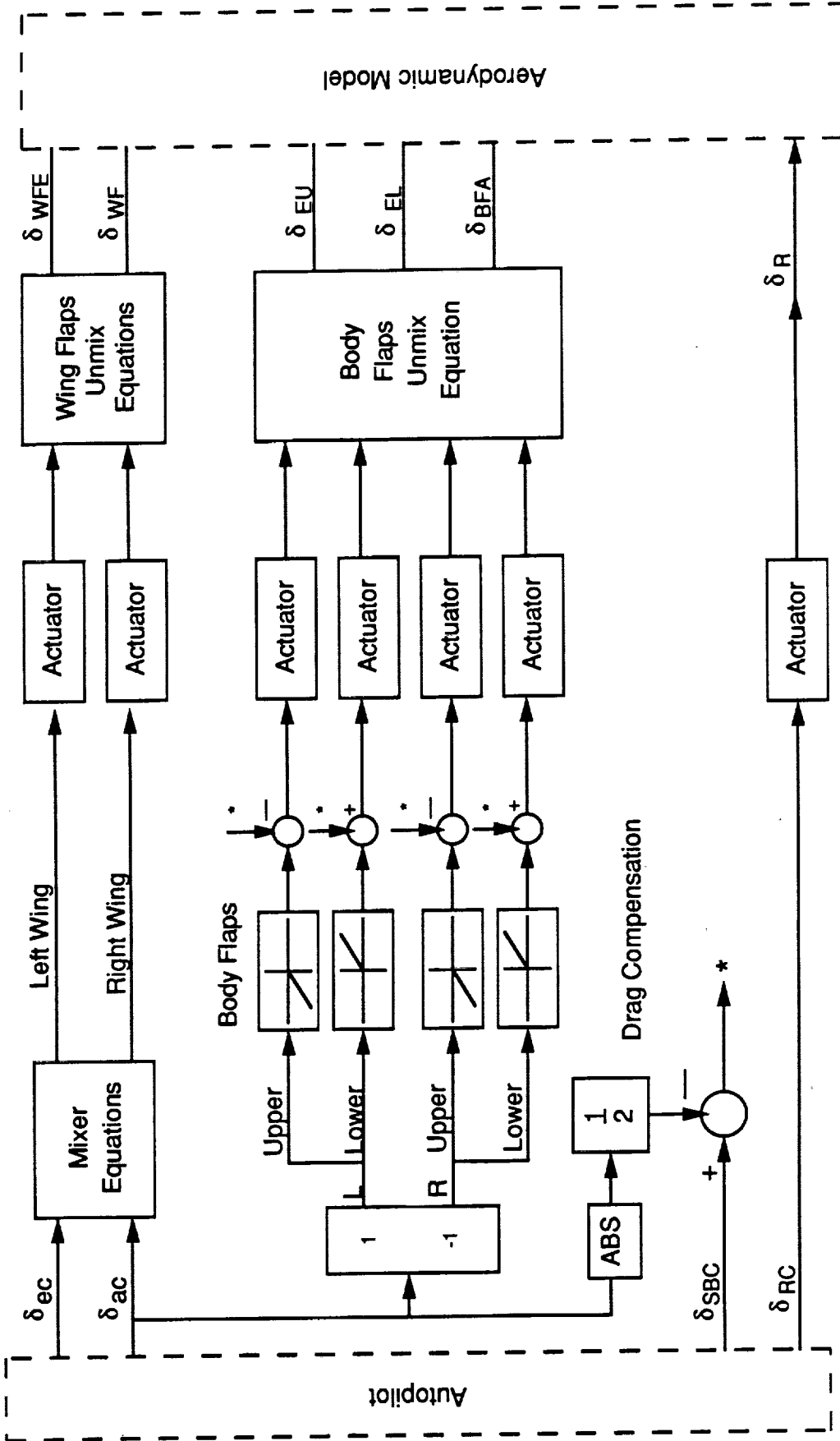
VAX

Figure B-2   CERV Simulation Block Diagram

Figure B-3 Control Surfaces Mixer Equations

150

Wing Flap Mixer Equations :

$$\begin{bmatrix} Left\ Wing \\ Right\ Wing \end{bmatrix} = \begin{bmatrix} 1 & 1 \\ 1 & -1 \end{bmatrix} \begin{bmatrix} S_{ec} \\ S_{ac} \end{bmatrix} \begin{matrix} (elevator\ command) \\ (aileron\ command) \end{matrix}$$

Wing Flap Unmix Equations :

$$\begin{bmatrix} S_{WFE} \\ S_{WF} \end{bmatrix} = \frac{1}{2} \begin{bmatrix} 1 & 1 \\ 1 & -1 \end{bmatrix} \begin{bmatrix} Left\ Wing \\ Right\ Wing \end{bmatrix}$$

Body Flap Unmix Equations :

$$\begin{bmatrix} S_{EU} \\ S_{EL} \\ S_{BFA} \end{bmatrix} = \frac{1}{2} \begin{bmatrix} 1 & 1 & 0 & 0 \\ 0 & 0 & 1 & 1 \\ -1 & -1 & 1 & 1 \end{bmatrix} \begin{bmatrix} Upper\ Left \\ Lower\ Left \\ Upper\ Right \\ Lower\ Right \end{bmatrix} Body\ Flaps$$

Figure B-3 Control Surfaces Mixer Equations
(Continued)

151

Appendix C

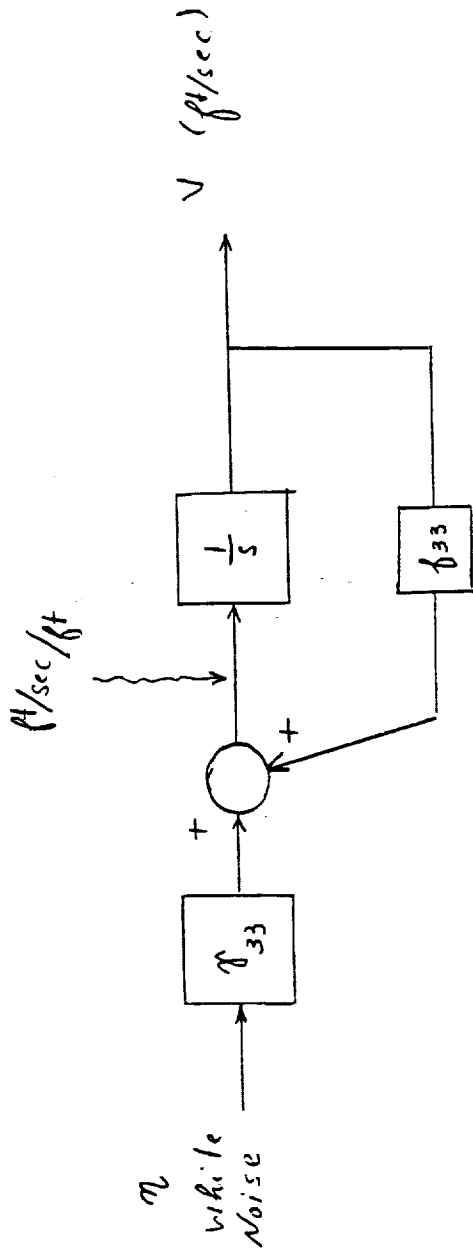WIND TURBULENCE MODEL

C.1 Introduction

A number of efforts have been directed toward generating mathematical models of wind turbulence near the surface of the earth. References 3-6 all recommend the use of the Von Karman isotropic power spectra over the Dryden spectra, apparently due to their greater accuracy at high frequency.

The Von Karman spectra provide a complex spacial distribution of wind velocity vectors, which must be converted to a temporal distribution, by aircraft speed and flight path, for use in a flight simulation. The size of the aircraft, in response to the gust velocities, must also be taken into account. Reference 3 proposes to approximate the Von Karman gust distributions by driving shaping filters with white noise. It proposes a second-order filter for the longitudinal direction and a third-order filter for the lateral and vertical directions. Reference 4 also proposes shaping filters, based on the landing conditions of a transport aircraft, for this approximation. It uses a first-order filter for the longitudinal direction and a second-order filter for the lateral and vertical directions. This is the model that has been implemented in our simulation.

C.2 Model Description

The form of the wind turbulence model shaping filters used in the flight simulation is taken from Reference 4. Block diagrams of the continuous froms of the filters, in terms of displacement along the flight path, are shown in figures C-1 and C-2. In the simulation these filters are discretized and the aircraft speed is used to convert time steps to distance steps. The parameters of the filters are determined from the aircraft wing span (b) and the chosen integral scale length (L), which determines the frequency response of the filters. The chosen variance level (sigma) of the wind components, along with the integral scale length, determines the level of the input white noise to drive the gust spectra.

The choice of appropriate integral scale length and turbulence variance is difficult since these vary with altitude and measured data show large variations. Figures C-3 and C-4 from Reference 4 provide an indication of the probabilities and measured variations in these values. Figure C-5 from Reference 6 gives altitude profiles of these values as chosen for use in Space Shuttle simulations.

η
White
Noise

γ_{33}

$\frac{1}{s}$

β_{33}

$V \ (ft/sec)$

$ft/sec/ft$

$\beta_{33} = -\dfrac{(1 + 1.5\beta)^{2/3}}{1 + 3\beta}$,

$\gamma_{33} = -1.4 \ \beta_{33}$

$E\left\{\eta(x_1) \ \eta^T(x_2)\right\} = \sigma^2 L * \delta(x_1 - x_2)$

$\beta = \dfrac{b}{2L}$

L = Turbulence Integral Scale

b = Wing Span of Aircraft $(2l \ ft)$

Figure C-1 Turbulence Model for X-Axis

153

Figure C-2 Turbulence Model for Y and Z-Axis

$$\beta^{21} = \frac{-(1+\beta)^{2/3}}{L^2} \beta^{-4/3}$$

$$\beta^{22} = \frac{-0.5(1+3\beta)}{L} \beta^{-4/3}$$
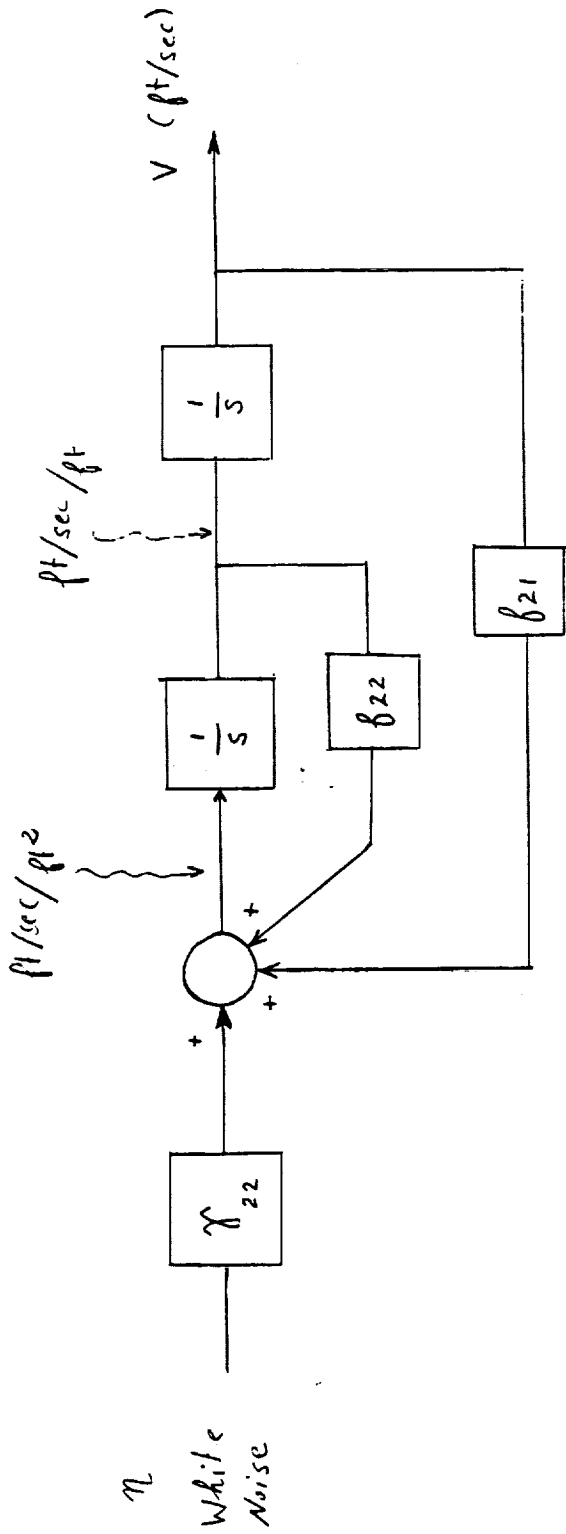
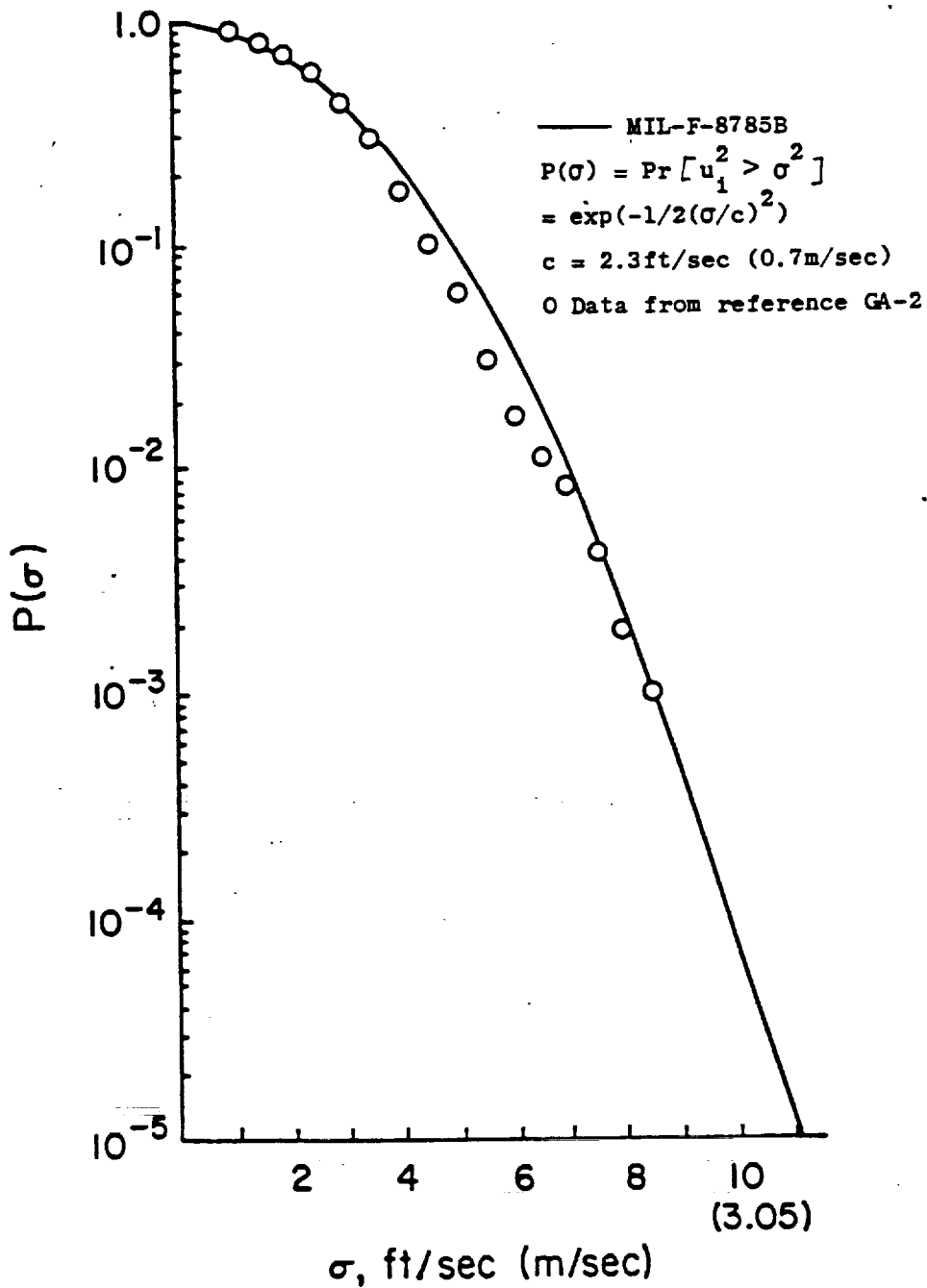$$\gamma_{22} = -\beta^{21}$$

$$E\left\{\eta(x_1)\,\eta^T(x_2)\right\} = \sigma^2_L * \delta(x_1 - x_2)$$

$$\beta = \frac{b}{2L}$$

L = Turbulence Integral Scale

b = Wing Span of Aircraft (21 ft)

154

PROBABILITY DISTRIBUTION OF THE
RMS TURBULENT VELOCITY
$$P(\sigma) = Pr\{\bar{v}_i^2 \geq \sigma^2\}$$

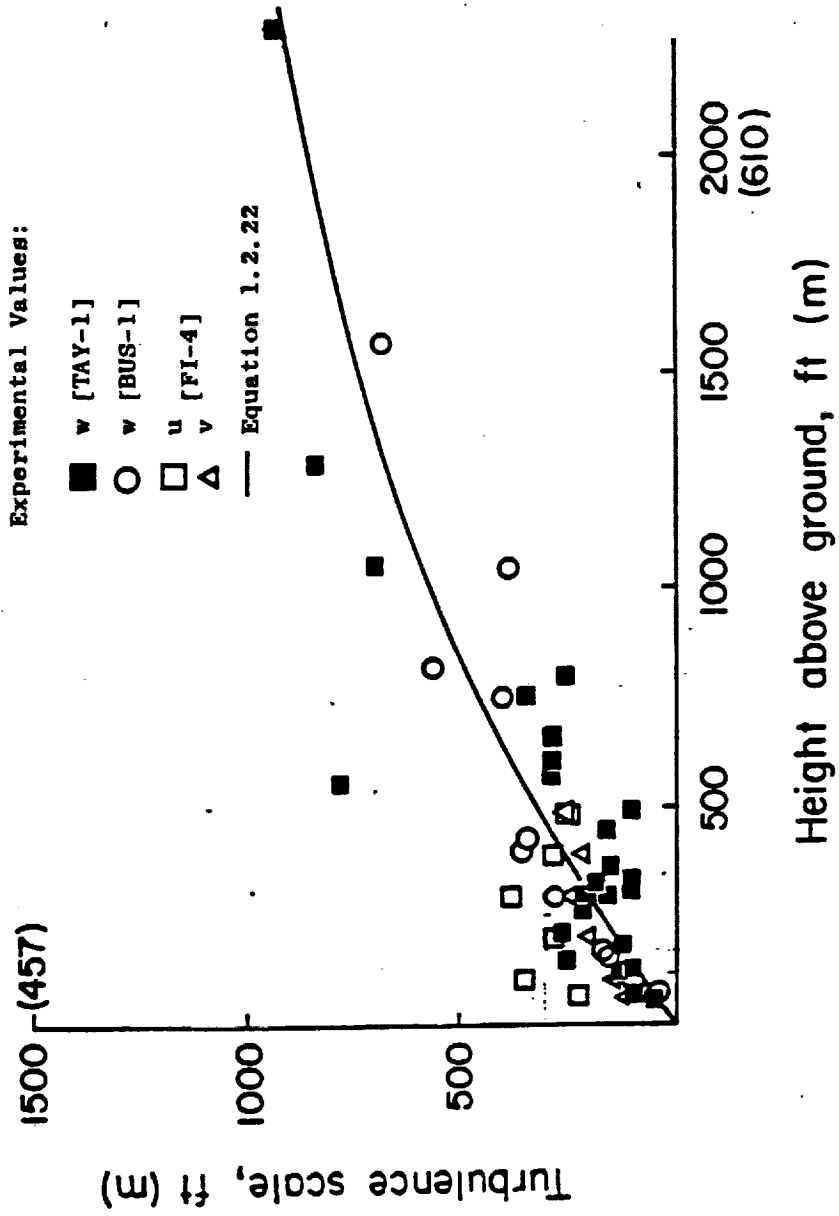Figure C-3 Probability Distribution of the RMS Turbulent Velocity

155

Figure C-4 Variation of the Turbulence Scale with Height

Experimental Values:

■ w [TAY-1]
○ w [BUS-1]
□ u [FI-4]
△ v
—— Equation 1.2.22

Height above ground, ft (m)

Turbulence scale, ft (m)

ALTITUDE (m)	STANDARD DEVIATION OF TURBULENCE			INTEGRAL SCALES OF TURBULENCE		
	σ_1(m/sec)	σ_2(m/sec)	σ_3(m/sec)	L_1(m)	L_2(m)	L_3(m)
10	2.31	1.67	1.15	21	11	5
20	2.58	1.98	1.46	33	19	11
30	2.75	2.20	1.71	43	28	17
40	2.88	2.36	1.89	52	35	23
50	2.98	2.49	2.05	61	42	29
60	3.07	2.61	2.19	68	49	35
70	3.15	2.71	2.32	75	56	41
80	3.22	2.81	2.43	82	63	47
90	3.28	2.89	2.54	89	69	53
100	3.33	2.97	2.64	95	75	59
200	3.72	3.53	3.38	149	134	123
304.8	3.95/4.37	3.95/4.37	3.95/4.39	196/300	190/300	192/300
400	4.39	4.39	4.39	300	300	300
500	4.39	4.39	4.39	300	300	300
600	4.39	4.39	4.39	300	300	300
700	4.39	4.39	4.39	300	300	300
762	4.39/5.70	4.39/5.70	4.39/5.70	300/533	300/533	300/533
800	5.70	5.70	5.70	533	533	533
900	5.70	5.70	5.70	533	533	533
1524	5.70/5.79	5.70/5.79	5.70/5.79	533	533	533
2000	5.79	5.79	5.79	533	533	533
3048	5.79/5.52	5.79/5.52	5.79/5.52	533	533	533
4000	5.52	5.52	5.52	533	533	533
5000	5.52	5.52	5.52	533	533	533
6096	5.52/5.27	5.52/5.27	5.52/5.27	533	533	533
7000	5.27	5.27	5.27	533	533	533
8000	5.27	5.27	5.27	533	533	533
9144	5.27/4.22	5.27/4.22	5.27/4.22	533	533	533
10000	4.22	4.22	4.22	533	533	533
20000	6.01	6.01	4.22	6691	6691	955

*Double entries for a tabulated altitude indicate a step
change in standard deviation or integral scale at that altitude.

Figure C-5 Variation of Standard Deviation and Length Scale With Altitude
Used in Space Shuttle Simulations (from ref. 6)

References

1. Blight, J., Coleman, E., Thompson, C., "Integral LQG Controller Design for a Fighter Aircraft", AIAA-87-2452-CP, Proc. of 1987 Guidance, Navigation, and Control Conference, Monterey, California, Aug. 1987.

2. Tsikalas, G., Dyer, D., "Shuttle Automatic Landing System", AAS-82-017, Proc. of 1982 Annual Rocky Mountain Guidance and Control Conference, Keystone, Colorado, Jan. 1982

3. Barr, N. M., Gangsaas, D., and Schaeffer, D. R., "Wind Models for Flight Simulator Certification of Landing and Approach Guidance and Control System", FAA-RD-74-206, Dec. 1974.

4. Holley, W. E., and Bryson, A. E., "Wind Modeling and Lateral Aircraft Control for Automatic Landing", Stanford University Department of Aeronautics and Astronautics Report No. 489, Jan. 1975.

5. Chalk, C. R., Neal, T. P., Harris, F. E., and Pritchard, F. E., "Background Information and User Guide for MIL-F-8785B (ASG), Military Specification - Flying Qualities of Piloted Airplanes", AFFDL-TR-69-72, Aug. 1967.

6. Tatom, F. B., and Smith, S. R., "Advanced Space Shuttle Simulation Model", NASA CR-3541, 1982.

15. Supplementary Notes

Langley Technical Monitor: Richard M. Hueschen

16. Abstract

The CERV autoland feasibility study focused on determining the controllability of the NASA Langley high lift over drag CERV for performing an automatic landing at a prescribed runway. An autoland system was developed using integral LQG design technique. The design was verified using a nonlinear 6 DOF simulation. Simulation results demonstrate that the CERV configuration is a very flyable configuration for performing an autoland mission. Adequate stability and control was demonstrated for wind turbulence and wind shear. Control surface actuator requirements were developed.

PREPARATION OF THE REPORT DOCUMENTATION PAGE

The last page of a report facing the third cover is the Report Documentation Page, RDP. Information presented on this page is used in announcing and cataloging reports as well as preparing the cover and title page. Thus it is important that the information be correct. Instructions for filling in each block of the form are as follows:

Block 1. Report No. NASA report series number, if preassigned.

Block 2. Government Accession No. Leave blank.

Block 3. Recipient's Catalog No. Reserved for use by each report recipient.

Block 4. Title and Subtitle. Typed in caps and lower case with dash or period separating subtitle from title.

Block 5. Report Date. Approximate month and year the report will be published.

Block 6. Performing Organization Code. Leave blank.

Block 7. Author(s). Provide full names exactly as they are to appear on the title page. If applicable, the word editor should follow a name.

Block 8. Performing Organization Report No. NASA installation report control number and, if desired, the non-NASA performing organization report control number.

Block 9. Performing Organization Name and Address. Provide affiliation (NASA program office, NASA installation, or contractor name) of authors.

Block 10. Work Unit No. Provide Research and Technology Objectives and Plans (RTOP) number.

Block 11. Contract or Grant No. Provide when applicable.

Block 12. Sponsoring Agency Name and Address. National Aeronautics and Space Administration, Washington, D.C. 20546-0001. If contractor report, add NASA installation or HQ program office.

Block 13. Type of Report and Period Covered. NASA formal report series; for Contractor Report also list type (interim, final) and period covered when applicable.

Block 14. Sponsoring Agency Code. Leave blank.

Block 15. Supplementary Notes. Information not included elsewhere: affiliation of authors if additional space is re-

quired for block 9, notice of work sponsored by another agency, monitor of contract, information about supplements (film, data tapes, etc.), meeting site and date for presented papers, journal to which an article has been submitted, note of a report made from a thesis, appendix by author other than shown in block 7.

Block 16. Abstract. The abstract should be informative rather than descriptive and should state the objectives of the investigation, the methods employed (e.g., simulation, experiment, or remote sensing), the results obtained, and the conclusions reached.

Block 17. Key Words. Identifying words or phrases to be used in cataloging the report.

Block 18. Distribution Statement. Indicate whether report is available to public or not. If not to be controlled, use "Unclassified-Unlimited." If controlled availability is required, list the category approved on the Document Availability Authorization Form (see NHB 2200.2, Form FF427). Also specify subject category (see "Table of Contents" in a current issue of STAR), in which report is to be distributed.

Block 19. Security Classification (of this report). Self-explanatory.

Block 20. Security Classification (of this page). Self-explanatory.

Block 21. No. of Pages. Count front matter pages beginning with iii, text pages including internal blank pages, and the RDP, but not the title page or the back of the title page.

Block 22. Price Code. If block 18 shows "Unclassified-Unlimited," provide the NTIS price code (see "NTIS Price Schedules" in a current issue of STAR) and at the bottom of the form add either "For sale by the National Technical Information Service, Springfield, VA 22161-2171" or "For sale by the Superintendent of Documents, U.S. Government Printing Office, Washington, DC 20402-0001," whichever is appropriate.